CONJUGATE HEAT TRANSFER ANALYSIS IN HYPERSONIC APPLICATIONS

A Thesis
Submitted in Partial Fulfillment of the Requirements for
the Award of the Degree of

DOCTOR OF PHILOSOPHY

By

RAVI KUMAR PEETALA

DEPARTMENT OF MECHANICAL ENGINEERING
INDIAN INSTITUTE OF TECHNOLOGY GUWAHATI
GUWAHATI, INDIA

May 2014

Declaration

I hereby certify that the work compiled in this dissertation is the outcome of the research work, performed by myself, else stated, under the guidance of Dr. Vinayak N. Kulkarni and Dr. Niranjan Sahoo.

Any part of this work has not earlier been submitted for the award of any degree, diploma, associate-ship, fellowship or its equivalent to any University or Institution.

Ravi Kumar Peetala
Registration No. 09610314
Department of Mechanical Engineering
Indian Institute of Technology Guwahati

CERTIFICATE

It is certified that the work contained in the thesis entitled Conjugate Heat Transfer Analysis in Hypersonic Flows, by Ravi Kumar Peetala (Registration No. 09610314), a student of the Department of Mechanical Engineering, Indian Institute of Technology Guwahati, India, for the award of the degree of Doctor of Philosophy, has been carried out under our supervision and this work has not been submitted elsewhere.

Dr. Vinayak N. Kulkarni
Assistant Professor
Department of Mechanical Engineering
Indian Institute of Technology Guwahati
Guwahati – 781039,
India

Dr. Niranjan Sahoo
Associate Professor
Department of Mechanical Engineering
Indian Institute of Technology Guwahati
Guwahati – 781039,
India

ABSTRACT

Transient heat transfer analysis is highly essential for design of many engineering objects, such as steam and gas turbines, diesel engine blocks, jet engines, rocket motors, nuclear reactors etc. It is of significant priority and of scientific relevance to understand the flow in hypersonic applications. High aerodynamic heating rates associated with high-speed flights portray even more severe transient heat transfer problems for the design of spacecraft and missiles. In view of this Conjugate Heat Transfer (CHT), solver is used to understand the interface properties and flow properties due to change in wall heating rates. It is also useful to examine the heat penetration of solid in various wall materials with different time scales. Therefore the main focus of the present work is on the accurate prediction of heat transfer, temperature at the interface and flow properties. This problem is critically important in efficient design of thermal protection system (TPS) for hypersonic vehicles. TPS, in-fact is traditionally designed with the help of one-dimensional heat transfer analysis. Since, uncertainties are more in these studies; CHT is used to overcome those uncertainties. It is clear that thermal protection system can be optimally designed from these studies. The present investigations can be summarized in two main steps which are described as follows; Empirical analysis and numerical simulation. These are the two techniques generally used to estimate the surface heat flux in the above applications.

In experimental analysis, the surface heating rates are predicted from the measured temperature by using one-dimensional heat transfer modeling and various methods like Laplace transform, Duhamel's integral, Schultz and Jones methods. The temperature histories obtained from the in-house one-dimensional finite volume computation solver, literature reported shock tunnel measurement and supersonic flight experiment are used to predict the surface heat flux using fore mentioned methods. Heat flux recovery from all the methods for smooth temperature signals is seen to be in good agreement with reasonable accuracy of ± 5%. However, it has been noticed that the spline based fitting techniques supersede the polynomial based fitting techniques for prediction of heat flux from discontinuous or noisy temperature signals. Spline based fitting techniques are found to be precise for trend prediction and quantification of heat flux for all types of temperature data. It has also been observed that lower order spline (i.e. linear spline) is equally effective in recovering the heat flux signal as compared to the higher order but is limited to short duration measurements of

the order of few milliseconds. However in large time scale applications, one-dimensional heat transfer analysis is not valid. These large time scales heat is transferred in multi-direction, so it is necessary to study the multi dimensional heat transfer studies.

In view of necessity of multidimensional heat transfer analysis, solid and fluid domain conservation equations are solved simultaneously in the numerical approach turned as conjugate heat transfer (CHT) analysis. The finite volume based explicit solver is used for conduction and flow solvers are used for this purpose. The AUSM-δ scheme is incorporated in the fluid flow solver for inviscid flux computations while the viscous fluxes are computed using discrete version of the Gauss divergence theorem. The main focus of the current studies is on CHT technique, which is carried out in three ways: decoupled, strongly coupled and loosely coupled. Thus analysis generalized CHT in-house solvers have been developed for hypersonic applications.

The CHT studies are focused to understand the limit of applicability of the assumptions which are considered to recover the experimental data. It is also considered as a potential tool for simultaneous prediction of wall heat flux and temperature. With these objectives, CHT solvers involving different couplings between solid and fluid domain computations are employed to assess the applicability of these coupling strategies for various time scales. The critical analysis discussed in these investigations, is very much useful to select a particular coupling technique as per the user requirement. It also leads to valuable comments about the comparison of wall heat flux obtained from conventional CFD analysis and the experimental measurements. The prediction of heat flux and temperature at the fluid and solid domain interface is done by the in-house solvers which solve various hypersonic flow problems (i.e. flow over a flat plate, cylinder, composite solids, double wedge) for two dimensional geometries. These computational studies demonstrate the effect of large simulation duration on the prediction of heat flux due to transient and multidimensionality of the heat transfer.

Flow over finite thickness flat plate has been studied using all the coupling techniques. These strategies are seen to be equally useful for prediction of local temperature and heat flux signals for short duration experiments of the order of 1ms. Effect of wall property variation on the fluid flow has also been studied for comparatively large time scale (~0.1s) using loosely coupled CHT technique. Thermal boundary layer and velocity boundary

layer thicknesses are used to understand the interaction between wall heating and hydrodynamic boundary layer.

CHT studies are extended to hypersonic flows over a cylinder by adopting various coupling techniques and examining their implementation abilities. The main focus of this study is to define a computationally cheaper CHT algorithm for the above mentioned application. This study is also focused to look into the effect of hypersonic flow field on wall heat flux for a finite thickness insulating cylinder at moderately large time scales. CHT analysis is further extended to composite solid domain, since thermal protection systems are generally configured with multiple solids. It has been noticed that, the composite CHT studies are useful for design of thermal protection systems for hypersonic vehicles.

Shock wave boundary layer interaction (SWBLI) phenomenon plays a critical role in the design of supersonic and hypersonic vehicles; hence the present studies are extended to understand the flow over a double wedge model. It has been observed that the interaction induce extremely high heating and pressure loads on the surface of the vehicle. Implementation of CHT is found useful to predict the separation bubble length, heat flux, skin friction coefficient and pressure distributions.

ACKNOWLEDGEMENT

I would like to make my deepest appreciation and gratitude to Dr. Vinayak N. Kulkarni and Dr. Niranjan Sahoo for their invaluable guidance, constructive criticism and encouragement during my thesis work. I must say I am blessed to have them as my supervisors.

My sincere acknowledgement goes to Prof. D. Chakraborty and Prof. P. Mahanta, former and present Heads of Mechanical Engineering Department. I thank them for their encouragement, guidance, and support from the initial to the final stages of my PhD work. I am also indebted to the members of Doctoral Committee Prof. U. K. Saha, Dr. C. Somayaji, and Dr. V.V. Goud for their precious suggestions about critical issues related to my work. Acknowledgement is made to all my well-wishers both faculty and students of Indian Institute of Technology Guwahati for their support, encouragement and critique.

I would like to extend my sincere thanks to all my beloved friends Mr. John Bibin, Mr. Dipankar Das, Mr. Vinod Pandey for helping me in coding and for their involvement in the discussions about research problems and Mr. Tharun Dolla, Mr. Ramesh Pallekonda, Mr. Pydi, Mr. Prasad, Mr. Charan, Mr. Sunku, Mr. Akshay, Mr. Anand, Mr. Suresh, Mr. Sumit, Mr. Suvayan, Miss. Sruthi, for their help in proof reading of my thesis. I am also thankful to my Lab mates and lobby mates with whom I have come in contact during my stay at IIT Guwahati. The friendship and unforgettable attachments shared with them has made my life pleasant. I extend my indebted gratitude towards the church, with whom I cherished my good times, for their support and encouragement in all tough times and most of all their prayers for me and my project.

A special thanks to my family. Words cannot express how grateful I am to my mother, father, and brothers for all of the sacrifices that they've made on my behalf. Their prayer for me was what sustained me this far. Finally I thank my God, my good Father, for letting me through all the difficulties. I have experienced your guidance day by day. You are the one who let me finish my degree. I will trust you in future as well. Thank you, Lord.

May 19, 2014

IIT Guwahati **Ravi Kumar Peetala**

Dedicated to my Parents....

Mrs. Nirmala Peetala
and
Mr. Peddiraju Peetala

Whose endless faith and blessings always
Inspired me to move forward

TABLE OF CONTENTS

NOMENCLATURE

a	Coefficient
a_N	Coefficient for North node
a_W	Coefficient for West node
a_S	Coefficient for South node
a_E	Coefficient for East node
A	Area of cell (m^2)
c_p	Specific heat $\left(\text{kJ/kg-k}\right)$
C_f	Skin friction
C_w	Chapman and rubesin parameter
$(dt)_s$	Thickness of solid domain (mm)
$(dt)_f$	Thickness of fluid domain (mm)
d_f	Outer diameter of fluid domain (mm)
d_i	Outer diameter of solid domain and inner domain of fluid domain (mm)
d_s	Inner diameter of solid domain (mm)
E	Total specific energy (kJ/kg)
e	Specific internal energy (kJ/kg)
$\overline{F}$	Laplace transform of the polynomial equation
H	Total specific enthalpy (kJ/kg)
h	Specific enthalpy (kJ/kg)
L	Length (m)
k	Thermal conductivity $\left(\text{W/m.k}\right)$
M	Mach number
$\hat{n}$	Unit normal vector
F	Fluxes
p	Pressure (N/m^2)
Pr	Prandtl number

q_0 Stagnation point heat flux $\left(\mathrm{W/m^2}\right)$

r_0 Outer radius of the cylinder (mm)

R Universal gas constant ($J/kg.K$)

Re Reynolds number

S Laplace transform

s Source term of energy equation

$\overline{S}$ Source average strength

St Stanton number

T_w Wall temperature $\left(\mathrm{K}\right)$

T_s Stagnation point temperature $\left(\mathrm{K}\right)$

t Time (ms)

u X-direction velocity (m/s)

v Y-direction velocity (m/s)

U Conservative variable

x, y Cartesian co-ordinate system

S Sutherland's constant

∂w Characteristic variables

Greek symbols

Ω Control volume

τ Shear stress (N/m^2)

ρ Density (kg/m^3)

λ Courant number

γ Specific heat ratio

δ *Shock stand-off distance*

μ Dynamic viscosity ($kg/m-s$)

Δ Difference

Subscripts

∞	Freestream quantities
i, j	Indices along x and y directions
k	Edge number reference
L, R	Left and right side properties
I, V	Inviscid and viscous fluxes
w	Wall

Superscripts

$\_$	Vector quantities
$\perp$	Perpendicular
*	Non-dimensional quantities

LIST OF TABLES

LIST OF FIGURES

ABBREVIATIONS

AUSM	Advection Upstream Splitting Method
BEM	Boundary Element Method
CFD	Computational Fluid Dynamics
DC-CHT	Decoupled Conjugate Heat Transfer
DQM	Differential Quadrature Method
FEM	Finite Element Method
FVM	Finite Volume Method
IHCP	Inverse Heat Conduction Problem
LC-CHT	Loosely Coupled Conjugate Heat Transfer
LES	Large Eddy Simulation
LIFTS	Langley Integrated Fluid-Thermal-Structural
MEM	Maximum Entropy Method
NGV	Nozzle Guide Vanes
N-S	Navier-Stokes
QR	Quadratic Regularization
SBLE	Swept-Back Leading Edge
SC-CHT	Strongly Coupled Conjugate Heat Transfer
SQP	Successive Quadratic Programming
SWBLI	Shock Wave Boundary Layer Interaction
TFFB	Temperature Forward Flux Back

CHAPTER 1

INTRODUCTION

1.1 History of the Flight

The pursuit to fly in the sky has led many researchers in the culmination of aerodynamics. Even though the quest to fly was conceived by the primitive man, it started progressing after the conception of notion that air has weight by Aristotle. Subsequently, Archimedes principle and discoveries of Galileo, Pascal, and Bacon that air is compressible and its pressure decreases with altitude has led further progress. In the year 1500, Leonardo da Vinci foresaw the things and designed certain machines that copied the action of bird's wings. His insight of the movement of wing relative to the air causes the lift necessary to fly has provoked many researchers to build machines lighter than air which lead to the culmination of first flying machine to carry man. In 1783, two Montgolfier brothers from France constructed the balloon of holding the distinction of initiating the first ascent of man into the atmosphere. But the quest to control the direction has led to the acquisition of small engines and steering devices, still remains lighter-than-air aerostat devices.

Sir George Cayley of England (1773-1857), who is generally recognized as the father of modern aerodynamics understood the basic forces acting on a wing. He built a glider with a wing and a tail unit which flew successfully. He realized the pivotal role of the angle of attack of wing and conceived the insight that curved surfaces would produce more lift force than flat ones. His designs were made stable with the use of dihedral. In 1853, it was believed that he built a man-carrying glider, which flew, once with one of his servants as a passenger. During the late 1800's, many inventors endeavored to use a steam engine to power their airplanes and made little progress. Meanwhile, towards the end of the nineteenth century, a German named Otto Lilienthal successfully flew in gliders of his own design. He recorded over 2000 successful flights before crashing to death in 1896. Lilienthal proved the concept of heavier-than-air flight. Today, this form of flying, now called hang-gliding, is enjoying a substantial comeback.

At the Smithsonian Institution in Washington, D.C., Dr. Samuel Pierpont Langley attempted to design small steam-powered airplanes and came up successfully with a 5-meter wing span tandem biplane "the Aerodrome," fitted with a steam engine driving two propellers, which flew over 1 kilometer in 1896. Backed by a grant from Congress, he built a

full-scale version of the same airplane to carry a pilot. Unfortunately, launching gear failure caused it to crash twice during October and December of 1903. On December 17, 1903, the Wright brothers eventually achieved success in a gasoline-engine-powered machine of their own design, which was improved further. Two world wars and numerous limited wars have leveraged advances in the airplane, which made Aerial combat as a commonplace by the end of World War I (1918), and German advanced concepts at the end of World War II (1945) pointed the way to the future.

Now-a-days, numbers of researchers are pushing forward their interest in the areas of hypersonic transports, lifting bodies, and the space shuttle. Hypersonic flight is arbitrarily defined as flight at speeds beyond Mach 5 with a spectacular flow changes are evident to define this. To date, speeds of this magnitude have been achieved only by rockets and spacecraft and the NASA X-15 research airplane. Several formidable problems are encountered at these speeds. First, the shock waves generated by a body trail back at such a high angle that they may seriously interact with the boundary layers around the body. For the most part, these boundary layers are highly turbulent in nature. Secondly, across the strong shocks, the air undergoes a drastic temperature increase, which is a major problem of the aerodynamic body. For sustained hypersonic flight, most normal metals used in today's airplanes would quickly melt; therefore new materials or methods that can withstand the high-temperatures are yet to come. Aerodynamic heating is one salient feature that has to be looked along with hypersonic flow due to the fact that temperatures at those surfaces will be so high that it could melt the surface. In order to control this heating, hypersonic vehicle's surfaces are made blunt. One must notice that heating still exists. In order to reduce the heating, various cooling techniques are considered. Cooling techniques to remove thermal energy from the surface of hypersonic spacecraft are broadly classified into two categories such as active cooling and passive cooling techniques. ‘Radiative shielding’ (e.g. Molybdenum and Zirconium) and ‘Insulation’ (e.g. Dynaquartz) cooling are the most widely used techniques in the area of passive cooling. These techniques are used to avoid the oncoming heat to the vehicle and therefore they are called passive cooling techniques. ‘Convective cooling’, ‘ablative cooling’, ‘transpiration cooling’ and ‘film cooling’ are classified as ‘active cooling techniques’. These techniques are directly used to cool the vehicle surface. Thus, in order to design a thermal production system or cooling system one must predict the surface heat flux properly. These predictions can be measured in two ways - numerically (using computational fluid dynamics (CFD)) and also experimentally. In CFD,

the following three different coupling techniques have been used to determine the interface properties like surface heat flux, surface temperature etc.

- Decouple Conjugate Heat Transfer (DC- CHT).
- Strongly Coupled Conjugate Heat Transfer (SC- CHT).
- Loosely Coupled Conjugate Heat Transfer (LC- CHT).

The literature describes the heat transfer analysis of hypersonic flows based on both analytical and numerical approaches. Both of these methods, used for many years to model hypersonic, are now-a-days replaced by digital technology. Over the past several years, a number of models on complex coupled heat transfer studies are investigated and understood. In subsequent sections, a detailed review on the analytical studies along with experimental and numerical methods based on CFD literature is discussed.

1.2 Literature Review on Analytical Heat Transfer Studies

In general, there is no direct method to measure transient convective heating rate. Nevertheless it can be inferred from the history of transient temperature-time. Heat transfer measurement experiments are generally carried out for these studies in short duration impulse facilities, such as hypersonic shock tunnels, using thin film sensors (Sahoo, 2003 and Kulkarni *et al.,* 2008). Thin film sensors are typically used to record the rate of change of temperature with time. These thin film sensors are made from sputtering or painting a sensing material (platinum, nickel, gold etc.) on a backing or insulating material (quartz, Macor etc). Various analytical and numerical heat transfer models are available for evaluating surface heating rates from the recorded temperature history in open literature. Generally, in these methods, one dimensional heat conduction equation along with the experimentally obtained temperature signal is given as input for estimation of heat flux.

Cook and Felderman (1966) had presented the surface temperature measurements with inbuilt assumptions like unidirectional heat transfer and semi-infinite sensor depth applicable to experiments of shorter duration (of the order 1ms). However, these evaluation techniques are not applicable for longer testing durations of the order of few seconds. Therefore, necessity of understanding transient conduction issues has been felt by various researchers for accurate estimates of heat transfer rates. Various methodologies and formulations, based on orthogonal expansion technique, Laplace transform method, Hermite approximation method, Green's function approach, finite integral transform technique,

separation of variables method etc, are reported in the literature by numerous researchers for different scientific problems.

Carslaw and Jaeger (1959) discussed the solution methodology in detail for problems of heat flow in some selected test cases. Tittle (1965) and Bulavin and Kascheev (1965) described the Laplace transform method for solving the heat conduction equation of a thin slab symmetrically heated on both sides. James (1970) has calculated the surface heat flux from the history of transient temperature measured at an interior position in a heat-conducting solid, possessing constant thermal properties. These methods involve the numerical inversion of a convolution integral. Each of the new methods employs a least-squares procedure. Furthermore, a comparison of simplest formulation of the new methods with an older numerical inversion procedure was also employed similar to that of Stolz (1960). In this comparison it was shown that the new method is stable with time interval of one sixth of the minimum allowable time in the Stolz method (Walker and Scott, 1998). Analysis of the stability was given for several formulations which have even more desirable characteristics. Beck (1986) had obtained Eigen function expressions for rectangular coordinate system using application of Green's function. James *et al.* (1987) verified the use of Green's function to solve heat conduction equation in three dimensions to obtain an integral equation for temperature in terms of the initial and boundary values of the temperature. Haji and Mashena (1987) investigated that Galerkin procedure can also be used for solving transient conduction problems in composite geometries. Although this procedure gives an approximate closed-form solution, it has been proved that it offers the benefits and limitations one expects from an exact solution.

Clarissa et al. (2000) and Jian (2001) described the usefulness of Hermite approximation method for fuel rod heat conduction model to study stability analysis and thermal hydraulic behavior of a pressurized water reactor (BWR). Sadat (2006) has described the functionality of second order perturbation method for high Biot number applications during the studies conducted for transient heat conduction analysis for a slab. Shahani (2007) investigated and implemented finite Hankel transform in thermoelasticity analysis for quasi-static structural problems to arrive at a closed form relations for the thermal stresses. Ostrogorsky (2008) and Ge *et al.* (2009) carried out explorations to advocate the applicability of Laplace transforms and perturbation method for transient heat conduction studies in spheres exposed to surroundings at a uniform temperature and finite Biot's numbers. Reports about the accomplishment of various numerical and computational

methods to solve the energy equation effectively are also available in literature. Using the higher order shell theory, Mehdi (2000), Mishra and Roy (2007), Miller and Hober (2008) and Sirilath and Cho (2008) described that finite element and finite difference methods as some of the effective tools to study the heat conduction analysis for various configurations.

Diego (1987) developed a numerical solution of the one-dimensional inverse heat conduction problem. This is based on the computation of the solution associated with a suitable filtered version of the noisy data by discrete mollification and a parameter choice criterion, which automatically determines the radius of mollification as a function of the amount of noise in the data. Several numerical examples of interest were also analyzed showing the accuracy and stability properties of the method.

Mehta *et al.* (1988) investigated the influence on the temperature distribution and heat transfer coefficient on the surface of a typical sounding rocket caused by normal and lateral conduction. Using finite element method, a two-dimensional heat conduction equation with a time dependent aerodynamic heating condition at one surface and a radiation boundary condition at the other end was solved. Unsteady heating of a thin-skinned body subjected to an aerodynamic heating rate has wide practical interest in high speed free-flight. These include normal and lateral heat conduction and heat loss into thermocouple lead wires. The measured thermocouple temperature history on the inner surface of the thin-skin is customarily employed to estimate heat-transfer coefficient while neglecting normal and lateral heat conduction terms. One dimensional heat conduction equation was solved using perturbation method with the assumptions of quasi isothermal surface, adiabatic and constant wall temperature and negligible thermal radiation. Two-dimensional heat conduction equation with a time dependent aerodynamic heating condition at one surface and a radiation boundary condition at the other end is solved using finite element method. The resulting differential equations are solved using a three time level difference scheme. The algorithm employed was unconditionally stable. The main purpose of the work was to investigate the influence of normal and lateral conduction on the temperature distribution and heat transfer coefficient on the surface of a typical sounding rocket.

Zukhova and Pimshtein (1990) studied the one-dimensional, steady-state thermal problem for a laminated cylinder consisting of concentric layers and subjected to internal pressure and external heating. Their calculations show that the radial compressive stress due to the internal pressure can permit external heating without layer separation. They found that

the distribution of temperatures and stresses depends on the manner of stress application and heating.

Taler (1996[a]) developed a mathematical procedure of transient methods of measuring surface heat transfer rates. This method provides a simple and accurate means for determining time-varying heat transfer coefficient for an accurate temperature history of the body at a selected point beneath the surface. The interior temperature measurements were converted into local instantaneous heat transfer coefficients by solving the inverse heat conduction problem for the gauge. In his paper, he discussed about three types of heat flux gauges, namely, semi-infinite 1-D gauges, thick wall gauge and thin-skin calorimeters. The effect of the inaccuracies in the measurement of the interior temperature was eliminated by cubic spline smoothing or digital filtering of the raw interior temperature data. Inverse heat conduction procedures of transient methods were employed for measuring surface heat transfer rates.

Taler (1996[b]) proposed a new approach for solving a semi-numerical method for solving the inverse heat conduction problems in homogeneous and composite bodies. The presented solution does not require either the initial temperature distribution in the body, or the whole temperature-time history at the temperature sensor locations. Sample calculations confirm that this approach produces stable and accurate results for both exact and noisy data. The extension of the method presented to two or three dimensions is straightforward.

There are two methods of solving the transient inverse heat conduction problems in complex shaped elements (Taler *et al.* (1997). First inverse method assumes the known temperature surface located inside the analyzed area. Second inverse method deals with over-determined problem, because the number of temperature measurement points is higher than the number of unknown heat transfers coefficients. The measured temperature histories at several points placed inside the element are used in reconstructing the time-space temperature distribution in whole element cross-section. Using Finite Element Analysis, thermal stresses are then evaluated. At the element inner surface the heat coefficient is unknown in both the methods.

Huang and Tsai (1998) have described a boundary element method (BEM) based on inverse algorithm utilizing iterative regularization method (i.e. Conjugate Gradient Method) to solve the inverse heat conduction problem (IHCP) for estimating the unknown transient boundary heat flux in a multi-dimensional domain with arbitrary geometry.

The direct heat conduction problems are concerned with the determination of temperature at interior points of a region when the initial and boundary conditions, thermo physical properties and heat generation are specified. The inverse heat conduction problem involves the determination of the surface conditions, energy generation and thermal properties from the knowledge of the temperature measurements taken within the body. For the multi-dimensional inverse problems with regular coordinates, i.e. the rectangular, cylindrical and spherical coordinates, the multi-dimensional inverse problems with irregular shape is very limited in the literature. There are various methods in solving the direct problem having irregular domain. For instance, the finite element method using mesh generation and the finite difference method using grid generation are irregular.

The domain meshes are needed for the two techniques mentioned above, which could affect the solutions of the direct problem, if the meshes are generated differently. The advantage of applying the boundary element method in IHCP lie in that it can be used to handle the irregular geometry problem without mesh generation within the domain under some conditions. For this reason, the BEM is most recommended to calculate the direct problem with irregular shape in the inverse calculations. Both BEM and conventional Regularization Method can be applied to two-dimensional IHCP for estimating boundary conditions in both steady-state and transient heat conduction problems. The sensors are placed far away from the boundary having unknown conditions or the measurement errors, thus the ill-posed phenomena of the inverse solutions can be improved by using the regularization method. The inverse solutions for two transient heat conduction problems with different geometry and boundary conditions will be illustrated to show the validity of using the CGM in the present inverse problem. They considered several test cases involving different measurement errors and domain shape. The results show that the inverse solutions obtained by CGM remain stable.

Guosm *et al.* (1998) studied the best combined heat transfer coefficient and effectiveness data currently available for a fully cooled, three-dimensional nozzle guide vanes (NGVs) at engine conditions. Thin-film technology is used to measure the heat transfer coefficient and cooling effectiveness over heavily film cooled nozzle guide vanes (NGVs). The measurements were performed in a transonic annular cascade which has a wide operating range that simulates the flow in the gas turbine jet engine. The aerodynamic and thermodynamic characteristics of the coolant flow are modeled to represent engine conditions by using a foreign gas mixture of SF6 and Argon. Engine-level values of heat transfer

coefficient and cooling effectiveness have been obtained by correcting the different molecular (thermal) properties of the gases used in the engine-simulated experiments to those which exist in the true engine environment.

The efficiency and specific thrust of gas turbine engines increase with higher gas temperature after combustion and typical modern aero engines experience turbine entry temperatures of up to 1700K. In practice, there are no metals for turbine components that can withstand uncooled operation at these elevated gas temperatures. At such temperatures the turbine blade must be safeguarded against the hot gases and film cooling is one of the major methods employed. Cooling technology involves the use of relatively cool air which is taken from the compressor exit and bypasses the combustion process to cool the vanes through the rows of discrete cooling holes.

Lisa *et al.* (2001) developed a thin film sensor that provides accurate surface temperature, strain, and heat flux measurements. Test environments included both air-breathing and space propulsion-based engine and burner rig environments at surface temperatures up to 1100°C and under high gas flow and pressure conditions. This is achieved by integrating a heat flux gauge into a single multifunctional gauge for simultaneous real time measurement of surface temperature, strain, and heat flux sensors and multifunctional gauge. In addition, the material systems are demonstrated along with the sensors. Finally, the results of the current effort will be provided to demonstrate the capabilities of the multifunctional gauge.

Thin film sensors provide minimally intrusive means of measuring surface parameters in engine systems such as temperature, strain and heat flux. These are needed to evaluate the advanced materials and components to provide experimental verification of computational models. The advantage of the thin film heat flux gauge over conventional gauges is its capability to measure steady as well as excellent transient response. The technologies developed for the thermocouple, strain gauge and heat flux sensors are being integrated into a single multifunctional gauge for the simultaneous real-time measurement of surface temperature, strain and heat flux.

Kim and Oh (2001) developed an inverse heat formulation using a two dimensional finite element method as a tool to evaluate heat transfer coefficient during heat treatment process. The formulation has a function to provide a time profile of heat transfer coefficient on various surface locations with measured temperature at proper locations within work piece under heat treatment. By that formulation heat transfer coefficients can be evaluated for fan

and water cooling of solid cylindrical carbon steel specimens. Comparison of the obtained heat transfer coefficients against the existing results were found in reasonable accuracy.

Chantasiriwan (2002) proposed an experimental setup for the inverse determination of steady-state heat transfer coefficient in a two-dimensional system. Instead measuring the of heat flux at the surface, where heat transfer coefficient is to be determined, the experiment can also be designed in such a way that temperature measurements can be taken at locations where sensors can be conveniently placed and would not disturb the fluid flow field. The mathematical model of the system is solved numerically by using the boundary element method. It was shown that, due to the uncertainty in the temperature measurement, the estimated heat transfer coefficient also contains uncertainty. This can be reduced by varying experimental parameters. However, by prudent experimental design, the uncertainty in the estimated heat transfer coefficient may be reduced.

Abderrahmane *et al.* (2004) developed analytical and numerical solutions for fast transient conduction in an infinite plate, subject to sudden and violent thermal effects on its surface. These data were found useful for the optimization of numerical codes in fluid mechanics, in association with the heat transfer and the inverse methods for the determination of thermal characteristics of the surface phenomena in various cases. These diagrams belong to specific ranges of F_0 and B_i (Fourier and Biot numbers) numbers corresponding to the fast transient problems characterized by the low Fourier numbers. As well those diagrams constitute a substantial improvement of the well known Heislers charts. It overcomes the problem of very slow convergence. The main difficulty was encountered for solving characteristic equations based on a combination of the parameters involved in the particular equations of temperature and energy. The results were successfully compared to those based on a different calculation procedure. Distribution and evolution of the temperature in an infinite plate is also studied. The initial distribution of temperature in the plate was a function f(x), symmetrical with respect to the median plane of the plate (x=0). After studying the general case, a plate is treated initially at uniform temperature (T_0) and thereafter suddenly submitted to an environment with a constant temperature (T_e) associated to a finite value of a surface conductance (h). The thermal conductivity (k) of the body and the conductance h are considered as constant all along the thermal phenomena. The proposed diagrams turn out to be an appropriate and easy tool to solve numerous industrial problems. These diagrams can be used in the automotive and aeronautic industries to study the heat generated during the braking. The results seem to be optimized for numerical codes that deal with coupled

problems of fluid mechanics and heat transfer. This is especially useful to set space and time increments in modeling problems.

Alifanov and Golub (2003) derived the solution of the transient heat conduction equation of two axially bounded heterogeneous cylinders. They considered the temperature and heat flux to be continuous at the junction. They evaluated the temperature distribution using the finite Hankel and the Laplace transform.

Piotr *et al.* (2003) used two methods: space marching method and finite element method. The space marching method was used to solve inverse multidimensional heat conduction problems. This method was designed to reconstruct the transient temperature distribution in a whole construction element based on measured temperatures taken at selected points on the outer surface of the construction element. The finite element method was used to calculate thermal stresses and stresses caused by other loads. The developed method for solving temperature and total stress distribution was tested using the measured temperatures generated from a direct solution. Transient temperature and total stress distributions obtained from the method presented below were compared with the values obtained from the direct solution.

The present method can be applied to monitor the systems that work in inverse methods which are widely applied in practice. These methods are useful to reconstruct the heat transfer distribution based on temperature measurements taken at chosen points on the construction element. Simple algorithms based on the finite difference method can only be applied to solve one-dimensional inverse problems that occur in simply shaped bodies. The algorithms used for inverse problems in two dimensions were recently solved. The solution of an inverse problem in complex-shaped bodies is possible by using finite element control volume method.

The space marching method can calculate temperature and stress distributions on the basis of temperature measurements, which can sometimes be taken on an outer, more easily accessible surface. This method can extend the life of power boiler components by improving the power boiler operation. Due to the implementation of the finite element control volume method, the space marching method can be applied to complex shaped bodies with the temperature dependent thermo physical properties. This method is also stable in terms of measurement data, which often becomes disturbed by measurement errors.

Alzaharnah *et al.* (2004) conducted a study to analyze the solid and liquid together by simulating the conjugate heat transfer in a pipe. When formulating the problem, the flow was

assumed to be fully developed and the uniform heat input through the external surface of the pipe. Control volume approach was used to solve the governing equations numerically. The study was extended to include the effect of the diameter to length (L/D) ratio of the pipe.

Mahulikar (2005) investigated the calculation of convective coefficients and heat fluxes analytically, caused by aerodynamic heating on critical surface of hypersonic vehicle. The recovery temperature for stagnation region, convective coefficient for the bi-curvature forward stagnation region was obtained directly from two dimensional stagnation region correlations, using the two principal radii of curvatures. Convective heat flux to swept-back leading edge (SBLE) surface was obtained from two dimensional stagnation region and flat plate heat fluxes, using the respective velocity vector components. These results expose the concepts of temperature-minimized-sweepback, and the thermally-benign sharp SBLE effect at high sweepback angles.

Kim *et al.* (2007) applied maximum entropy method (MEM) to estimate the surface temperature from the temperature measurement. In this work, a typical IHCP in one-dimensional slab with a finite thickness was considered. The unknown temperature of interest was estimated on one boundary. At the same time, temperature readings were acquired on the other boundary which was thermally insulated. The inverse heat conduction problem was reformulated for MEM and a three-phase solution method utilizing the successive quadratic programming (SQP) was proposed. The inverse estimation was remarkably improved by MEM for a rectangular profile compared with the result by CGM. In this study, the total sum was calculated using both the quadratic regularization (QR) by the constrained optimization and the conventional conjugate gradient method. Computational results by the proposed MEM were presented and compared with the results obtained from conventional methods. By comparing the results of these two methods, the QR calculates the total sum more accurately. Consequently, the accuracy of the MEM estimation near the final time had been improved.

Ming-I *et al.* (2008) employed the differential quadrature method (DQM) for inverse determination of thermal conductivity in one-dimensional slab. This approach does not require a priori assumption on the functional form of the estimates and the estimated thermal conductivity can also be obtained directly in the calculation process. Of interest were the effects of the number of the measurement points and magnitude of the measurement errors on the accuracy of the estimations. The estimated thermal conductivities and exact forms were compared and found to comply with each other. Some examples including spatially dependent and temperature dependent thermal conductivities were solved to illustrate the

accuracy and efficiency of the DQM. Numerical results demonstrated that the DQM is effective and stable in treating this type of problem.

Radu *et al*. (2008) developed the analytical solution for the elastic thermal stress in a long hollow cylinder under sinusoidal transient thermal loading. They also used finite Hankel transformation to obtain the solution. They assumed that the cylinder is in plane strain condition and it is made of homogeneous isotropic material. It was assumed that the thermo-mechanical properties do not change during a thermal transient and that the strain rates due to the thermal loading are small. They used the properties of Bessel functions to get the complete solution for associated thermal stress components for simple boundary conditions. They implemented the numerical solution and compared with the FEA results performed with commercial software (ABAQUS)

1.3 Literature Review on Numerical Heat Transfer Studies

The trend in computational mechanics is to adopt coupled-field analysis to obtain computational models which attempt to better mimic the physics under consideration. These CFD simulations are generally carried out with adiabatic or isothermal wall boundary conditions which are inherently very rigid. However in reality, it is very difficult to have prior knowledge of exact boundary details. Apart from this, conventional heat transfer analysis for the fluid domain has rigid assumptions of constant and uniform heat flux or temperature at the wall or at the fluid-solid interface. This interface heat flux or temperature, in general, is not always constant or uniform but it depends on convective properties of flow and conductive properties of fluid and solid. Hence the energy equation for solid and fluid domains must be solved simultaneously with the continuity and momentum equations for fluid domain alone. This physical interaction between the conductive heat transfer in the solid and the convective heat transfer in the fluid is referred to as conjugate heat transfer (CHT) analysis which has been successfully used for designing various engineering objects such as automotive engine blocks, fuel injectors, cooling of turbine blades/vanes, solar equipments, nuclear reactors, heat exchangers etc.

Various CHT investigations are reported in open literature for diverse scientific and technological advances. Mark and Patankar (1985) carried out CHT analysis for electronic equipments by considering infinite viscosity in the solid domain. Kaminski (1986) also reported results of CHT analysis to study the effect of conduction in natural convection flow over one of the vertical walls in a square enclosure. Apart from these, wide ranges of

applications are covered in the incompressible range for heat transfer analysis in solid and fluid domain simultaneously. The laminar flow in a circular tube (Nakayama *et al.* 1996) , forced convection (Hwang,1998), flow over wall based heat source (Chiu et al. 2001), channel flow (Qinghua et al. 2004), solidification process in casting (Amin and Gawas, 2003), fluid flow in a backward facing step (Kanna and Das, 2004) etc. are the reported applications of CHT studies.

Ramesh et al. (1994) conducted investigation on the heat transfer, from a uniformly powered strip source of heat that is located on the surface of a two-dimensional conducting substrate. The upper and lower surfaces of the substrate were cooled by forced laminar flow that is two-dimensional, steady, and with constant properties. The problem is a paradigm for the investigation of the competing effects of substrate conduction and fluid convection in the cooling of electronic components, i.e. chips or chip carriers on boards or substrates that are cooled by air flowing parallel to the surface. The objectives of the study were to investigate the conjugate heat transfer mechanisms in great detail and in a precise way, such as to use the results as a baseline for succeeding more complex situations of air-cooling of component on board situations. In these studies, a fully-developed laminar parallel planes channel flow was considered.

Divo and Kassab (2006) investigated the flow in a channel with a square step conduction obstruction problem using an effective domain decomposition mesh less methodology for the conjugate heat transfer problems. The proposed algorithm was modeled by convecting fully inverse viscous incompressible fluid interacting with the conducting solids. The messless formulation for fluid flow modeling was based on a radial basis function interpolation using hardy inverse multi quadrics and a time-progression decoupling of the equations using a Helmholtz potential. The decomposition approach effectively reduces the conditioning numbers of the resulting algebraic systems. The mess less solutions compared with finite volume methods, showed good agreement.

He et al. (1995[a,b]) adopted the BEM/FVM approach in further studies of CHT in incompressible flow in ducts subjected to constant wall temperature and constant heat flux boundary conditions.

These investigations were mainly centered on subsonic or incompressible flows. However, CHT analysis is still underutilized in the field of hypersonic or hypervelocity flows where high heat transfer rate is the major concern for the flight vehicle design. Very few

researchers have attempted CHT analysis in the compressible flow regime for supersonic or hypersonic applications.

Wetting et al. (1991) studied hypersonic vehicles operated in a hostile aero thermal environment which has a significant impact on their aerothermostructural performance. Significant coupling was observed between the aerodynamic flow fields, structural heat transfer, structural response and creating a multidisciplinary interaction. Interfacing state-of-the-an disciplinary analysis methods was found to be inefficient. Hence, inter-disciplinaty methods integrated into a single aerothermostructural analyzer were needed. The NASA (Wieting et al., 1988) Langley Research Center is developing such methods in an analyzer called Langley Integrated Fluid-Thermal-Structural (LIFTS), an acronym for Langley Integrated Fluid-Thermal-Structural analyzer. The evolution and status of LIFTS was reviewed and illustrated through applications.

Kontinos(1997) used BEM/FVM coupling algorithm to solve the conjugate heat transfer over the metallic thermal protection panels at the leading edge of the X-33 in the Mach 15 hypersonic flow. Xia and Spel (1997) carried out the topology-based algebraic grid generator used in the examples presented in TIL (Topology Input language) which allowed the multi-grid option. Several levels of coarse discretization can thus be readily obtained. Furthermore, the BEM/FVM method offers the additional advantage of providing heat flux values and it stems from the fact that nodal unknowns which appear in the BEM are the surface temperatures and heat fluxes. Consequently, solid/fluid interfacial heat fluxes which are required to enforce continuity in CHT problems are naturally provided by the BEM (Boundary Element Method) conduction analysis. This is in sharp contrast to domain meshing methods such as FVM and FEM where heat fluxes are computed by numerical differentiation in a post-processing stage.

Hassan et al. (1998) presented an iterative loose coupling between a FVM computational fluid dynamics code and a finite element material thermal response code and used it to study the ablation of a re-entry vehicle flying through a ballistic trajectory.

Ye et al. (1998), developed a BEM-based CHT algorithm, thereby avoiding meshing of the solid region for the conduction solution. The method coupled the boundary element method (BEM) to a FVM Navier-Stokes solver and was applied to solve two-dimensional steady state compressible subsonic CHT problems over cooled and uncooled turbine blades. The conduction problem required solution of the Laplace equation for the temperature (or the Kirchhoff transform in the case of temperature dependent conductivity), and, as such, that

required a boundary discretization thereby eliminating the onerous task of grid generation within intricate regions of the solid. The boundary discretization utilized to generate the computational grid for the external flow-field can be considerably coarsened to provide the discretization required for the boundary element method.

Rahaim et al. (1997) and Rahaim and Kassab (2000) adopted a BEM/FVM strategy to solve time- accurate CHT problems for supersonic compressible flow over a 2-D wedge. They presented experimental validation of this CHT solver. In their studies, the dual reciprocity BEM was used for transient heat conduction, while a cell-centered FVM was chosen to resolve the compressible turbulent Navier-Stokes equations. Blobner et al. (2000) used the CHT analysis of solid domain heat transfer studies in boundary element method (BEM), for the thermal shock problem achieved by a pure boundary domain integral formulation and this paper solved the conjugate natural convection in a cavity with conducting side wall.

Wang (2000) investigated three-dimensional conjugate heat transfer analyses for the manifold located upstream of the ramjet fuel injector. Using CF design, the flow field of the hot fuel flowing through the manifold was simulated and the wall temperature was computed. Numerical results of the fuel temperature are compared with one-dimensional analysis based on empirical equations, which showed good agreement. The numerical results revealed that the fuel temperature has dropped about $3^{o}C$ from the inlet to the exit of the manifold and it takes 30-40 s to reach equilibrium.

Dowell and Hall (2001) carried out coupled field solution that require complete meshing of both fluid and solid regions while enforcing solid/fluid interface continuity of fluxes and temperatures. Kassab and Aliabadi (2001) addressed the conjugate heat transfer study i.e.: the coupling of convective heat transfer external to the solid body of a thermal component coupled to conduction heat transfer within the solid body of that component.

Divo et al. (2002) developed BEM-based temperature forward / flux back (TFFB) coupling algorithm for conjugate heat transfer analysis. Heat conduction within the structure was coupled to heat transfer to external flow. There were two different approaches used in CHT technique i.e. direct coupling and loosely coupling. The fluid flow studies were used in Finite volume method (FVM). The loosely coupled CHT strategy was particularly attractive when coupling auxiliary field equations to computational fluid dynamics codes.

Heidmann et al. (2002) carried out separate flow and heat conduction analyses. The in heat transfer coefficient as well as film effectiveness values were predicted using two independent external flow solutions each computed by imposing a different constant wall temperature at the surfaces of the turbine blade exposed to hot gases and film cooling air. The film effectiveness determines the reference temperature for the computed film coefficients. In turn, these values are used to impose convective boundary conditions to a conduction solver to obtain the metal temperatures. The shortcomings of this approach neglect the effects of the wall temperature distribution on the development of the thermal boundary layer. They are readily overcome by a CHT analysis in which the coupled nature of the field problem is explicitly taken into account in the analysis.

Liu et al. (2005) developed numerical schemes for tightly coupling fluid and solid solver through the constant computation of the heat flux at the fluid-solid interface. Madhusudhan et al. (2007) studied the conceptual design, thermal response and thermo-structural analyses for the control surface (elevon) of a wing-body hypersonic vehicle. Convective heating rates on elevon were computed using semi-empirical methods. Based on the heat flux levels and pressure loads, a multi-layered design with carbon-carbon and inconel was chosen for elevon. Thicknesses of the layers were sized using one-dimensional transient thermal analysis. The adequacy of the design was checked by detailed thermal and structural analyses. Thermal response analysis showed that maximum temperature in carbon-carbon outer shell is 1597 K and temperatures of all other materials are within the limits. Thermo-structural analysis was carried out at seven critical flight conditions and the results show that the stresses in all the components are below the specified limits.

Duchaine et al. (2009) studied coupling strategy of a Large Eddy Simulation (LES) solver and a heat transfer code within solids on parallel architectures. The numerical methods used in the solvers were explained and then coupling strategy in terms of physical quantities to exchange (fluxes and temperature), stability and parallel efficiency are discussed. The coupled strategy applied to a cooled turbine blade model where results demonstrated both the efficiency of the parallel implementation and the quality of the results. Coupled and non-coupled simulation were compared to experimental results and discussed in terms of cooling efficiency and flow structures.

Xiaoli et al. (2010) introduced a new flow-thermal-structural coupling approach based on coupled heat transfer simulation for a hypersonic aerodynamically heated leading edge. These studies were carried out for Mach number 6.47 flow over a cylinder for which the

flow behavior and aero-thermal loads are calibrated by experimental data and the numerical results of the surface pressure, cold wall heating rate, hot wall heating rate and temperature distributions were all well consistent with experimental data.

Saha et al. (2012) numerically studied the base flow of a long range flight vehicle and presented for different flight conditions. In this study, the Navier-stokes equations are solved along with $k-\varepsilon$ turbulence model using the CFD software. These studies captured all essential flow features including flow separation at base shoulder, shear layer formation at the jet boundary, recirculation at the base region. With increase in altitude, the plume of the rocket exhaust was seen to bulge more, causing more intense free stream and rocket plume interaction leading to higher gas temperature in the base cavity. The flow field in the base cavity was investigated in more detail, which is found to be fairly uniform at different instant of time. Presence of the heat shield is seen to reduce the hot gas entry to the cavity region due to different recirculation pattern in the base region. Computed temperature history obtained from conjugate heat transfer analysis was found to compare very well with flight measurement data.

Nikas and Panagiotou (2013) investigated a numerical simulation of the conjugate heat transfer effects inside a computer chassis which is cooled by fans forcing heat convection. The temperature distribution on the heat sources and the air path lines were investigated in order to get a clear picture about the case that fully satisfies the operating conditions. The simulation was conducted by the commercial CFD software. The solution was based on the Navier-Stokes equations applying into a three dimensional model. The turbulence model used in these studies was well validated by corresponding experimental data consisting mainly of velocity profiles and temperature distribution provided in the open literature review.

Murthy et al. (2013), carried out CHT studies in an axi-symmetric double cone at Mach number 4.57 and turbulent flow past circular cylinder at Mach number 6.7 to, predict the interface temperature distribution and cold wall heat flux distribution along the surface of the solid. The results were in well agreement with the experimental results.

In line with the present literature, investigations are planned to extend the applicability of CHT analysis for high Mach number flows using the well established computational techniques

1.4 Motivation for PhD Work

Prediction of aerodynamic heating is an extremely important aspect in the design of hypersonic vehicle. Understanding and accurate estimation of surface heat flux is a vital part in the design phase. Conversion of kinetic energy of high-speed hypersonic flow into heat energy in the thin shock layer is the major reason for higher convective heating rates. Therefore, knowledge of convective heating rates becomes essential for designing the thermal protection system for launch vehicles or re-entry space-crafts. This information can be obtained from experimental measurements, flight tests or through computational simulations. Over the past five decades, there has been intensive research and development in the experimental and computational hypersonic aerodynamics towards prediction of surface properties. These efforts have resulted in the development of sophisticated high enthalpy wind tunnels, shock tunnels and Computational Fluid Dynamics (CFD) methods.

The convective heat transfer measurement experiments are generally carried out through flight tests or in short duration impulse facilities, such as hypersonic shock tunnels, using thin film gauges. Some researchers proposed heat-conduction models based on thin-film or thick film concept [Schultz and Jones (1973), Taler (1996), Sahoo, (2003), Kulkarni *et al.* (2008) and Bertolazzi et al. (2012)]. Some of the methodologies or formulations for the heat conduction problem are based on Hermite approximation method (Narayanan and Zabaras, 2004), perturbation method (Sadat, 2006), Hankel transform technique (Hui and Tan, 2006) and inverse methods [Walker and Scott (1998), Walker et al. (2000), Liu et al. (2010)]. One of the simplest methods, used in short-duration transient measurements (~1ms) is to construct the temperature time history using piecewise linear function and subsequently use it for one-dimensional semi-infinite heat conduction modeling (Cook and Felderman, 1996). When, the experimental time duration of measurement is more, the semi-infinite assumption does not hold good. So, the concept of thin film and thick-walled gauge has been introduced in the literatures (Taler, 1996[a]). In these techniques, experimentally measured transient temperatures data are fitted using polynomial and cubic-spline techniques. Subsequently, temperature histories, obtained from above methods are used for prediction of surface heat fluxes. With developments in computational tools, other techniques such as,

inverse analysis using control volume heat balance (Sahoo and Peetala, 2011), inverse finite-element analysis [Bertolazzi et al. (2012), Reza and Ahmad (2008)] and genetic algorithm (Liu, 2008), have been reported in the literatures for prediction of surface heat flux. Analytical one-dimensional heat transfer models are used for evaluating the surface heating rates from the recorded temperature history using thermal sensors. However these techniques are based on fitting the experimentally obtained temperature signal. Therefore, efforts need to be extended to access the effectiveness of these methodologies. Such studies are essential to compare the performance of all the techniques in recovering heat flux in a given situation which in turn would be helpful to arrive at the 'efficient method' among the existing ones.

Computational fluid dynamics has been used for simulating hypersonic flow around objects of interest to predict aerodynamic heating. Such CFD simulations are invariantly carried out assuming the wall to be adiabatic or isothermal. These extreme assumptions make it very difficult to estimate all the boundary details. Moreover, either wall temperature or heat flux is obtainable from such computational simulations. Thus, it is not possible to estimate both, temperature and heat flux, simultaneously. Therefore, it is extremely essential to develop a conjugate heat transfer solver to overcome this drawback of conventional CFD methodology and also the limitations involved in post-processing the experimental data. Such computational strategy can provide the wall temperature and heat flux simultaneously which is essential in many engineering applications. Conjugate heat transfer analysis has been routinely used by various researchers in the subsonic or incompressible flow situations. However, limited numbers of findings are reported in the literature which relate to hypersonic flow regime. Therefore development of a CHT solver for hypersonic application is extremely essential due to its immense advantages over conventional CFD methodology. Moreover, establishment of a CHT framework demands for development of a compressible flow solver for fluid domain and conduction solver for solid domain. Further, these solvers need to be validated and verified individually. Apart from this, a CHT solver should have provision of various couplings between fluid flow solver and conduction solver. In the simpler manner, two solvers can be executed serially in the decoupled form. However, strong and loose coupling techniques are generally exercised to device the CHT algorithm. Thus, possibility of CHT simulation with either of three methods provides flexibility in the solver. In light of this, it is very much apparent to evaluate the applicability of assumptions involved in reducing the experimental data for a hypersonic situation.

The CHT methodology is very much beneficial to design the heat transfer measurement experiment in hypersonic impulse facility. The measured temperature signals would be useful for selecting the thermal sensor, possible mounting location of the sensor, data acquisition settings and heat transfer recovery technique. In view of this, an explanatory simulation for the hypersonic flow over a finite thickness flat plate can demonstrate the heat transfer measurement experiment. The temperature signals can be conveniently used to carry out the performance assessment of various heat transfer recovery techniques by comparing the recovered heat flux signal with the one obtained from CHT simulation.

Simultaneous prediction of wall temperature and heat flux is the major advantage of CHT based analysis. As an initial guess, decoupled CHT technique can be implemented. Moreover, comparison among the coupling techniques for analyzing a particular hypersonic flow situation is highly desirable to arrive at a cost effective computational technique. Such investigations are very limited in the open literature. The test case of hypersonic flow over a finite thickness circular cylinder can be considered to compare the effectiveness of available coupling techniques.

It has been noticed that, the CHT analysis has not been explored exhaustively for hypersonic applications. The limited numbers of findings which concentrate in this speed regime use homogeneous material for fluid flow and heat transfer analysis. However, application of a composite material in real hypersonic flights demands to test such configuration to demonstrate the capability of the CHT solver. Such studies are also useful to analyze the solid-fluid and solid-solid interface properties in the presence of hypersonic flow. Philosophy of thermal protection system design can also be built through such simulations.

Shock wave boundary layer interaction (SWBLI) is most widely studied research topic in supersonic and hypersonic flows. However most of these investigations are carried out using conventional wall boundary conditions viz. isothermal and adiabatic. But, change in wall temperature with time due to finite thermal diffusivity of the wall material leads to change in interaction dynamics. Therefore, separation and interaction studies related to SWBLI should be explored using a CHT solver. Exposure of the solver to such problems would as well test its applicability in practical situations and in turn helps to widen its range of application.

1.5 Objective of the Thesis

Implementation of conjugate heat transfer methodology for hypersonic applications is the central theme of present investigations. In the above mentioned fallouts of conventional analytical, numerical and experimental methodologies, following objectives are set for the present studies.

- Development of a simpler method for prediction of heat transfer rate is the foremost objective for present studies. Comparative assessment of this technique along with the literature reported heat flux recovery techniques is planned using the temperature signals obtained from numerical simulations, shock tunnel testing and flight testing. Performance evaluation of all the methods to arrive at the robust or suitable technique is the central theme of these investigations.
- Development of a two dimensional conjugate heat transfer analysis solver is one of the thrust area of present research. This objective demands for the development of a two dimensional fluid flow solver and two dimensional conduction solver. Logical extension of this development is the validation of these individual solvers.
- Provision of loose and strong coupling methodologies completes the development of CHT solver.
- Numerical simulation of heat transfer measurement experiment on a finite thickness flat plate in a conventional shock tunnel is planned using the in-house solver. Evaluation of the heat transfer prediction techniques using the simulation based temperature signals in comparison with the heat transfer rates obtained from CHT solver can also be achieved here. Effect of wall heating on the thermal and hydrodynamic boundary layers is also planned during these studies.
- Comparative study for computational cost in simulating the hypersonic flow over finite thickness cylinder using various coupling techniques is set to define a computationally cheaper CHT algorithm. This study can be extended to analysis the effect of simulation time on interface heat flux and thus on the fluid domain.
- Hypersonic flow over finite thickness composite flat plate and composite cylinder are planned to understand the effect of change in wall material in the streamwise direction on the interface properties. Capability of present solver with multiple interfaces (solid-solid and fluid-solid) will also be evaluated.
- Finally in-house CHT solver will be employed to understand the effect of wall material on the shock wave boundary layer interaction.

1.6 Organization of the Thesis

Mathematical details of one-dimensional heat conduction equation for recovery of heat transfer rate in relation to Laplace based technique, Schultz and Jones method, Duhamel's integral methods [Schultz and Jones (1973), Taler (1996[a]), Sahoo and Peetala, (2010)] are disused in **chapter-2.** This chapter also deals with the comparative assessment of noted techniques using know temperature signals from various sources. **Chapter 3** deals with governing equations and numerical formulations for the compressible viscous fluid flow solver and heat conduction solver in finite volume formulation. Various coupling techniques in relation with development of in-house development of CHT solver is the subject of discussion of **Chapter-4**. Conjugate heat transfer analysis for hypersonic flow over finite thickness flat plate and associated effects on fluid domain are covered in **Chapter-5.** The cost effectiveness of various coupling techniques for cylindrical configurations is central theme of **Chapter-6** which cylindrical configuration. The conjugate heat transfer analysis for hypersonic flow over composite plate and cylinder are discussed in **Chapter-7**. Shock wave boundary layer interaction and effect of wall material on the interaction dynamics is the subject of **Chapter-8.** Finally the overall conclusion and the scope for future work are mentioned in **Chapter-9**.

CHAPTER 2

PREDICTION OF TRANSIENT HEAT FLUX USING VARIOUS ANALYTICAL TECHNIQUES

2.1 Preface

Transient heat transfer is one of the important phenomena in the design of many high performance engineering systems or sub-systems. Design of a proper cooling system for electronic equipments, transpiration cooling technique for gas and steam turbine blades, thermal protection system for missiles and space vehicles are few application areas where the transient heat transfer plays a vital role. Normally, the transient temperature histories are obtained by using suitable sensors. Thin film platinum sensors or thermocouples are the most widely used sensors for such applications. A typical thin film sensor has a sensing material film painted or sputtered on an insulating backing material. Platinum and nickel are widely accepted sensing materials while Macor (Machinable Ceramic) and quartz are the routinely used backing materials. Current of constant magnitude is passed through the sensing material during the experiment in which it is exposed to the fluid flow. Frictional heating of the film changes its resistance which in turn changes the voltage output. Thus recorded voltage corresponds to change in temperature in accordance with the temperature coefficient of resistance of the film material. This temperature time history is then post processed using one dimensional heat conduction equation for prediction of surface heat transfer rate. The major assumptions involved in this inverse process are the semi-infinite depth of the backing material, uni-directional flow of heat and smaller experimental duration (of the order 1ms).

This chapter describes the mathematical details of the techniques related to prediction of transient surface heat flux from temperature signals using one-dimensional heat conduction modeling. The techniques based on spline fitting (linear and cubic) and least square polynomial fitting of temperature data are evaluated for prediction of surface heat flux. Also, presently devised Laplace based technique is considered here to predict surface heat flux where least square polynomial based temperature fitting is incorporated. The temperature time histories obtained from in-house one-dimensional finite volume computation solver, literature reported shock tunnel measurement and supersonic flight experimental temperature data are used to predict the surface heat flux using all the above methods.

Present studies are planned to device a new heat flux recovery technique and to evaluate the effectiveness of widely used techniques to recover the heat flux from the temperature data. Chosen techniques for present investigations include the established ones viz. polynomial fitting [Taler (1996), Sahoo and Peetala (2010)], cubic spline technique [Taler (1996), Sahoo and Peetala (2010)] and linear spline [Cook and Felderman (1966), Sahoo and Peetala (2010)]. Presently devised Laplace based technique is also used for the comparative studies. The flow chart for entire process is shown in Fig. 2.1. Temperature signals obtained from the CFD simulations, ground based experimental testing and flight-testing are used to evaluate the performance of a particular technique to predict the heat flux. Details of the prediction techniques, CFD results and the assessment of heat flux recovery techniques are explained in detail in the following sections.

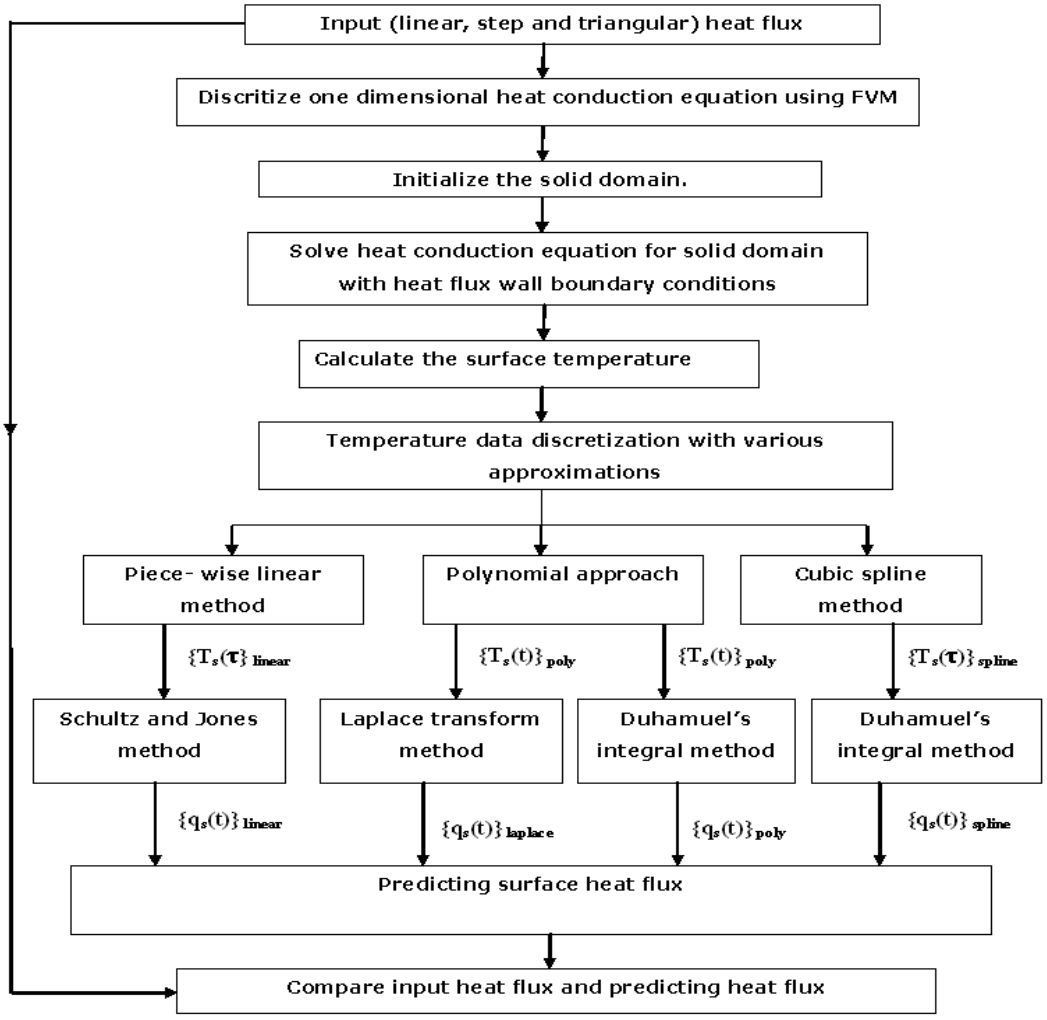

Fig. 2.1: Flow chart showing the methodologies of simulations for different test cases.

2.2 Computational Technique for Surface Temperature Prediction

A finite volume based one-dimensional implicit solver is developed for the heat conduction equation (Veersteeg and Malalasekera, 1995). The typical heat conduction model implemented for a thin film senor by neglecting the sensing material is shown in Fig. 2.2(a).

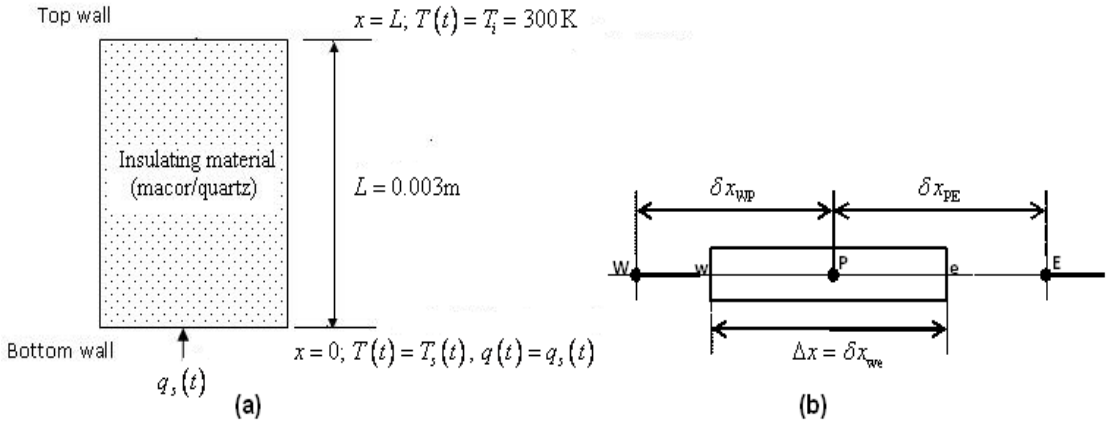

Fig. 2.2: One dimensional modeling of heat conduction equation; (a) schematic representation; (b) finite-control volume formulation.

The governing equation for heat transfer analysis of the one-dimensional unsteady heat conduction equation is given as below;

$$\rho c_p \frac{\partial T}{\partial t} = \frac{\partial}{\partial x}\left(k \frac{\partial T}{\partial x} \right) + s \tag{2.1}$$

Where, ρ, c_p and k are the density, specific heat and thermal conductivity of the material and s is the heat source term. Considering the control volume shown in Fig. 2.2(b), one can integrate Eq.(2.1) over a fixed control volume in the space and with time.

$$\begin{aligned} &\int_t^{t+\Delta t}\int_{cv} \rho c_p \frac{\partial T}{\partial t} dV dt = \int_t^{t+\Delta t}\int_{cv} \frac{\partial}{\partial x}\left(k \frac{\partial T}{\partial x} \right) dV dt + \int_t^{t+\Delta t}\int_{cv} \bar{S} dV dt \\ &\text{or, } \int_W^E \left[\int_t^{t+\Delta t} \rho c_p \frac{\partial T}{\partial t} dt \right] dV = \int_t^{t+\Delta t} \left[\left(kA \frac{\partial T}{\partial x} \right)_E - \left(kA \frac{\partial T}{\partial x} \right)_W \right] dt + \int_t^{t+\Delta t} \bar{S}\, \Delta V dt \end{aligned} \tag{2.2}$$

In the above equation, A and V are the area and the volume, $\bar{S}$ is the source average strength for the elemental finite volume. The temperature at a node is assumed to be same for the entire control volume. Hence, the left hand side of Eq. (2.2) can be written as,

$$\int_{cv} \left[\int_t^{t+\Delta t} \rho c_p \frac{\partial T}{\partial t} dt \right] dV = \rho c_p (T_p - T_p^{\,0}) \Delta V \tag{2.3}$$

Here, the superscript '0' refers to temperature at time t and the temperature without any superscript belongs to next time interval. Finite volume formulation for the term of right hand side Eq. (2.2) leads to,

$$\rho c(T_p - T_p^{\,0})\Delta V = \int_t^{t+\Delta t}\left[\left(k_e A\frac{T_E - T_P}{\partial x_{PE}}\right)_e - \left(k_w A\frac{T_P - T_W}{\partial x_{WP}}\right)_w\right]dt + \int_t^{t+\Delta t}\bar{S}\Delta V dt \tag{2.4}$$

With fully implicit scheme and linearized source term $\bar{S}\Delta x = S_u + S_p T_P^{\,0}$, Eq. (2.4) can be simplified (Veersteeg and Malalasekera, 1995). Referring to Fig. 2.2(b), the final form of equation is given as follows, for a fully implicit scheme ($\theta = 1$) above expression reduces to

$$a_P T_P = a_W T_W + a_E T_E + a_P^{\,0} T_P^{\,0} + S_u \tag{2.5}$$

where, $a_P = a_P^{\,0} + a_W + a_E - S_p, a_P^{\,0} = \rho c\left(\frac{\Delta x}{\Delta t}\right), a_W = \frac{k_w A_w}{\delta x_{WP}}, a_E = \frac{k_e A_e}{\delta x_{PE}}$;

The coefficients of T_W and T_E are taken as a_W and a_E, respectively. The temperature (T_P) at any point 'P' is associated with its corresponding coefficient a_P. Both sides of the Eq. (2.5) contain the temperature at new time step and constitute a system of algebraic equations for the complete computational domain. These equations are solved simultaneously by tri-diagonal matrix algorithm (TDMA) at each level, as mentioned in the reference (Veersteeg and Malalasekera, 1995). The present finite volume based solver bears the capability of composite heat conduction with continuity of heat flux and uniqueness of temperature at the interface. Since, the current investigation deals with short duration measurements, it is expected that thermal conductivity of the material does not vary with time. Hence, constant values of thermal properties of the material are assumed [Sahoo and Peetala (2010), Holman (1989)] and are given in Table 2.1.

Table 2.1: Material properties used in the simulation

Material	Thermal conductivity (k) $(\mathrm{W/m.K})$	Density (ρ) $(\mathrm{kg/m^3})$	Specific heat (c_p) $(\mathrm{J/kg.K})$	Thermal diffusivity $\alpha = k/(\rho c_p)$ $(\mathrm{m^2/s})$
Macor	1.46	2520	790	7.3×10^{-7}
Quartz	1.4	2200	670	9.498×10^{-7}

2.2.1 Surface temperature and heat flux histories for standard cases

First, the surface temperature histories are obtained by one dimensional finite-volume based computational technique for the boundary conditions as shown in Fig. 2.2(a). During the present studies, input heat flux is applied at the bottom wall while the top surface is considered as isothermal wall with initial temperature of 300K. Three different nature of time varying heat loads (Fig. 2.3) are applied at the bottom surface.

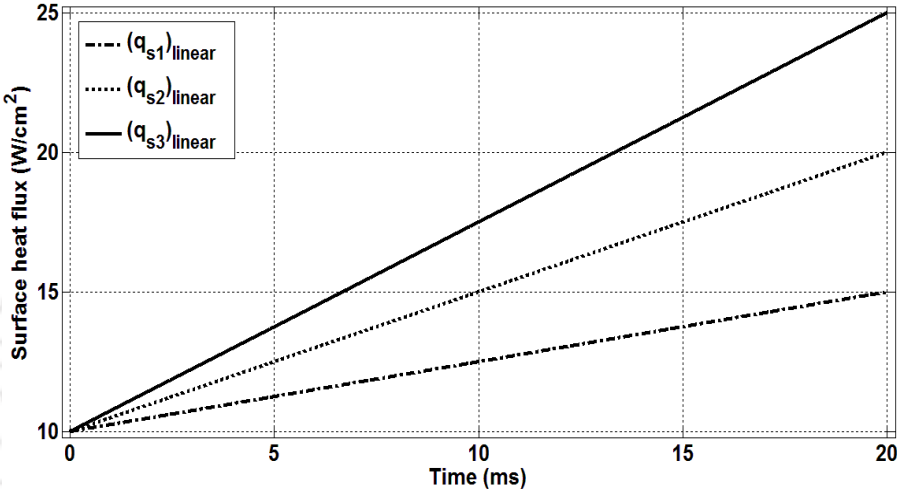

(a)

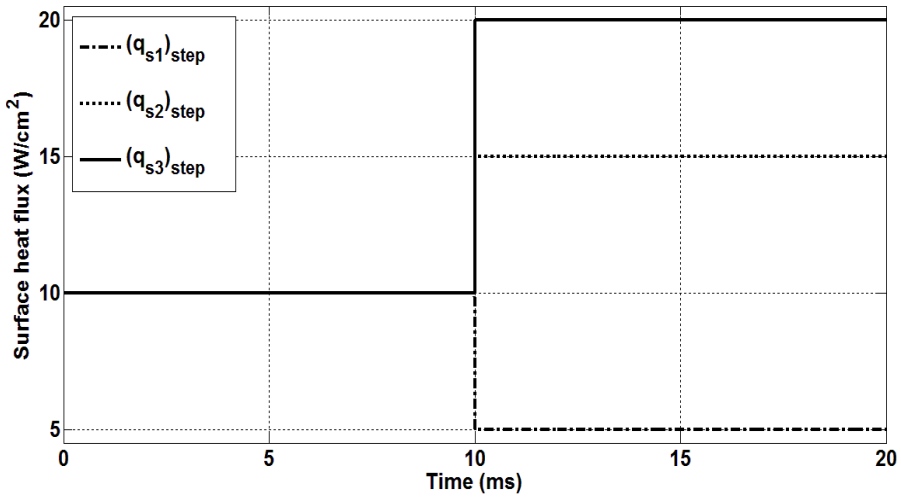

(b)

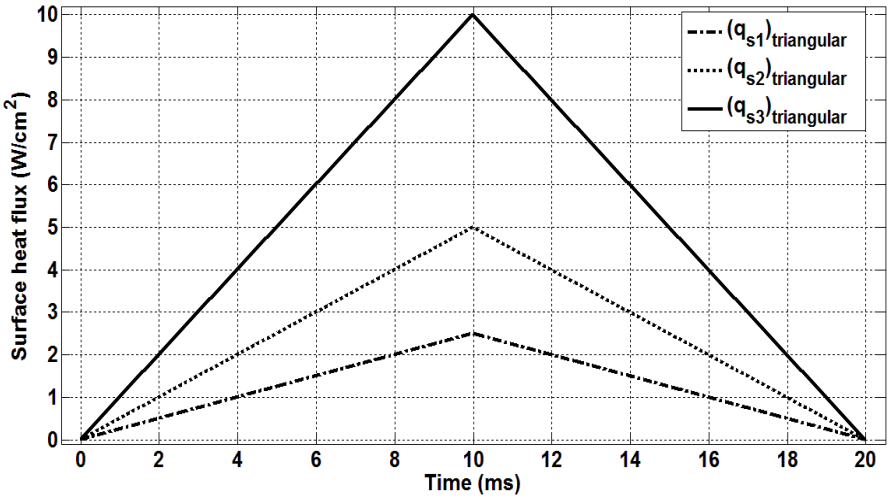

(c)

Fig. 2.3: Time varying applied heat fluxes used in finite-volume method: (a) linear heat fluxes; (b) step heat fluxes; (c) triangular heat fluxes.

It is desired that the heat should not reach the constant temperature boundary end of the substrate during the simulation (i.e. 20ms). Hence, the properties of the surface should be taken as that of an insulator. In the present case, shown in Fig. 2.2(a), Macor is taken as the insulator for which the material properties are given in Table 2.1. The temperature signal for each test case has a special feature. In case of a linear heat loads (Fig. 2.4-a), the rate of temperature rise is seen to be dependent on the rate of change of applied heat flux. The time histories of temperatures for different step heat loads (Fig. 2.4-b) are seen to follow the same trend as that of constant heat flux until the temporal location of the heat flux discontinuity is seen at 10ms. After this step discontinuity, rate of temperature rise is observed to be again dependant on the step height. When there is a sudden decrease in heat flux from 10 W/cm^2 to 5 W/cm^2, the temperature drops momentarily. The possible reason for this phenomenon is the higher rate of heat transfer from the surface by conduction in the solid in comparison with the applied heat flux at the same time which leads to decrease in surface temperature. The trend of temperature time history is seen to be similar for all the triangular heat load cases (Fig. 2.4-c), where temperature time histories are seen to be inflated from lower values of peak heat load to the higher ones. All these, linear, step and triangular time variations of heat flux conditions might represent some non-physical condition. But, they provide perfect test cases to assess the various heat flux recovery techniques from the temperature time histories.

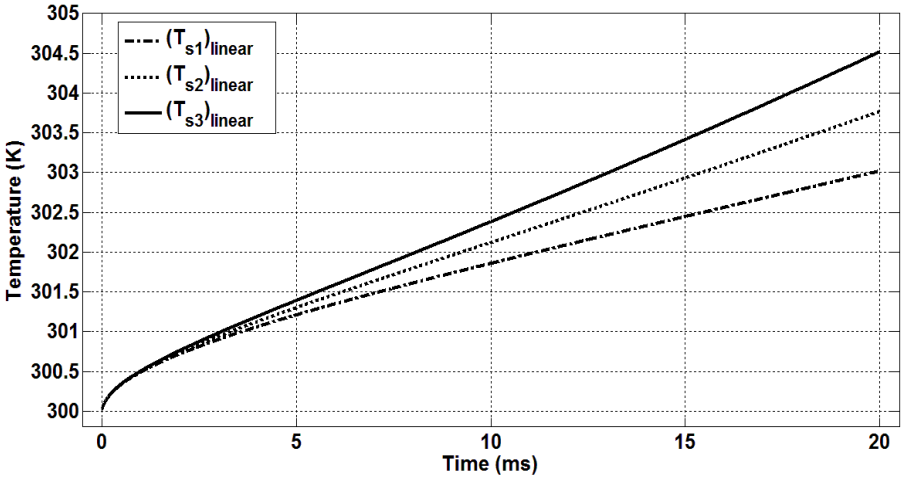

(a)

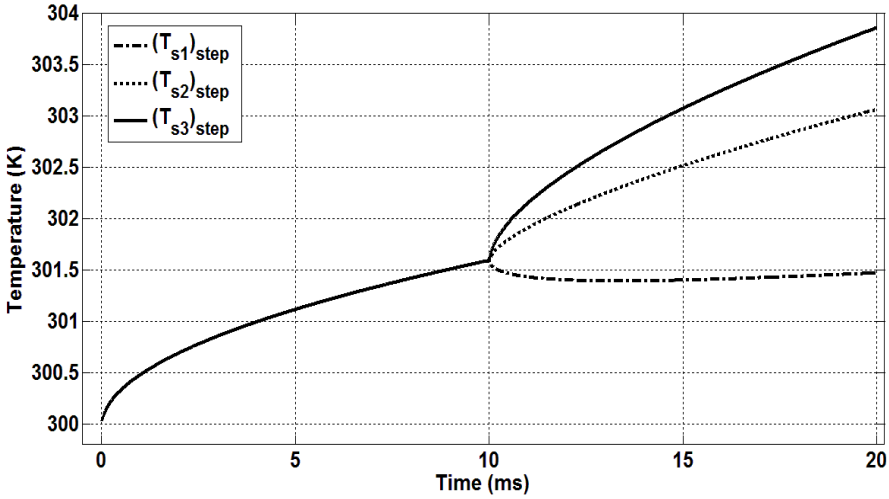

(b)

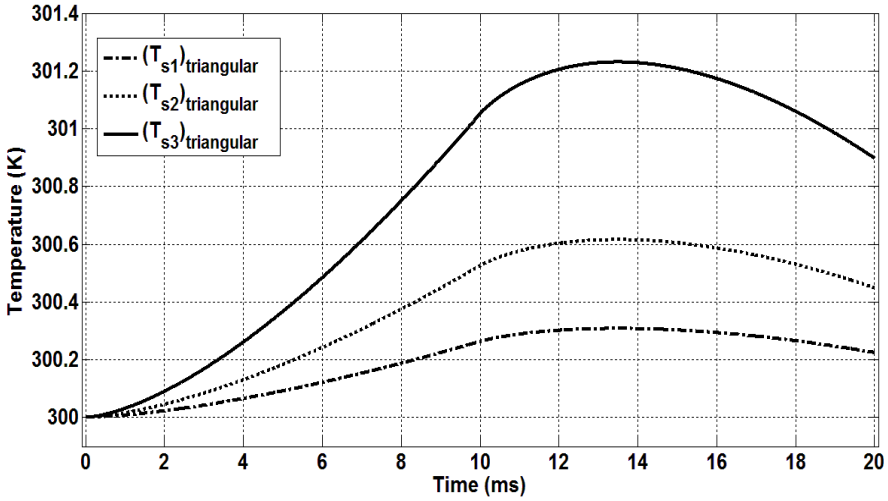

(c)

Fig. 2.4: Surface temperature obtained from finite-volume simulation: (a) linearly varying heat fluxes; (b) step heat fluxes; (c) triangular heat fluxes.

2.3 One-Dimensional Heat Conduction Modeling

Most of the short duration measurements rely on surface temperature histories for prediction of heat flux. They are either measured directly from the temperature sensors or obtained from the flow fields using computational techniques. Subsequently, the surface heat flux is computed by suitable one-dimensional heat conduction modelling involving the concepts such as semi-infinite principle, thin film or thick film gauges (Taler, 1996). In all cases, the basic equation is the one-dimensional unsteady heat conduction equation (Schultz and Jones, 1973) which is,

$$\frac{\partial^2 T}{\partial x^2} = \frac{1}{\alpha}\frac{\partial T}{\partial t} \tag{2.6}$$

Here, $T(t)$ is the measured transient temperature, x is co-ordinate along the depth the substrate and α is thermal diffusivity of the substrate. It may be noted here that the materials of sensing element and surface on which temperature sensor is mounted (substrate), are different. However, during short time duration of measurement, it is assumed that the temperature measured by the sensing element is same as that of substrate surface temperature. Thus, the substrate is considered as of infinite length due to which there will be no temperature change at the far end of the substrate. Moreover, the thermal properties of the substrate material do not change and there is no lateral heat conduction. Initially, the temperature is same at all locations in the substrate. The temperature-time history at the gauge surface and isothermal wall boundary condition at the extreme end of the substrate are the standard boundary conditions. If the surface heat transfer is $\dot{q}_S(t)$ and the corresponding surface temperature is $T_S(t)$ then, the initial and boundary conditions are written as below,

$$\begin{aligned} &T(0,t) = T_s(t) \quad \text{and } \dot{q}_s(t) = -k\left.\frac{\partial\{T_s(t)\}}{\partial x}\right|_{x=0} \\ &T(\infty,t) = T_i \end{aligned} \tag{2.7}$$

The general solution of this type of heat conduction problem is obtained by using Duhamel's superposition integral, given by the following equation (Carslaw and Jaeger, 1959);

$$\dot{q}_s(t) = \sqrt{\frac{\rho c_p k}{\pi}}\int_0^t \frac{1}{\sqrt{(t-\tau)}}\frac{d\{T_s(\tau)\}}{d\tau}d\tau \tag{2.8}$$

2.3.1 Temperature discretization and heat flux predictions.

The most convenient form of predicting the transient heating rates from temperature history is given by the Eq. (2.8). However, there is a singularity in the integral term at $t = \tau$ that introduces errors in heat flux estimation. These errors are large when the experimental time duration is small. In many practical cases, the function $T_s(t)$ cannot be described by simple expression. So, it is necessary to perform numerical integration by discretizing temperature data. There are various methods available in the literature for discretizing the temperature data such as piece-wise linear fitting (Cook and Felderman, 1966), polynomial fitting and cubic-spline methods [Taler (1996), Sahoo and Peetala (2011), Sahoo and Peetala (2010)]. These techniques are used here to obtain the closed form solution of temperature history. Subsequently, transient heat transfer rates are predicted by analytical expressions from Eq. (2.8).

If the surface temperature between successive times is assumed to vary linearly with time, then piece-wise linear function can be assumed for temperature data [Cook and Felderman (1966), Sahoo and Peetala (2010), Sahoo and Peetala (2011)].

$$\{T(t)\}_{\text{linear}} = T(t_{i-1}) + \frac{T(t_i) - T(t_{i-1})}{\Delta t}(\tau - t_{i-1}) \qquad (2.9)$$
$$\text{where, } \tau = t_i = i(t/n) = i\,\Delta t; \quad i = 1, 2, 3, \ldots\ldots\ldots, n$$

Here n is number of temperature data points recorded by the acquisition system during the experiment. The simplified expression for Eq. (2.8) is given as below;

$$\{\dot{q}_s(t)\}_{\text{linear}} = 2\sqrt{\frac{\rho c_p k}{\pi}} \sum_{i=1}^{n} \frac{T(t_i) - T(t_{i-1})}{(t_n - t_i)^{1/2} - (t_n - t_{i-1})^{1/2}} \qquad (2.10)$$

Polynomial regression data fitting technique can also be applied for transient surface temperature response and is given by the expression,

$$\{T(t)\}_{\text{poly}} = A_0 + A_1 t + A_2 t^2 + A_3 t^3 + A_4 t^4 + .. + A_m t^m = \sum_{i=0}^{m} A_i t^i \qquad (2.11)$$

Here m is degree of the polynomial considered for constructing the temperature signal. The corresponding surface heat flux obtained from Eq. (2.8) is given by the following expression [Taler (1996), Sahoo and Peetala (2010), Sahoo and Peetala (2011)]. With regression analysis, the coefficients $A_0, A_1, A_2 \ldots\ldots A_m$ for Eq. (2.11) are obtained.

$$\{\dot{q}_s(t)\}_{\text{poly}} = 2\sqrt{\frac{\rho c_p k}{\pi}} \left(\left[A_1 \sqrt{t} + \sum_{i=2}^{m} i A_i t^{(2i-1)/2} \right] \left[1 + (i-1)! \sum_{n=1}^{i-1} \frac{(-1)^n}{(2n+1) n! (i-1-n)!} \right] \right) \qquad (2.12)$$

The polynomial smoothing of temperature data allows the calculation of high-order derivatives, but may not reproduce real data points, especially when the time spread of the fitted data is large (Taler, 1996). However, it can be avoided by using another smoothing technique based on spline. A third-order spline method is used here to discretize the temperature data.

$$\{T(\tau)\}_{\text{spline}} = a_{1,i} + a_{2,i}(\tau-\tau_i) + \frac{1}{2}a_{3,i}(\tau-\tau_i)^2 + \frac{1}{6}a_{4,i}(\tau-\tau_i)^3 \quad \left(\text{For } \tau_i \le \tau \le \tau_{i+1}, i = 1,2,.....,M\right) \tag{2.13}$$

The constants appearing in this equation can be determined by the following expressions [Taler (1996), Sahoo and Peetala (2011), Sahoo and Peetala (2010)];

$$a_{1,i} = T_2(\tau_i);\;\; a_{2,i} = T_2{}'(\tau_i);\;\; a_{3,i} = T_2{}''(\tau_i);\;\; a_{4,i} = T_2{}'''(\tau_i); \tag{2.14}$$

The surface heat flux is then estimated for $M = 1,2,....(n-1)$ as,

$$\{\dot{q}_s(t)\}_{\text{spline}} = \begin{bmatrix} 2\sqrt{\dfrac{\rho c_p k}{\pi}}\displaystyle\sum_{i=1}^{M-1}\left\{V_i\left(P_i^{1/2}-R_i^{1/2}\right)-\frac{W_i}{3}\left(P_i^{3/2}-R_i^{3/2}\right)+\frac{a_{4,i}}{10}\left(P_i^{5/2}-R_i^{5/2}\right)\right\} \\ +2\sqrt{\dfrac{\rho_2 c_2 k_2}{\pi}}\left(V_M P_M{}^{1/2}-\frac{W_M}{3}P_M{}^{3/2}+\frac{a_{4,M}}{10}P_M{}^{5/2}\right) \end{bmatrix} \tag{2.15}$$

where,

$$\begin{aligned} &P_i = \tau_{M+1}-\tau_i;\; R_i = \tau_{M+1}-\tau_{i+1};\; F_i = a_{1,i}+a_{2,i}P_i+\frac{a_{3,i}}{2}P_i^2+\frac{a_{4,i}}{6}P_i^3 \\ &V_i = \frac{dF_i}{d\tau_{M+1}};\; W_i = \frac{d^2F_i}{d\tau^2{}_{M+1}} \quad (i = 1,2,.....,M) \end{aligned} \tag{2.16}$$

2.3.2 Laplace technique for heat flux prediction

The mathematical technique using Laplace transform can be applied to one-dimensional unsteady heat conduction technique to obtain heat flux on the surface of the substrate (Schultz and Jones, 1973). Taking the $\bar{T}$ as the Laplace transform of temperature T in Eq. (2.6), we get,

$$\frac{d^2\bar{T}}{dx^2} = \left(\frac{S}{\alpha}\right)\bar{T} \tag{2.17}$$

The general solution for this ordinary differential equation is,

$$\bar{T}(x,S) = c_1 e^{\left(\sqrt{S/\alpha}\right)x} + c_2 e^{-\left(\sqrt{S/\alpha}\right)x} \tag{2.18}$$

$$\text{At } x = \infty,\;\; T = 0, \bar{T}(\infty,S) = 0 \;\Rightarrow c_1 = 0$$

$$\text{At } x = 0 \text{ and } T = f_1(t),\ \overline{T} = \overline{F}$$

Thus, the transformed boundary conditions given by Eq. (2.7) reduces to,

$$\overline{T}(0,S) = \overline{F}(S) = \overline{F} \text{ and } \overline{T}(\infty,S) = 0 \tag{2.19}$$

Using the Eq. (2.19), the constants c_1 and c_2 appearing in the Eq. (2.18) can be evaluated. Then the modified general solution is,

$$T(x,S) = \overline{F}\, e^{-\left(\sqrt{S/\alpha}\right)x} \tag{2.20}$$

The surface heat flux $\dot{q}_S(t)$ is then obtained by differentiating Eq. (2.20) with respect to x and evaluating the differential at $x = 0$,

$$\frac{\partial\{T(x,S)\}}{\partial x} = \overline{F}\left(-\sqrt{S/\alpha}\right)e^{-\left(\sqrt{S/\alpha}\right)x}$$
$$\text{or, } \left\{\dot{q}_s(0,S)\right\}_{\text{laplace}} = -k\left.\frac{\partial\{T(x,S)\}}{\partial x}\right|_{x=0} = k\overline{F}\left(\sqrt{S/\alpha}\right) \tag{2.25}$$

The fitting of temperature data is also required to predict the surface heat flux. Polynomial fitting technique given by Eq. (2.11) is used here for constructing the temperature signal.

2.3.3 Surface temperature and heat flux histories for standard cases

Various techniques discussed in Sec.2.3 are adopted subsequently for prediction of surface heat flux. The temperature time histories along with the surface material properties (Macor) are used with temperature as a boundary condition for prediction of surface heat flux. Initially temperature signals shown in Fig.2.4 are considered for recovery of heat flux. These results are plotted and compared with the applied heat flux in Figs 2.5(a-c). The legends used in this figure are given in Table 2.2. The recovery of linear heat flux (Fig. 2.5-a) and triangular heat flux (Fig. 2.5-c) are seen to be very good from all the techniques not only in terms of magnitude but also in terms of the temporal nature of the heat load. However, recovery of step heat load (Fig. 2.5-b) is different for all the techniques. The main reason for this discrepancy is the polynomial representation of the temperature signal, which makes it difficult for capturing the discontinuity in the temperature signal with a continuous polynomial fit. The temporal location of step is captured more precisely by methods adopted in the piece-wise linear spline and cubic spline as compared polynomial fitting techniques mentioned Table 2.2. With respect to time duration of prediction of 20ms, all the temperature and surface heat flux signals seem to be in good agreement.

Table 2.2: Methods used for temperature discretization and surface heat flux calculations.

Sl. No.	Temperature discretization Techniques	Surface temperature history $T_s(t)$	Surface heat flux $q_s(t)$
1	Piece-wise linear fitting	$\{T_s(\tau)\}_{\text{linear}}$ (Eq. 2. 9)	$\{\dot{q}_s(t)\}_{\text{linear}}$ (Eq. 2.10)
2	Polynomial fitting	$\{T_s(\tau)\}_{\text{poly}}$ (Eq. 2.11)	$\{\dot{q}_s(t)\}_{\text{poly}}$ (Eq. 2.12)
3	Cubic-spline method	$\{T_s(\tau)\}_{\text{spline}}$ (Eq. 2.13)	$\{\dot{q}_s(t)\}_{\text{spline}}$ (Eq. 2.15)
4	Polynomial fitting	$\{T_s(\tau)\}_{\text{poly}}$ (Eq. 2.11)	$\{\dot{q}_s(t)\}_{\text{laplace}}$ (Eq. 2.25)

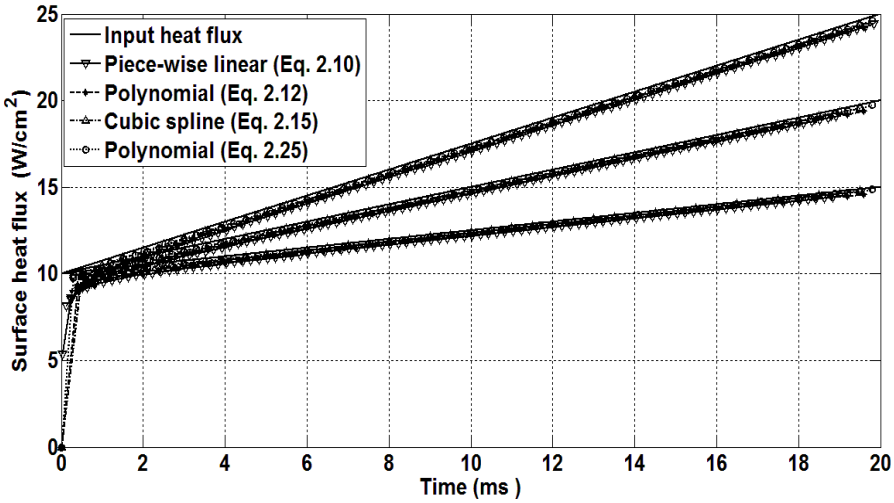

(a)

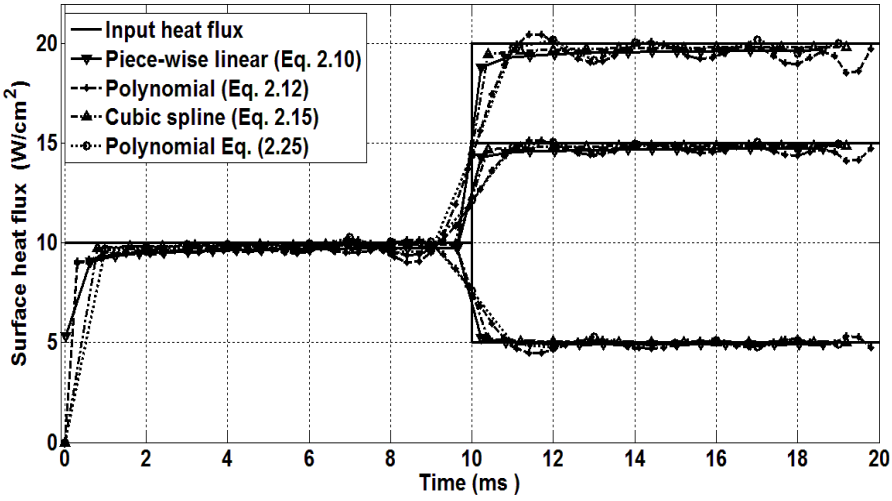

(b)

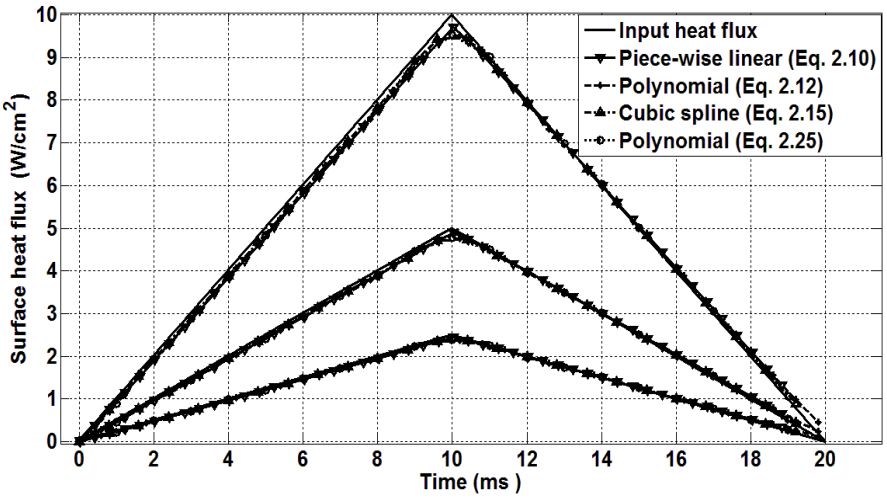

(c)

Fig. 2.5: Recovery of applied heat flux using various analytical techniques: (a) linearly varying heat fluxes; (b) step heat fluxes; (c) triangular heat fluxes.

2.3.4 Surface temperature and heat flux histories for experimental cases

In order to evaluate the effectiveness of analytical techniques and Laplace transform method of surface heat-flux recover, two different real-time experimental signals of temperature histories are considered. The first one is obtained from a platinum thin film sensor mounted on an insulated substrate (i.e. Macor). Experiments were performed for test duration of around 2 ms in a free piston driven shock tunnel (Kulkarni and Reddy, 2009). The time history of temperature for the second one is 10s and it is obtained from a nickel thin film sensor mounted on a quartz substrate during a supersonic flight experiment (Sahoo and Peetala, 2010). It may be noted that these temperature sensors will have to face very harsh testing atmosphere in terms of impulsive nature of heat loads and composition of test gas during the experiment. Therefore, the temperature signal obtained during tunnel testing is not necessarily smooth (Fig. 2.6-a and 2.7-a). Hence, temperature discretization techniques play an important role to obtain closed-form equation of temperature data. Experimental temperature discretization are as shown in (Fig.2.6-b and 2.7-b). All discussed techniques are considered to recover the surface heat flux in both the cases (Fig. 2.8-a and 2.8-b). During heat flux calculations, the properties of surface materials (Macor or quartz) are taken into consideration (Table 2.1). Referring to Fig (2.8-a), it is observed that the surface heat fluxes predicted by Eqs. (2.10) and (2.15) provide an excellent match with the data reported in the literature (Kulkarni and Reddy, 2009). However, Eqs. (2.12) and (2.25) show the same trend of heat flux with certain disagreement with the trend predicted by Eqs. (2.10) and (2.15). It may be due to the polynomial fitting technique adopted by these methods. The fitting

technique of temperature signal for entire time range using a polynomial although leads to simplicity for calculation of heat flux but makes it difficult to replicate the actual temperature signal. So, the polynomial fitting techniques are effective only for smooth temperature signals while piece-wise linear fitting and cubic-spline based temperature discretization can handle the discontinuity in temperature signal and truly resembles the nature of experimental signals.

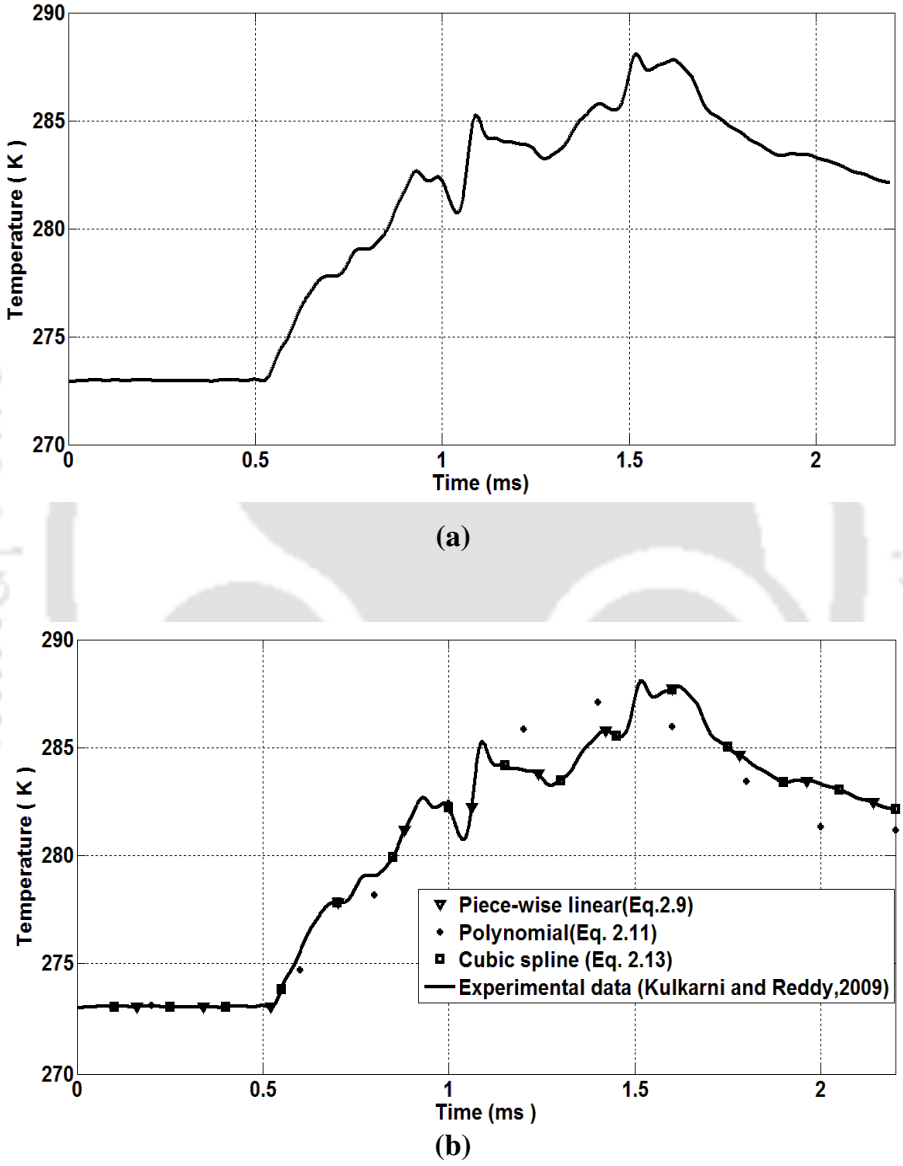

Fig. 2.6: Shock tunnel studies; (a) Experimental temperature history (Kulkarni and Reddy, 2009); (b) Comparison experimental temperature with fitting techniques temperature data.

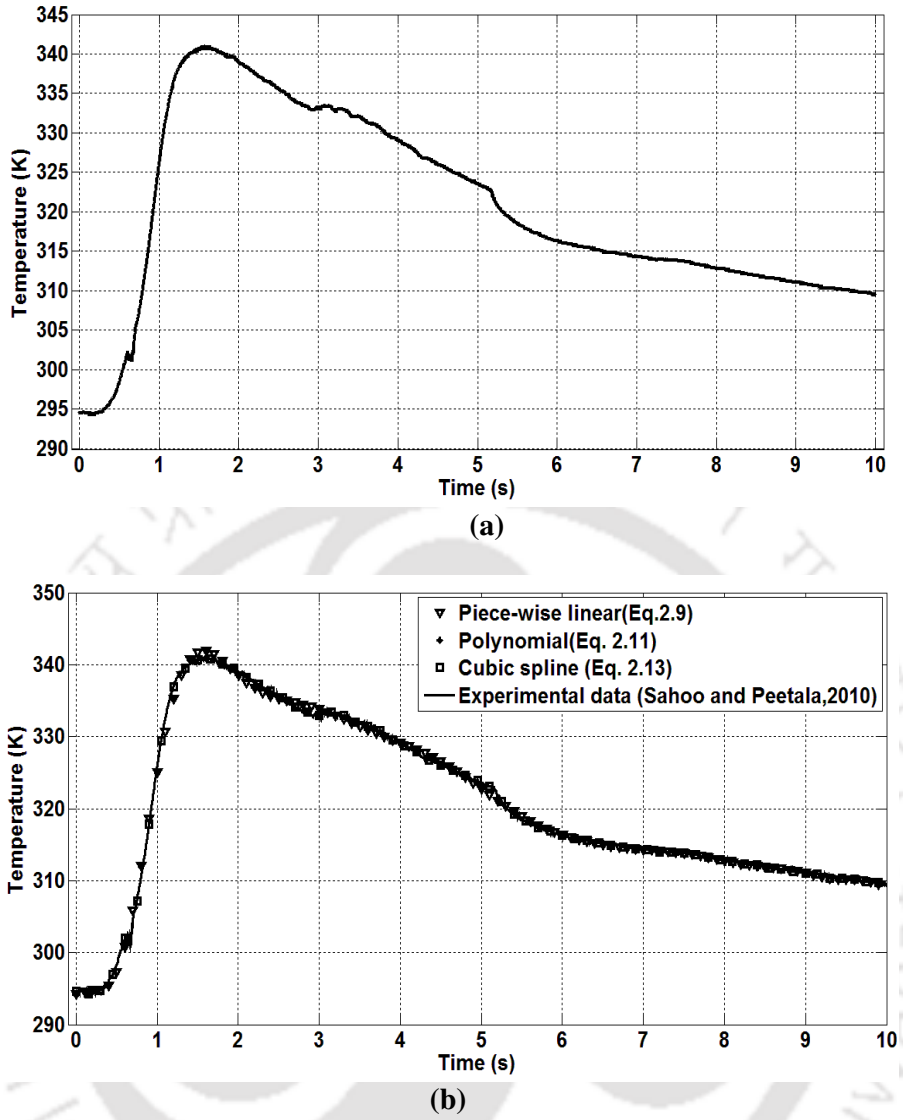

Fig. 2.7: Flight test studies; (a) Experimental temperature history (Sahoo and Peetala, 2010); (b) Comparison experimental temperature with fitting techniques temperature data.

The transient temperature data, acquired from a nickel thin film sensor mounted on a quartz surface during a supersonic flight experiment is taken as another test case where the experimental time duration is 10s (Sahoo and Peetala, 2010). All the methods discussed above are implemented here, for recovery of surface heat flux history and are presented in Fig. 2.8-b. The heat flux signals obtained from all the methods seem to be in close agreement as reported in the literature [Sahoo and Peetala (2010), Sahoo and Peetala (2011)]. It is mainly because of sufficiently smooth signals acquired during the flight experiments. Based on the results presented above, one can infer that discretization of temperature data plays a vital role to recover surface heat flux. When experiments are performed in a harsh

environments, one must follow the piece-wise linear fitting or spline based technique to recover the surface heat fluxes. Polynomial fitting of temperature data reduces the complexity in modeling and seems to be accurate for smooth experimental data. Irrespective of techniques of temperature discretization, surface heat fluxes predicted through one-dimensional analytical modeling and Laplace transform techniques matches closely in the range of ± 5%.

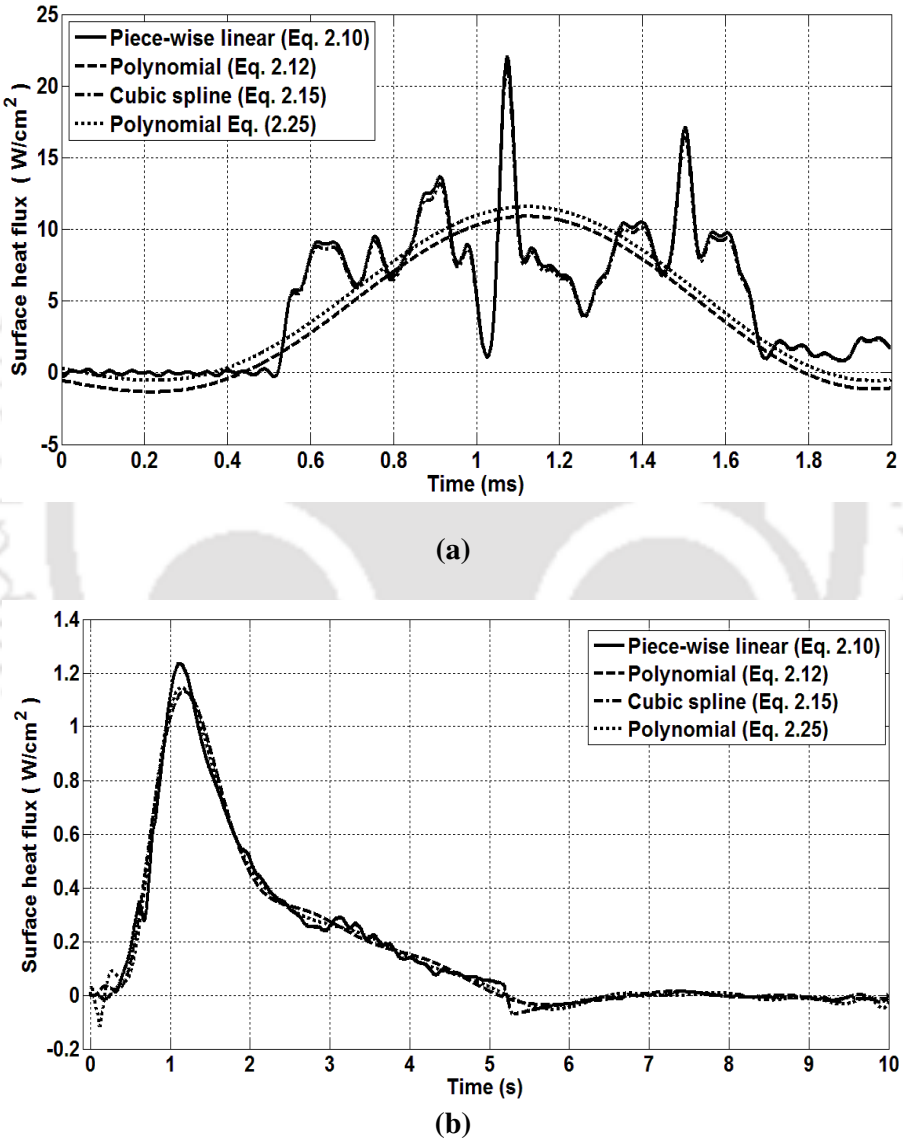

Fig. 2. 8: Recovery of surface heat flux and comparison with various techniques; (a) Shock tunnel temperature history; (b) Transient temperature data from flight test.

2.4 Summary

Performance assessment of various heat flux recovery techniques from known temperature time history has been reviewed in the present work. Temperature signals obtained from one-dimensional finite volume based computational investigations are considered for various heat flux signals (linear, triangular and step) of different magnitudes. Temperature signals obtained from shock tunnel testing and flight testing are also considered during present studies. Three different temperature discretization techniques (piece-wise linear fitting, polynomial fitting cubic-spline) are used here for constructing the temperature signals. The surface heat fluxes are predicted through one-dimensional analytical modeling and Laplace transform techniques. Encouraging agreement in terms of trend and magnitude has been observed for heat flux recovery from all the methods for smooth or non-noisy temperature signal obtained from computational study and experimental test cases. Heat flux recovery from all the methods for smooth temperature signals is seen to be in good agreement with a reasonable accuracy of ± 5%. However, it has been noticed that the spline based fitting techniques supersede the polynomial based fitting techniques for prediction of heat flux from discontinuous or noisy temperature signals. The applicability of polynomial based techniques is seen to be restricted only to smooth temperature signal due to their qualitative prediction of heat flux for discontinuous or noisy temperature signals. It can also be concluded from present investigations that prediction of heat flux is seen to be independent of introduction of polynomial fit of temperature data in the derivation of heat flux. Spline based fitting techniques are found to be precise for trend prediction and quantification of heat flux for all types of temperature data. It has also been observed that lower order spline (i.e. linear spline) is equally effective in recovering the heat flux signal as compared to the higher order spline but limited to short duration measurements (~ few milliseconds duration).

CHAPTER 3

DEVELOPMENT OF SOLVERS FOR FLUID FLOW AND SOLID CONDUCTION

3.1 Preface

This chapter explains the finite volume method used for fluid flow and conduction solver. It is the very first step towards the development of conjugate heat transfer (CHT) solver. The governing equations for two dimensional fluid flow (Navier-Stokes) and the corresponding boundary conditions are discussed in this chapter. In the simulation, flow over a flat plate problem is considered as the test case and the boundary of the wall is assumed to be isothermal. Variations of Stanton number, skin friction and boundary layer thickness along the length of the plate are considered for validation of the fluid flow solver. Therefore the results are compared with the corresponding analytical results. A generalized finite volume two-dimensional heat conduction solver for solid domain has been developed and tested with different test cases.

3.2 Governing Equations for Fluid Flow

Hypersonic flows are governed by Navier-Stokes (N-S) equations. Present studies deal with laminar flow. Hence, unsteady two dimensional Navier-Stokes equations i.e. mass, momentum and energy equations are considered in conservative form for fluid flow analysis. Following are the mass, x-momentum, y-momentum and energy equations, considered for fluid flow.

$$\frac{\partial(\rho)}{\partial t}+\frac{\partial(\rho u)}{\partial x}+\frac{\partial(\rho v)}{\partial y}=0 \tag{3-1-a}$$

$$\frac{\partial(\rho u)}{\partial t}+\frac{\partial(\rho u^2+p)}{\partial x}+\frac{\partial(\rho v)}{\partial y}=\frac{\partial(\tau_{xx})}{\partial x}+\frac{\partial(\tau_{yx})}{\partial y} \tag{3-1-b}$$

$$\frac{\partial(\rho v)}{\partial t}+\frac{\partial(\rho uv)}{\partial x}+\frac{\partial(p+\rho v^2)}{\partial y}=\frac{\partial(\tau_{xy})}{\partial x}+\frac{\partial(\tau_{yy})}{\partial y} \tag{3-1-c}$$

$$\frac{\partial(\rho E)}{\partial t}+\frac{\partial(\rho uH)}{\partial x}+\frac{\partial(\rho vH)}{\partial y}=\frac{\partial(u\tau_{xx}+v\tau_{yx}-\dot{q}_x)}{\partial x}+\frac{\partial(u\tau_{yx}+v\tau_{yy}-\dot{q}_y)}{\partial y} \tag{3-1-d}$$

where 'u' and 'v' are the velocity components in x and y directions, 'ρ' is density, 'a' is velocity of sound and p is pressure, τ is the shear stress, E is the total specific energy,

$E = e + \frac{1}{2}(u^2 + v^2)$, e is the specific internal energy, $H = h + \frac{1}{2}(u^2 + v^2) = E + \frac{p}{\rho}$, h is specific enthalpy given by $h = e + \frac{p}{\rho}$, $\dot{q}_x$ and $\dot{q}_y$ heat flux in x and y direction, respectively. The above governing equations are reduced to non-dimensional form using freestream variables and characteristic object dimension which leads to following non-dimensional variables.

$$x = \frac{x^*}{L}, y = \frac{y^*}{L}, u = \frac{u^*}{V_\infty}, v = \frac{v^*}{V_\infty}, \rho = \frac{\rho^*}{\rho_\infty}, p = \frac{p^*}{\rho_\infty {V_\infty}^2}, T = \frac{T^*}{T_\infty}$$

$$E = \frac{E^*}{{V_\infty}^2}, H = \frac{H^*}{{V_\infty}^2}, e = \frac{e^*}{{V_\infty}^2}, h = \frac{h^*}{{V_\infty}^2} \qquad (3.2)$$

$$t = \frac{t^* V_\infty}{L}, \mu = \frac{\mu^*}{\mu_\infty}, q_x = \frac{{q_x}^*}{\rho_\infty {V_\infty}^3}, q_y = \frac{{q_y}^*}{\rho_\infty {V_\infty}^3}$$

Here we are assuming x, y, u....etc as non-dimensional variables and x*, y*, u*....etc are the dimensional variables for simplicity.

Using the non-dimensional variables the governing equations reduce to following form;

$$\frac{\partial \rho}{\partial t} + \frac{\partial (\rho u)}{\partial x} + \frac{\partial (\rho v)}{\partial y} = 0 \qquad (3\text{-}3\text{-a})$$

$$\frac{\partial (\rho u)}{\partial t} + \frac{\partial (\rho u^2 + p)}{\partial x} + \frac{\partial (\rho v)}{\partial y} = \frac{\partial (\tau_{xx})}{\partial x} + \frac{\partial (\tau_{yx})}{\partial y} \qquad (3\text{-}3\text{-b})$$

$$\frac{\partial (\rho v)}{\partial t} + \frac{\partial (\rho uv)}{\partial x} + \frac{\partial (p + \rho v^2)}{\partial y} = \frac{\partial (\tau_{xy})}{\partial x} + \frac{\partial (\tau_{yy})}{\partial y} \qquad (3\text{-}3\text{-c})$$

$$\frac{\partial (\rho E)}{\partial t} + \frac{\partial (\rho uH)}{\partial x} + \frac{\partial (\rho vH)}{\partial y} = \frac{\partial (u\tau_{xx} + v\tau_{yx} - \dot{q}_x)}{\partial x} + \frac{\partial (u\tau_{yx} + v\tau_{yy} - \dot{q}_y)}{\partial y} \qquad (3\text{-}3\text{-d})$$

where,

$$\tau_{xx} = \frac{1}{\mathrm{Re}_\infty}\left\{\lambda\left[\frac{\partial u}{\partial x} + \frac{\partial v}{\partial y}\right] + 2\mu\frac{\partial u}{\partial x}\right\}, \ \tau_{yy} = \frac{1}{\mathrm{Re}_\infty}\left\{\lambda\left[\frac{\partial u}{\partial x} + \frac{\partial v}{\partial y}\right] + 2\mu\frac{\partial v}{\partial y}\right\}$$

$$\tau_{xy} = \tau_{yx} = \frac{1}{\mathrm{Re}_\infty}\left\{\mu\left[\frac{\partial u}{\partial y} + \frac{\partial v}{\partial x}\right]\right\}, \ q_x = \frac{-\mu}{(\gamma - 1){M_\infty}^2 \mathrm{Re}_\infty \mathrm{Pr}}\frac{\partial T}{\partial x}, \ q_y = \frac{-\mu}{(\gamma - 1){M_\infty}^2 \mathrm{Re}_\infty \mathrm{Pr}}\frac{\partial T}{\partial y} \qquad (3\text{-}3\text{-e})$$

In the above equations Re_∞ is free stream Reynolds number, Pr_∞ is Prandtl number and M_∞ is freestream Mach number. Since numbers of unknowns are more than the number of

equations, closure problem is solved by using an additional equation which is nothing but the non dimensional form of equation of state that is given by,

$$p = \rho \bar{R} T \text{, where } \quad \bar{R} = \frac{1}{\gamma M_{\infty}^{2}} \tag{3.4}$$

where , $\bar{R}$ non-dimensional gas constant.

Viscosity of the fluid varies with temperature. (T) and is calculated using Sutherland's formula.

$$\frac{\mu}{\mu_{ref}} = \left[\frac{T}{T_{ref}}\right]^{3/2} \left[\frac{T_{ref} + S}{T + S}\right] \tag{3.5}$$

Therefore the governing equations in compact vector (conservative form) are,

$$\frac{\partial U}{\partial t} + \frac{\partial F_i}{\partial x} + \frac{\partial G_i}{\partial y} = \frac{\partial F_v}{\partial x} + \frac{\partial G_v}{\partial y} \tag{3.6}$$

where,

$$U = \begin{bmatrix} \rho \\ \rho u \\ \rho v \\ \rho E \end{bmatrix}; F_i = \begin{bmatrix} \rho u \\ \rho u^2 + p \\ \rho uv \\ \rho uH \end{bmatrix}; G_i = \begin{bmatrix} \rho v \\ \rho uv \\ \rho v^2 + p \\ \rho vH \end{bmatrix}$$

$$F_v = \begin{bmatrix} 0 \\ \tau_{xx} \\ \tau_{yx} \\ u\tau_{xx} + v\tau_{xy} - \dot{q}_x \end{bmatrix}; G_v = \begin{bmatrix} 0 \\ \tau_{xy} \\ \tau_{yy} \\ u\tau_{yx} + v\tau_{yy} - \dot{q}_y \end{bmatrix} \tag{3.7}$$

where $\vec{U}$ is conservative variable matrix, $\vec{F}_i$, $\vec{G}_i$ are the inviscid fluxes and $\vec{F}_v$, $\vec{G}_v$ are viscous fluxes.

3.3 Finite Volume Method (FVM)

The finite volume formulation demands for the integration of above discussed governing equation on the volume. Thus integral form of the governing equations for finite volume formulation is as follows,

$$\frac{\partial \overline{U}}{\partial t} + \frac{1}{A} \oint \vec{F}\, \vec{n} dS = 0 \tag{3.9}$$

Here $\overline{U} = \frac{1}{A}\iint U dA$ (Average value of U over the entire volume)

The flux is given by $\vec{F} = \vec{F}_I - \vec{F}_V$

$\vec{F}_I = F_I\,\vec{i} + G_I\,\vec{j}$ (Total inviscid flux), $F_V = F_V\,\vec{i} + G_V\,\vec{j}$ (Total viscous flux)

$\vec{F}$ is the flux vector and $\vec{n}$ is the unit normal to the surface ds. Considering a cell, governing equations can be represented as,

$$\frac{\partial U_{ij}}{\partial t} + \frac{1}{A}\left\{\sum_{i=1}^{4} \vec{F}.\vec{n}dS\right\}_{ij} = 0 \tag{3.10}$$

Here the bar notation over U is dropped for simplicity.

3.4 Discretisation Schemes for Flux calculation.

The critical part of Euler or inviscid part of the solver is the discretisation of inviscid or convective fluxes. Various schemes are reported in the literature for these computations. In the present development, advection upstream splitting method with delta (AUSM) from the family of flux vector splitting schemes is implemented.

The AUSM scheme [Liou (1996), Blazek (2001)] is based on splitting the convective flux into convective and pressure part as,

$$\vec{F}_c = V\begin{bmatrix}\rho\\ \rho u\\ \rho v\\ \rho H\end{bmatrix} + \begin{bmatrix}0\\ n_x p\\ n_y p\\ 0\end{bmatrix} \tag{3.11}$$

Therefore the convective fluxes at face (I+1/2) of the control volume are given as, in Fig. 3.1

$$(\vec{F}_c)_{I+1/2} = (M_n)_{I+1/2}\begin{bmatrix}\rho c\\ \rho c u\\ \rho c v\\ \rho c H\end{bmatrix}_{L/R} + \begin{bmatrix}0\\ n_x p\\ n_y p\\ 0\end{bmatrix}_{I+1/2} \tag{3.12}$$

where,

$$(\bullet)_{L/R} = \begin{Bmatrix}(\bullet)_L & \text{if } M_{I+1/2} \geq 0\\ (\bullet)_R & \text{Otherwise}\end{Bmatrix} \tag{3.13}$$

Advection Mach number is evaluated as the sum of the left and right split Mach number.

$$(M_n)_{I+1/2} = M_L^{+} + M_R^{-} \tag{3.14}$$

The computation of the left and right state flow variables (ρ, u, v, w, p, H) is based on the interpolation of the values from the centroid to the cell faces.

The pressure at the face $(I+1/2)$ is given as

$$p_{I+1/2} = p_L^{+} + p_R^{-} \tag{3.15}$$

The split pressures

The left split pressure and right spilt pressure are

$$p_L^{+} = \begin{cases} p_L & \text{if } M_L \geq +1 \\ \frac{p_L}{4}(M_L+1)^2(2-M_L) & \text{if } |M_L| < 1 \\ 0 & \text{if } M_L \leq -1 \end{cases} \tag{3.16}$$

$|M| < 1$

$$p_R^{-} = \begin{cases} 0 & \text{if } M_R \geq +1 \\ \frac{p_R}{4}(M_R-1)^2(2+M_R) & \text{if } |M_R| < 1 \\ p_R & \text{if } M_R \leq -1 \end{cases} \tag{3.17}$$

AUSM can also be written in the form,

$$(\vec{F}_c)_{I+1/2} = \frac{1}{2}(M_n)_{I+1/2}\left\{\begin{bmatrix}\rho c\\ \rho cu\\ \rho cv\\ \rho cH\end{bmatrix}_L + \begin{bmatrix}\rho c\\ \rho cu\\ \rho cv\\ \rho cH\end{bmatrix}_R\right\} - \frac{1}{2}\left|(M_n)_{I+1/2}\right|\left\{\begin{bmatrix}\rho c\\ \rho cu\\ \rho cv\\ \rho cH\end{bmatrix}_R - \begin{bmatrix}\rho c\\ \rho cu\\ \rho cv\\ \rho cH\end{bmatrix}_L\right\} + \begin{Bmatrix}0\\ n_x(p_L^{+}+p_R^{-})\\ n_y(p_L^{+}+p_R^{-})\\ 0\end{Bmatrix} \tag{3.18}$$

Second term in the above equation has dissipative character, which is scaled by the scalar value $\left|(M_n)_{I+1/2}\right|$. When advection Mach number $(M_n)_{I+1/2}$ tends to zero, the dissipation term in the Eq.3.18 approaches zero. Thus, any disturbances cannot be damped by the scheme. Hence the dissipation term is modified as follows.

$$\left|(M_n)_{I+1/2}\right| = \begin{cases} \left|(M_n)_{I+1/2}\right| & \text{if } \left|(M_n)_{I+1/2}\right| > \delta \\ \dfrac{(M_n)^2_{I+1/2} + \delta^2}{2\delta} & \text{if } \left|(M_n)_{I+1/2}\right| \le \delta \end{cases} \quad (3.19)$$

Where δ is a small value ($0<\delta \le 0.5$). Hence there will be always sufficient amount of numerical dissipation. In order to retain the accuracy of the scheme for boundary layers, the parameter δ could be reduced in the wall normal direction.

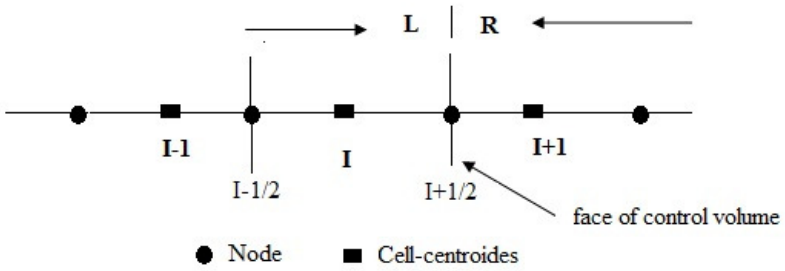

Fig. 3.1: Left and right state at cell face I+1/2.

3.5 Discretization of Viscous Fluxes

Evaluation of the viscous fluxes at the faces of the control volume requires flow quantities and their first derivatives at the faces. In the present cell-centered formulation, the values of any flow quantity at the faces is achieved by averaging the values of same quantity at the left and right cell of that particular face. The next requirement is the evaluation of first derivatives of velocity components and temperature. In the present solver the derivatives of primitive variables are calculated at the cell centroid by making use of a discrete version of the Gauss divergence theorem [Blazek (2001)]. The first derivatives of velocity components and temperature are then evaluated at the faces of each cell from the known values at the cell centroids. Here the assignment of gradients at the faces does not follow the simple averaging strategy that is followed in case of flow quantities because such simple averaging leads to decoupling of the gradients at boundaries. So in order to avoid such decoupling, in the present solver the gradients are passed to nodes of the domain and then they are assigned to the face centroid just by taking the average values at the end nodes of a particular face. The net convective flux is finally computed by summing the inviscid and viscous terms.

3.6 Fluid Flow Boundary Conditions

Various boundary conditions implemented in the present solver are as follows.

❖ Inlet and Outlet

For the hypersonic inlet boundary, values of all the flow variables are equated to the known freestream quantities. Supersonic outlet boundary condition has been implemented at the outlet. By the virtue of this boundary condition, all the variables at the outlet boundary cell are obtained from the immediate inner cell.

❖ Wall Boundary Condition

In the present solver, at the wall boundary, no-slip isothermal or no-slip adiabatic condition has been considered. Temperature of known value has been assigned to all the boundary faces for isothermal condition while adiabatic wall condition demands for zero temperature gradient at the wall.

❖ Symmetry

The symmetry wall boundary condition is incorporated using mirror cell approach. Implementation of this method is based on explanation given by Blazek [Blazek (2001)]. Assumption of a mirror cell at the symmetry wall is the central theme of this strategy. The flow variables for this cell are obtained by equating all the variables from the neighbouring fluid cell except for the wall normal velocity. For the impermiability condition, this velocity is equated by magnitude but reversed in direction.

3.7 Governing Equations for Solid Domain Conduction Solver

The governing equation for heat transfer analysis is the unsteady heat conduction equation. Two dimensional (2D) form of the same is considered for current studies. This equation is given below,

$$\rho c \frac{\partial T}{\partial t} = \frac{\partial}{\partial x}\left[k \frac{\partial T}{\partial x} \right] + \frac{\partial}{\partial y}\left[k \frac{\partial T}{\partial y} \right] + S \qquad (3.20)$$

Mathematical formulation for the heat conduction equation is demonstrated for one-dimensional heat conduction discussed in **Chapter 2**. Further it is extended to two-dimensional heat transfer using finite volume analysis by considering a control volume as shown in Fig. 3.2. When a similar procedure is extended to two dimensions, Eq.3.20 takes the following form.

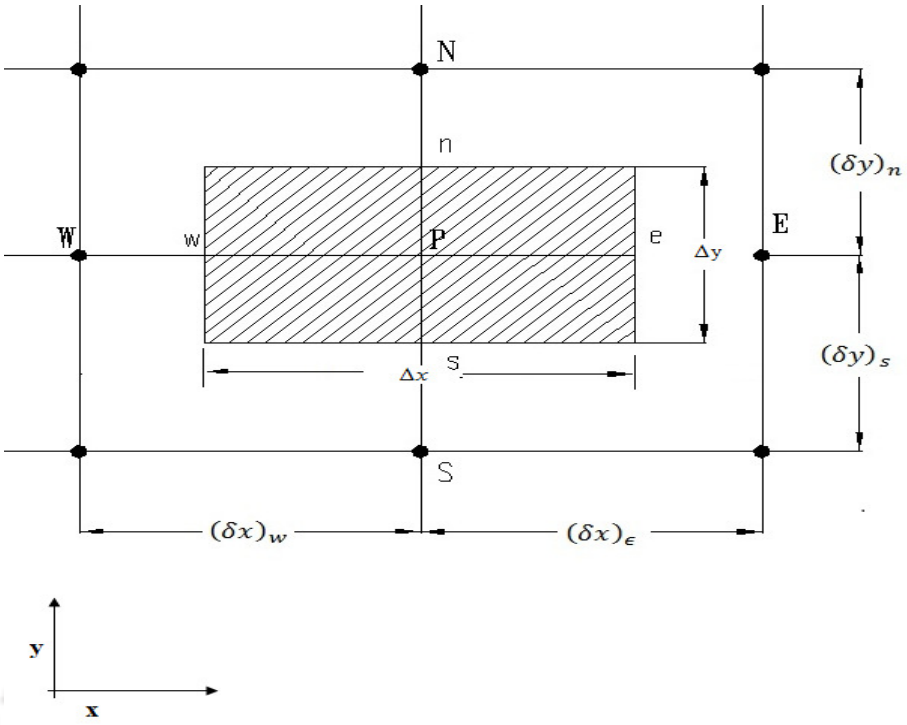

Fig. 3.2: Typical two dimensional control volume.

$$a_P T_P = a_W\left[\theta T_W + (1-\theta)T_W^{\,0}\right] + a_E\left[\theta T_E + (1-\theta)T_E^{\,0}\right] + a_S\left[\theta T_S + (1-\theta)T_S^{\,0}\right] + a_N \left[\theta T_N + (1-\theta)T_N^{\,0}\right] + \left[a_P^{\,0} - (1-\theta)a_W - (1-\theta)a_E - (1-\theta)a_S - (1-\theta)a_N\right]T_P^{\,0} + b \quad (3.21)$$

The source term 'S' is linearised as $b = \bar{S}\,\Delta x = S_u + S_p T_P^{\,0}$ (3.22)

For a fully explicit scheme ($\theta = 0$) Eq.3.21 reduces to

$$a_P T_P = a_W T_W^0 + a_E T_E^0 + a_S T_S^0 + a_N T_N^0 + [a_P^0 - (a_W + a_E + a_S + a_N - S_P)]T_P^{\,0} + S_u \quad (3.23)$$

Where,

$$a_P = a_P^{\,0} = \rho c\left(\frac{\Delta V}{\Delta t}\right), a_W = \frac{k_w A_w}{\delta x_{WP}}, a_E = \frac{k_e A_e}{\delta x_{PE}}, a_S = \frac{k_s A_s}{\delta y_{SP}}, a_N = \frac{k_n A_n}{\delta y_{PN}}, \Delta V = \Delta x \Delta y \quad (3.24)$$

The values of S_p and S_u depend on boundary conditions at the boundary nodes. Similar formulation is carried out for 2D heat conduction analysis for single material or composite material.

3.8 Boundary Conditions for Solid Domain Conduction Solver

For boundary conditions of heat conduction studies are discussed in below as;

- **Heat flux wall**

  Uniform or non-uniform heat flux of known value is assigned to the faces falling on the wall of this type.

- **Adiabatic wall**

  Temperature gradient normal to the corresponding face is equated to zero for implementation of this boundary condition.

- **Isothermal wall**

  Temperature of known value is given for all the cell faces falling on this wall.

- **Interface**

At the interface "continuity in heat flux" and equality of temperature are considered. The heat flux equation can be expressed as,

$$[\text{Heat flux}(x, \text{interface}, t)]_{\text{solid1}} = [\text{Heat flux}(x, \text{interface}, t)]_{\text{solid2}}$$

Regarding temperature, same value of the interface temperature is considered for either side of the domain which is comprised of different materials.

3.9 Results and Discussion

3.9.1 Test Case 1: Hypersonic flow over an isothermal flat plate

Successful formulation for the Navier-Stokes equations is performed. It's validation for the test case of hypersonic flow over an isothermal or adiabatic flat plate is performed. Schematic of the computational domain is as shown in Fig 3.3. Freestream conditions of a typical hypersonic shock tunnel are considered at the inlet. Outlet flow is considered as supersonic, top wall is assumed as the symmetry wall while bottom wall is considered as isothermal. Computations are performed for Mach number of 8, Reynolds number of 85000 and static temperature of 113 K. Isothermal wall boundary condition is implemented using constant wall temperature of 300 K. Fluid domain is meshed with the structured grid as shown in Fig. 3.4. Fine mesh is used at the wall to capture the boundary layer properly.

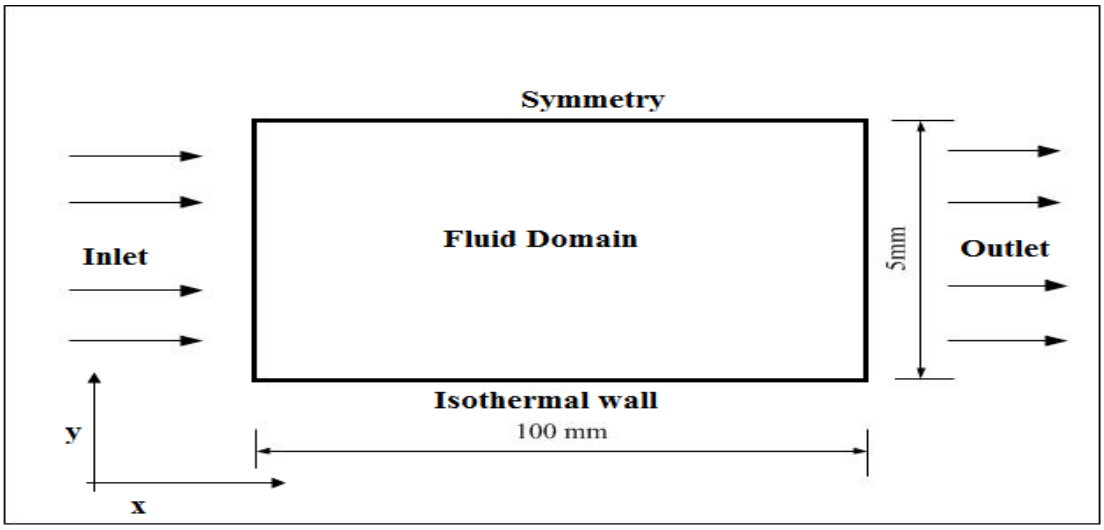

Fig. 3.3: Schematic of the domain of flat plate with boundary conditions

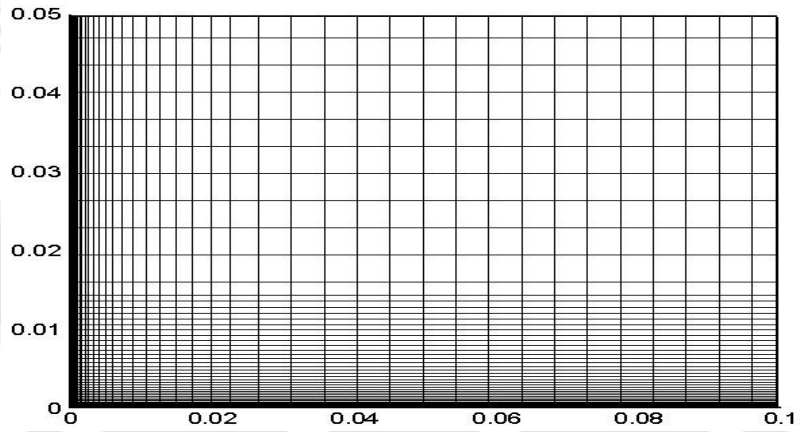

Fig. 3.4: Grid in fluid domain for flat plate.

Results obtained from present solver for the test case of hypersonic flow over an isothermal flat plate are compared with the standard analytical predictions. The major parameters considered for this comparison are skin friction coefficient, Stanton number and boundary layer thickness. Expressions for these parameters are as mentioned below [White, 1991].

$$\text{Skin friction } C_f = \frac{0.664 C_w^{1/2}}{\text{Re}_x^{1/2}} \tag{3.25}$$

$$\text{where, Chapman and Rubesin parameter } C_w = \frac{\rho_w \mu_w}{\rho_\infty \mu_\infty} \approx \left[\frac{T_w}{T_\infty}\right]^{-1/2} \tag{3.26}$$

$$\text{Stanton number } S_t = C_f \times 0.5 \,\text{Pr}^{-2/3} \tag{3.27}$$

$$\text{Boundary layer thickness } \delta = \left(\frac{C_w^{1/2}\left[5.0+\left(0.2+0.9\frac{T_w}{T}\right)(\gamma-1)Ma_\infty^2\right]x}{\mathrm{Re}_{x\infty}^{1/2}} \right) \tag{3.28}$$

Variation of all the parameters is seen to be in good agreement with the analytical equivalent as seen from Figs 3.5-3.7. Here, the skin friction (C_f) and Stanton number decrease along the length of the plate. Major reason for this decrement is the increase in boundary layer thickness as displayed by Fig 3.7. Therefore the reduced near wall gradients of velocity and temperature reduce the wall shear and heat flux. This agreement of various wall parameters, in local magnitude and global variation, confirms the accuracy of the present solver.

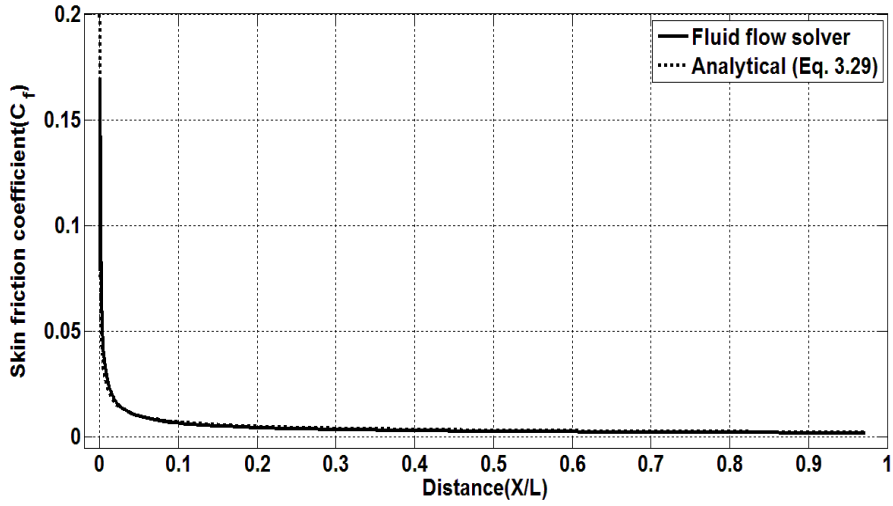

Fig. 3.5: Variation of skin friction coefficient along the length of plate.

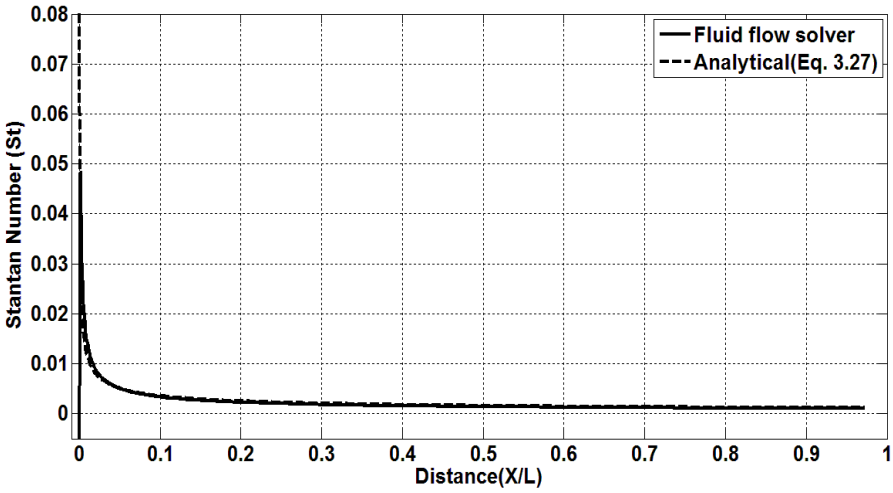

Fig. 3.6: Variation of Stanton number along the length of plate.

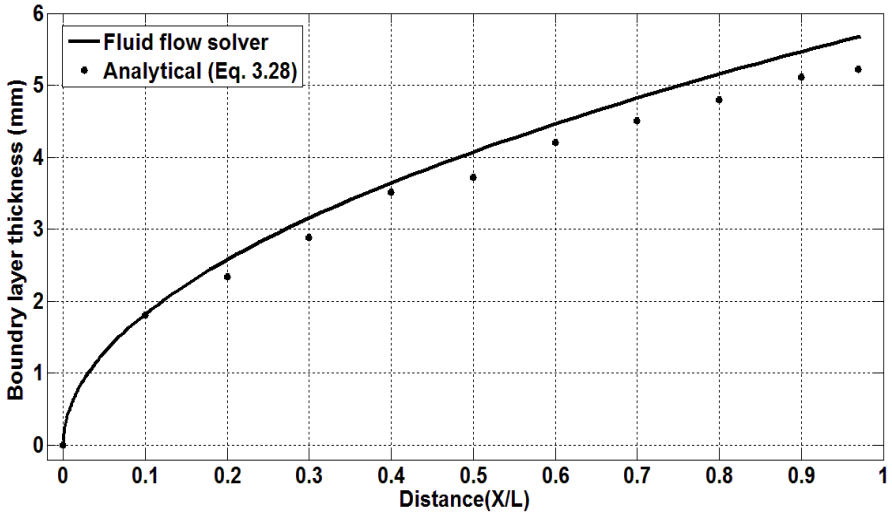

Fig. 3.7: Variation of boundary layer thickness along the length of plate.

3.9.2 Test Case 2: Transient heat conduction in a slab

Conduction solver is validated for the test case of transient heat conduction through a finite thickness plate. Typical computational domain is as shown in Fig. 3.8. Top wall is considered as heat flux wall where heat flux of $2x10^5$ W/m^2 is applied. Side walls are considered as adiabatic while the uniform constant temperature of 200 K is maintained at bottom wall. These boundary conditions imitate the one dimensionality in the two dimensional computational domain. Moreover, analytical formulation for the temperature variation along the depth of the plate at a particular instance is given as [Holman (1989)].

$$T - T_i = \frac{2q_w\sqrt{\frac{\alpha\tau}{\pi}}}{k}\exp\left(\frac{-x^2}{4\alpha\tau}\right) - \frac{q_w x}{k}\left(1 - erf\,\frac{x}{2\sqrt{\alpha\tau}}\right) \tag{3.29}$$

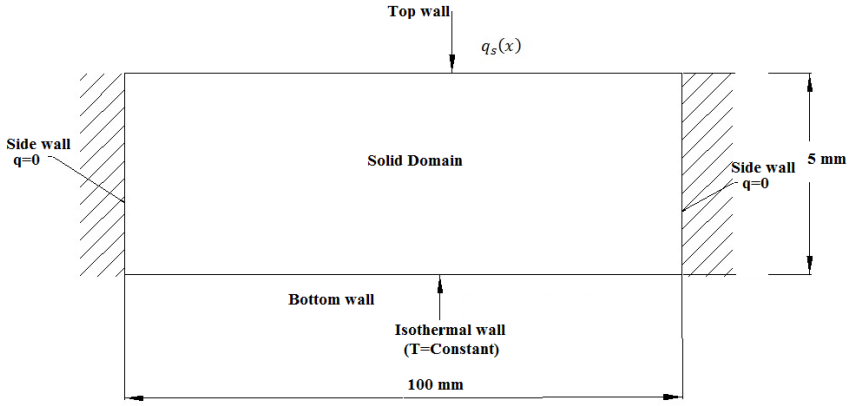

Fig. 3.8: Schematic diagram of single domain.

Comparison of thus obtained temperature with one dimensional and two dimensional computations is shown in Fig. 3.9. This figure clearly displays the spatial accuracy of the present conduction solver. The expected match between different dimensionalities is also evident from this figure. Surface temperature variation with time, derived from the Eq. (3.29) in comparison with the same obtained from present solver, is shown in Fig. 3.10. This figure confirms the temporal accuracy of the conduction solver. Hence the chosen test case of transient heat conduction in a finite thickness slab is found effective in confirming the spatial and temporal accuracy of the in-house conduction solver.

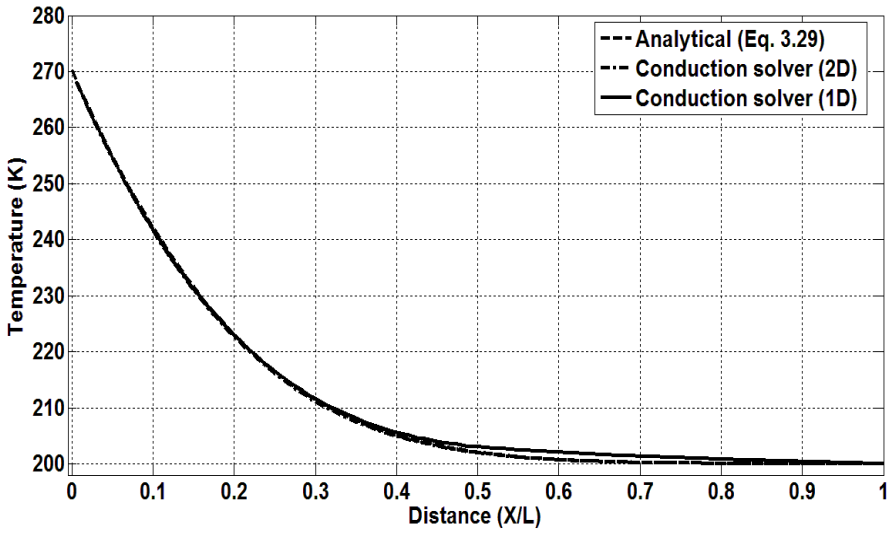

Fig. 3.9: Temperature variation along the depth of plate.

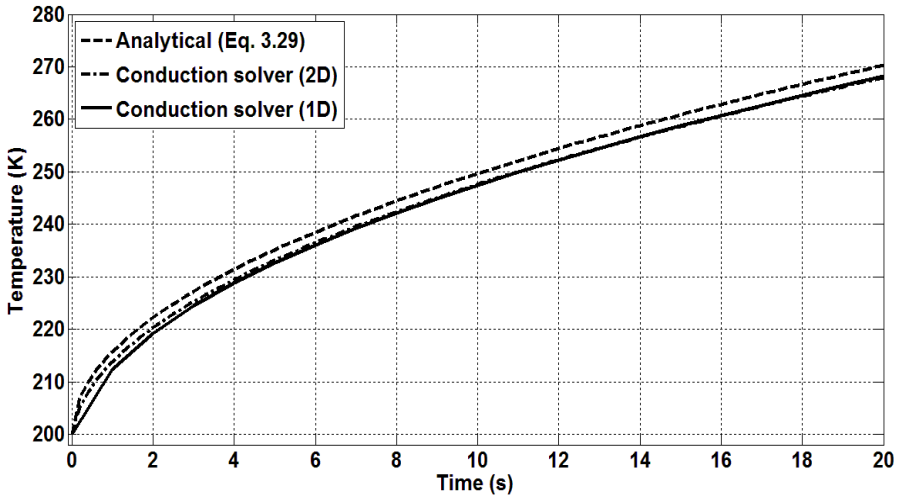

Fig. 3.10: Surface temperature change with respect to time.

3.9.3 Test Case 3: Transient heat conduction through a composite slab

In these studies, ability of the solver to handle composite solid domain is tested. This test case is reported by Pietro and Domenic (2008). Therefore, the set up and the boundary conditions are the same as reported in the literature. Basically, computational domain is a 0.3x0.9m rectangular slab which is equally divided into three sub blocks [Pietro and Domenic (2008)] as shown in figure 3.11. Each sub-block is made of a different material and it is discretized using 51x51grid points. A constant heat flux of 9000 W/m^2 is imposed on the lower surface of the domain, while the other three boundaries are held at a fixed temperature of 400 K. The initial temperature of all the solids is assumed as 300 K and the simulation lasts for 80 seconds with a time step $\Delta t = 0.01$ s. The materials used in the simulations along with their thermal characteristics are taken from reference [Incropera and DeWitt (2002), Table 3.1].

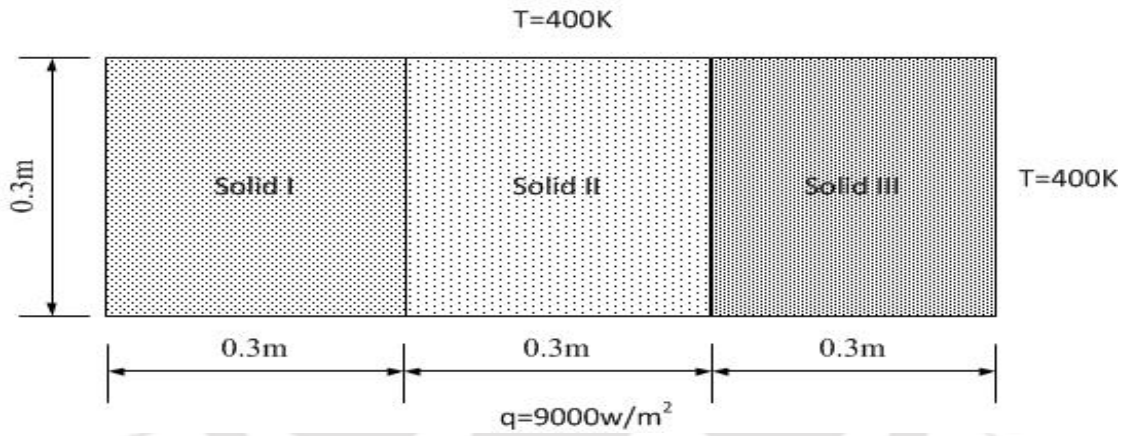

Fig. 3.11: Schematic diagram of composite domain.

Temperature contours obtained for combination of various materials and its comparison with the literature reported results are shown in Figs 3.12-3.15. A more interesting result is obtained when three different materials, copper, brass and bronze, are used together. In this case, heat flux of 90000 W/m^2 is imposed on the bottom boundary, constant temperature (300 K) is maintained at top wall while the left and right surfaces are assumed as adiabatic. The initial temperature and the time step are the same as in the earlier case. Comparison of the results for this variant is shown in Fig. 3.15. It can be seen from these figures that the heat transfer is faster in copper than in brass and bronze due to its higher thermal diffusivity. Along the same line, more heat transfer from copper to brass than from brass to bronze can be explained. Encouraging agreement with such physical expectation and with the literature reported results reassert the accuracy of the conduction solver. It also

confirms the implementation of interface boundary condition in the conduction solver. This test case provides the confidence, necessary for integrating the fluid flow and conduction solver, for development of CHT solver which indeed demands for a fluid-solid interface which bears same mathematical formulation.

Table 3.1: Material properties (Pietro and Domenic, 2008)

Material	Thermal conductivity ($W/m.K$)	Density (kg/m^3)	Specific Heat ($kJ/kg.K$)	Viscosity (m^2/s)	T_{melt} (K)
Copper	401	8920	384.91	1.1676×10^{-4}	1350
Aluminum	204	2720	895	8.38×10^{-5}	933
Bronze	26	38670	340	8.82×10^{-6}	727
Brass	104	8520	380	3.21×10^{-4}	735

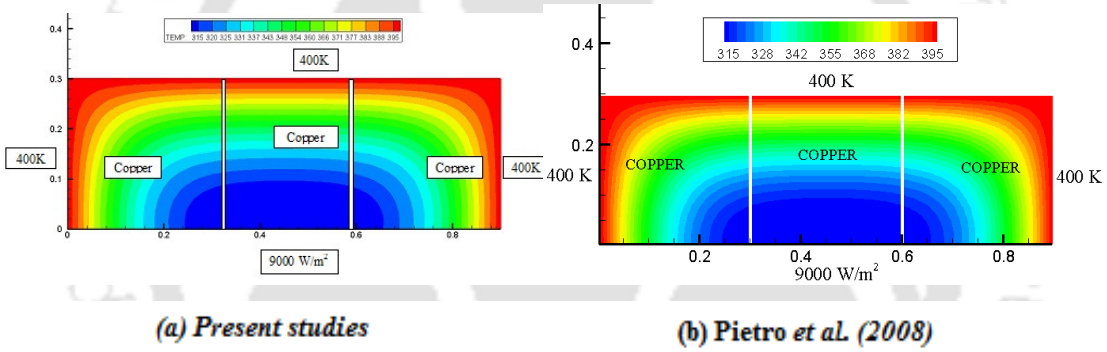

Fig. 3.12: Temperature for three copper blocks at t = 80s

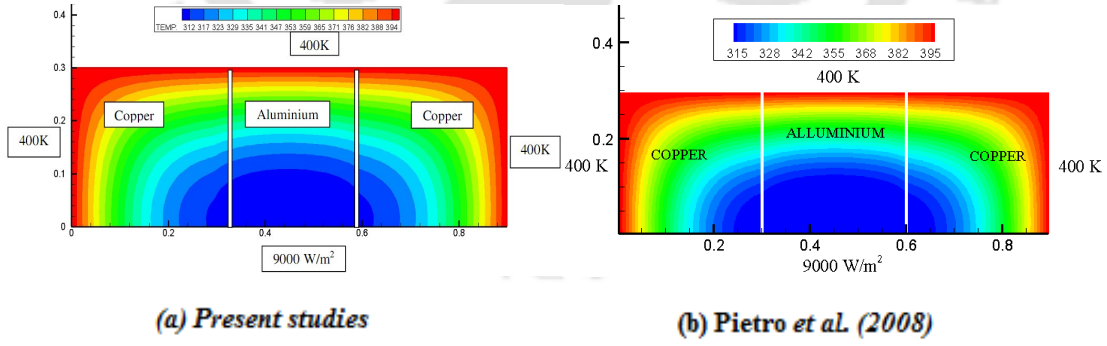

Fig. 3.13: Temperature field for copper-aluminum blocks at t = 80s

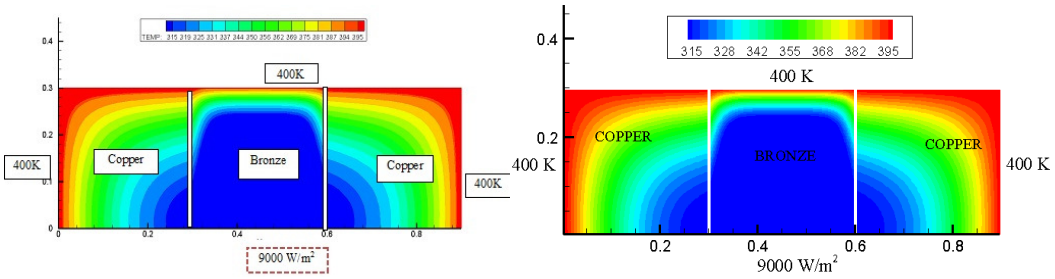

(a) Present studies **(b) Pietro *et al.* (2008)**

Fig. 3.14: Temperature for copper-bronze blocks at t = 80s.

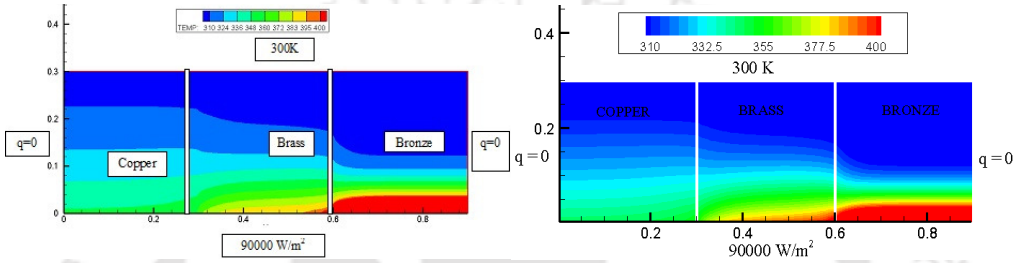

(a) Present studies **(b) Pietro *et al.* (2008)**

Fig. 3.15: Temperature for copper-brass-bronze blocks after 300s.

3.10 Summary

Finite volume formulation has been successfully implemented for the fluid flow and conduction solvers. The AUSM-δ scheme is incorporated in the present fluid flow solver for inviscid flux computations while the viscous fluxes are computed using discrete version of the Gauss theorem. Various boundary conditions, necessary to solve a particular hypersonic flow situation, are incorporated in the fluid flow solver. Conduction solver is equipped with all the required boundary conditions for transient heat conduction analysis. Thus developed solvers are validated for the standard test cases viz. hypersonic flow over isothermal plate for the fluid flow solver and transient heat conduction in a finite thickness flat plate. Encouraging agreement has been noticed for both the solvers with the respective analytical results. Possibility of simulation for composite domain conduction has also been successfully verified.

CHAPTER 4

COUPLING TECHNIQUES FOR THE CONJUGATE HEAT TRANSFER SOLVER

4.1 Preface

Conjugate heat transfer studies have advantages over the conventional CFD analysis due to its potential of simultaneous monitoring of changes in fluid flow and conduction based heat transfer in solid. Therefore simultaneous prediction of wall temperature and heat transfer rate is possible through such a vital technique. However formulation for a typical CHT solver remains a task where proper communication between fluid and solid domain becomes a major target. Such communication is termed as coupling and the associated strategies as coupling techniques. Various techniques involved for this methodology and employed in the present solver are discussed in the following sections. Outcome of fluid flow solver (wall heat flux) has been considered as input for the solid solver in decoupled manner to obtain the wall temperature variation. This procedure demonstrates the necessity of active or bilateral coupling between fluid and solid domains.

This chapter explains various coupling techniques of CHT. Three methodologies incorporated to integrate the fluid flow and conduction solvers are decoupled CHT (DC-CHT), strongly coupled analysis (SC-CHT) and loosely coupled analysis (LC-CHT). Details of individual methodologies are given herein. Necessity of coupling is explained through a case study of hypersonic flow over a finite thickness plate using DC-CHT technique. Computationally obtained temperature time trace clearly demonstrates the requirement of detailed CHT studies.

4.2 Computational Methodology for CHT studies

The conjugate heat transfer analysis for the hypersonic flow over a flat plate involves both fluid as well as solid domain. The methodologies of coupled and decoupled CHT analysis are given in Fig. 4.1-4.2. These methodologies are incorporated to integrate the fluid flow and conduction solvers and their salient features are listed in Table 4.1. The first case is termed as decoupled CHT (DC-CHT). This strategy is the most obvious and simplest way of analysis. In this case, simulations for CHT analysis are carried out as shown in Fig. 4.1, where the fluid flow solver is initially converged using isothermal wall boundary condition at the interface. Then, the wall heat flux obtained from this simulation is used to solve the solid

domain conduction solver to obtain the temperature time history at the interface for the desired time duration. This methodology thus bears the simplest initial guess and would be useful for smaller simulation times. This strategy lags in bilateral communication between solid and fluid domain since only fluid domain data is passed to the solid domain solver. So the fluid domain remains passive in these simulations. Thus it is interesting to understand the effect of change in wall temperature on the fluid domain. However, when the computations in the fluid and solid domain are carried out simultaneously using interface boundary condition as shown in Fig. 4.2, it is referred as strongly coupled analysis (SC-CHT). In this strategy, governing equations for fluid flow need to be solved with isothermal wall boundary condition in a time marching loop. Thus obtained wall heat transfer rate should be used or considered as boundary condition to solve the conduction solver for solid. In a way, outcome of this solid domain computation, which is the interface or wall temperature, remains the boundary condition for fluid domain computations for the next time marching loop. Here, the time marching of the solid domain should be carried while using the time step obtained from fluid domain. Therefore, solid and fluid domains remain in phase for all the iterations till the desired maximum time level is reached or steady state is reached. Thus, active coupling between solid and fluid domains for every iteration, justifies the name of this methodology as the strong coupling technique. Therefore this method is more elaborate and hence should be more accurate.

Larger time requirement to end the computations remains the prime requirement of strong coupling. Hence a faster computation technique with almost equal accuracy needs to be established. In view of this, the third method termed as loosely coupled CHT (LC-CHT) is as shown in Fig. 4.2. Here the governing equations for fluid flow and conduction are solved simultaneously till the residue of the fluid domain attains a preset/desired value using common time step obtained from the fluid domain. The maximum temperature in the solid domain is noted at this stage and computations in the fluid domain are terminated. Time marching in the solid domain is then continued with the increased time step till the maximum temperature of the solid domain attains a preset critical value. Pietro and Domenic (2008), during their investigations, kept the critical pre-set value as 1% of the noted maximum temperature. Attainment of this criterion re-initiates simultaneous computations of the solid and fluid domain using common time step obtained from the fluid domain. If there is no internal heat generation or presence of source of heat in the solid, then maximum temperature is expected to attain on the surface. Therefore only surface temperatures need to be monitored

to get the maximum value. Hence, maximum temperature is considered as criterion which also alters the fluid flow properties. This type of solution method, which is quasi or partially active, is known as loose coupling (LC-CHT) between fluid and solid domain computations. This methodology is expected to be a compromise between accuracy and computational cost. However investigations for this hypothesis need to be initiated to assert the immense advantage over the strong coupling due to equally accurate and more quicker computations. However, choices of all the critical variables would define the performance of this technique.

Table 4.1: Important features of CHT methodologies

Notations	Salient features
Decoupled conjugate heat transfer (DC-CHT)	- Boundary condition at the interface is isothermal uniform temperature. - Fluid domain computation is independent of solid domain.
Strongly coupled conjugate heat transfer (SC-CHT)	- Boundary condition at the interface is continuity of heat flux and identical temperature. - Fluid and solid domain computations are carried out simultaneously till the termination.
Loosely coupled conjugate heat transfer (LC-CHT)	- Boundary condition at the interface is continuity of heat flux and identical temperature. - Fluid and solid domain computations are either carried out simultaneously or only solid domain computations are performed. - Residue of the fluid flow solver and maximum temperature in solid domain are flags used for coupling and decoupling of solid and fluid domain computations.

4.3 Hypersonic Flow Over Flat Plate

The test case of hypersonic flow over flat plate is considered herein to demonstrate the necessity of bilateral active coupling. In view of this, same computational domain considered in Fig. 3.3 is used in this test case. The test conditions employed for the simulations are freestream Mach number of 9, Reynolds number of 85000 and isothermal wall temperature as 300 K. Mach contours obtained from (DC-CHT) on the fluid domain are shown in Fig. 4.3. Variation of the Mach number near the wall boundary depicts the presence of boundary layer. The leading edge weak shock in the presence of this boundary layer is clearly evident from this figure. To display the variation of thermal and hydrodynamic boundary layer, temperature and velocity profiles for their non-dimensional value are plotted in the normal direction at a location $0.01m$ from the leading edge, as shown in Fig. 4.4. Here freestream temperature and velocity are used as corresponding references for non-dimensionalisation. Velocity profile shows smooth and monotonic variation from the no-slip condition at wall to freestream velocity. However the temperature profile displays a non-monotonic variation. Near the wall, temperature initially increases from the wall conditions and reaches a maximum value which is 664.8 K in the boundary layer.

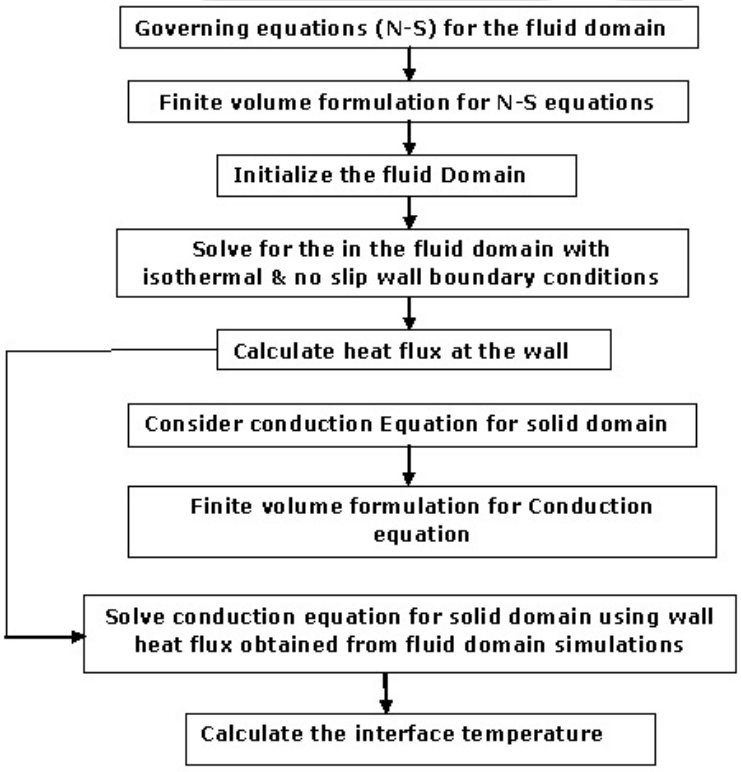

Fig. 4.1: Flow chart for decoupled conjugate heat transfer (DC-CHT) methodology.

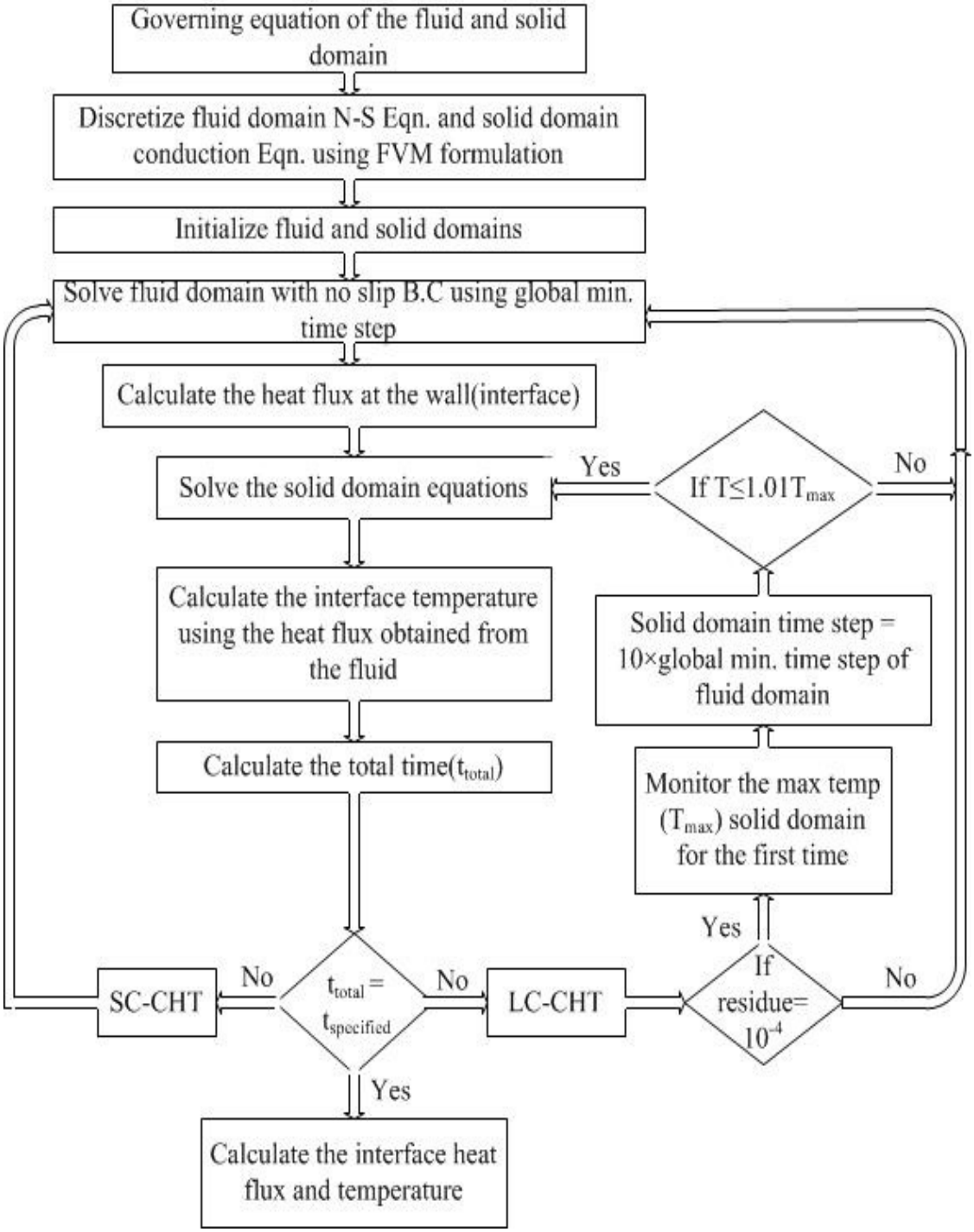

Fig. 4.2: Flow chart for coupled conjugate heat transfer (CHT) methodology.

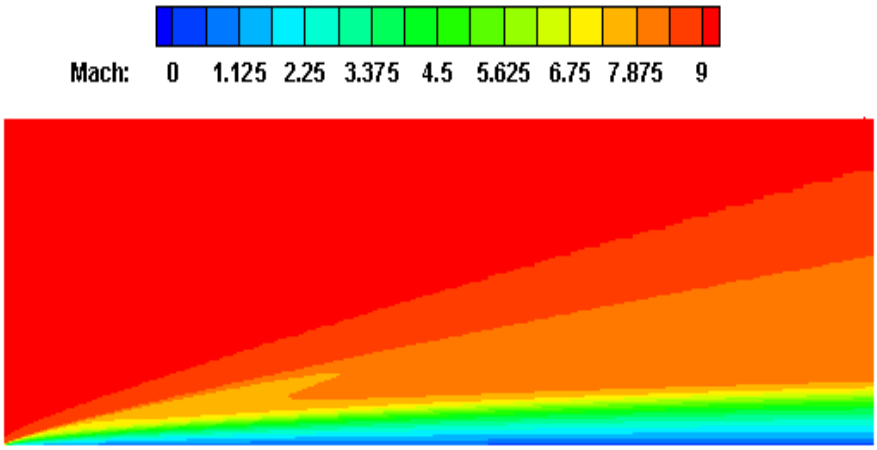

Fig. 4.3: Mach contours of fluid domain for hypersonic freestream of Mach number 9 used in DC-CHT

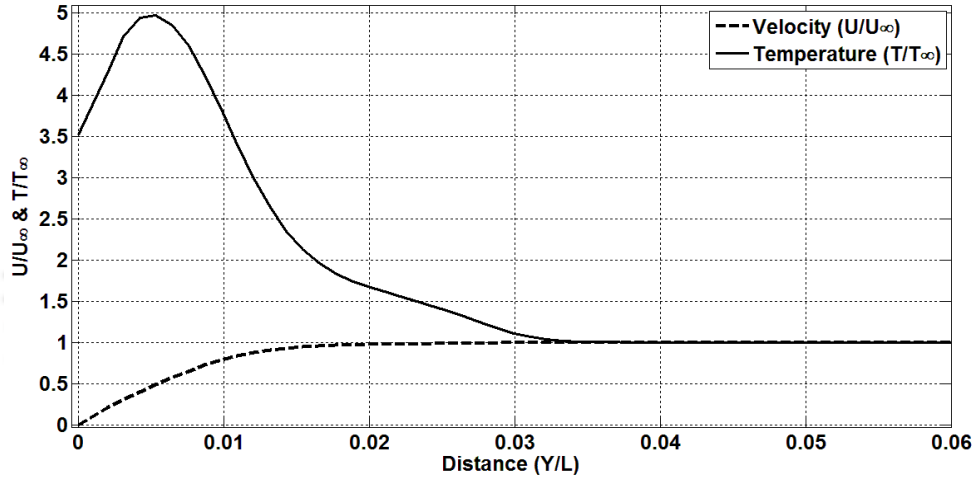

Fig. 4.4: Non-dimensional temperature and velocity profiles at x=0.01 m from the leading edge from DC-CHT.

Further decrease from the maximum value can be seen till the freestream temperature. It should be noticed here that the temperature profile attains a value inside the thermal boundary layer which is more than the wall temperature (300 K) and the freestream temperature (113 K). Frictional heating in the presence of hypersonic flow is the reason for this temperature enhancement or non-monotonic profile of temperature. This aerodynamic heating is the reason of thicker velocity boundary layer which follows the function relation Eq. (3.28) with the freestream and wall parameters. Therefore, the velocity boundary layer obtained from computations and the one from relation are plotted in Fig. 4.5. Previously encountered agreement in Fig.3.7 has also been observed here. The skin friction coefficient and Stanton number are evaluated from Eq. (3.25) and Eq. (3.27) respectively and are plotted

along with the computed values in Fig. 4.6 and Fig. 4.7 respectively. These figures also confirm the accuracy of present simulations through the encouraging agreement between analytical and computational results.

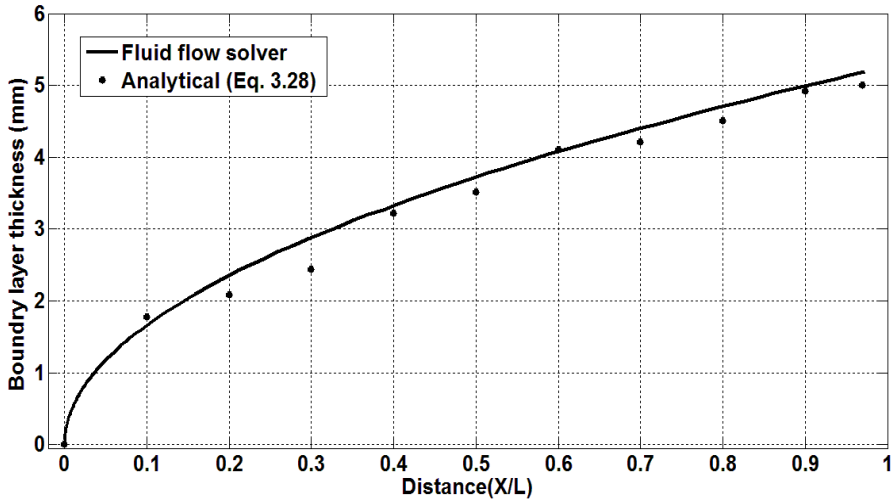

Fig. 4.5: Variation of velocity boundary layer thickness along the length of plate from DC-CHT

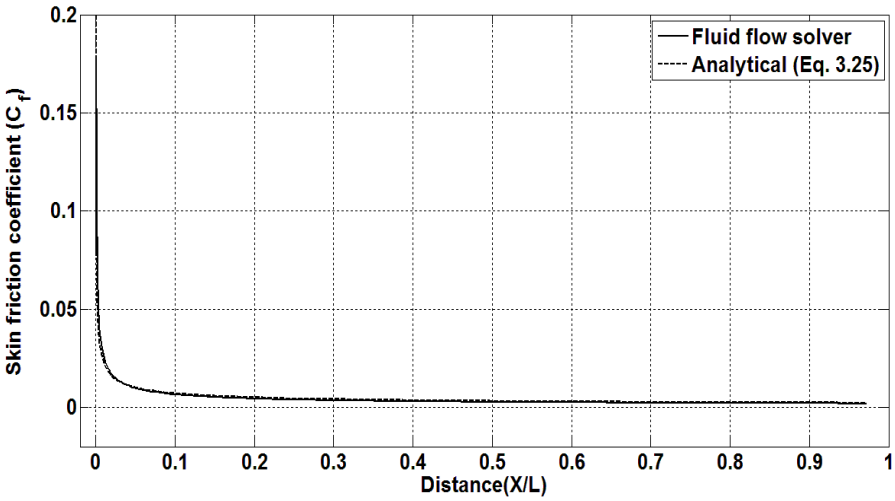

Fig. 4.6: Variation of skin friction coefficient along the length of plate obtained from DC-CHT.

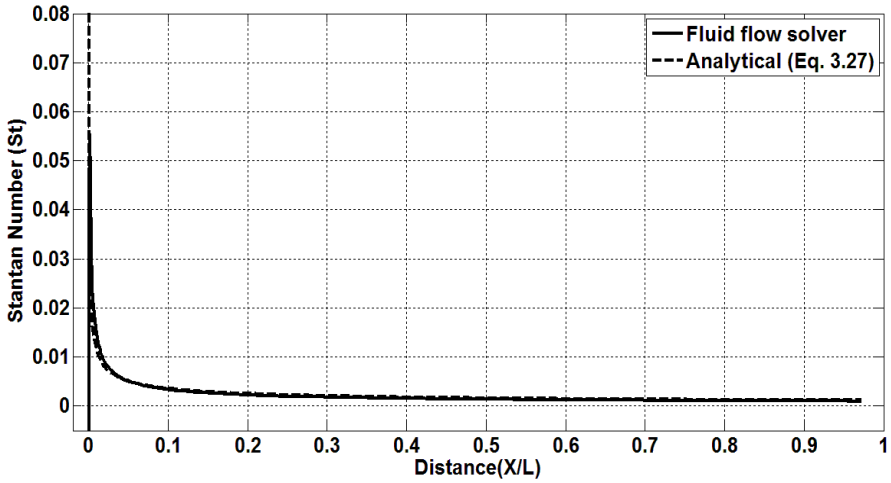

Fig. 4.7: Variation of Stanton number along the length of plate predicted using DC-CHT.

The main objective of present simulations is to conduct the heat transfer analysis between fluid and solid domains in the decoupled manner to evaluate the requirement of active coupling. Heat transfer is obtained analytically using equation below [White,1991],

$$q_{(s)} = St \times \rho_{\infty} \times C_p \left(T_0 - T_w\right) \tag{4.1}$$

$$\text{where,} \quad T_0 = T_{\infty}(1 + 0.5(\gamma - 1)M_{\infty}^2 \tag{4.2}$$

In view of this, the wall heat transfer rate given by present simulations and plotted in, Fig. 4.8. This profile forms the boundary condition for solid domain. Macor is considered as the solid material of same length of fluid domain and thickness of 5 mm. Schematic of the solid domain is same as the one shown in Fig. 3.8. During this simulation, initial solid temperature is considered as 300 K while the boundary conditions other than the heat flux are kept same as mentioned in Fig. 3.8.

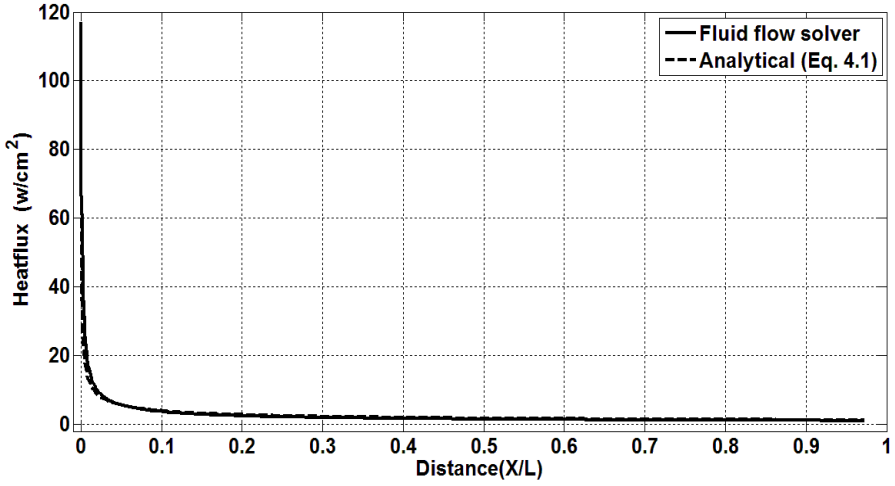

Fig. 4.8: Heat flux variation along the length of the plate obtained from DC-CHT.

The temperature contours for the solid at different time intervals are shown in Fig. 4.9. Application of non-uniform heat flux (Fig. 4.8) on the top wall has lead to non-uniform temperature variation at all the time instances. Highest temperature of 576.5 K, 740.68 K and 829.22 K has been obtained for the time instances 1s, 5s and 10s. This maximum value has been noticed at the leading edge.

(a)

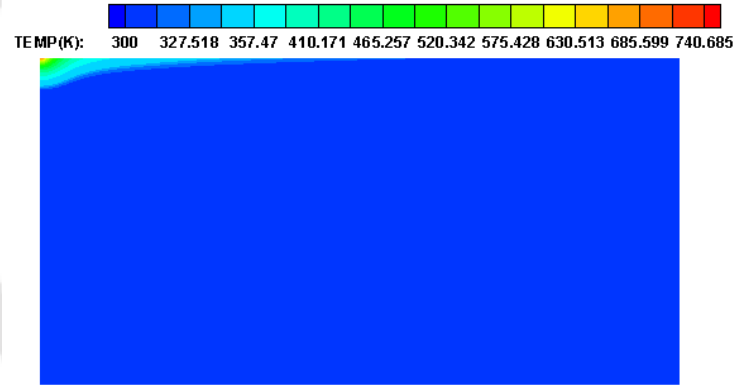

(b)

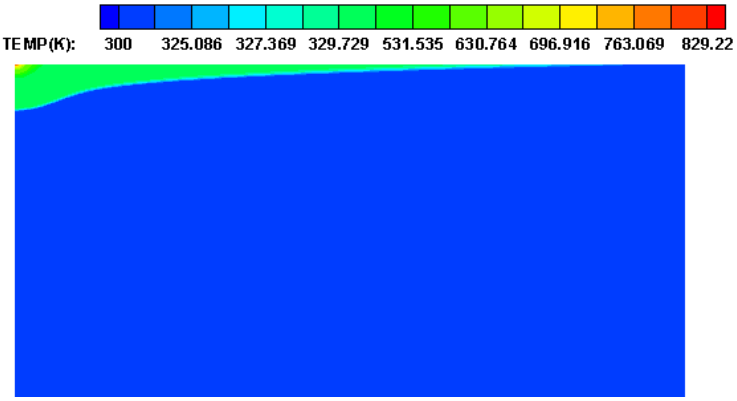

(c)

Fig. 4.9: Temperature contours at (a) 1s; (b) 5s; (c) 10s predicted using DC-CHT.

The variation of the fluid-solid interface temperature with time is as shown in Fig. 4.10. This figure also provides the evidence of higher wall temperature at the leading edge and decrement in the same towards the trailing edge. Beyond the 10% of length past the leading edge, uniform temperature of 559.2 K can be noticed at 1s. Thus the varition of temperature is only for first 10% of the length at 1s. However this length corrsponding to temperature variation increases to 20% and 40% at 5s and 10s respectively. This uniform temperature is 259.2 K, 440.685 K and 529.22 K in the increasing order of those time instances. However, this temperature variation has not been communicated to the fluid flow solver in this decoupled or uni-lateral way of heat transfer analysis. Hence the fluid properties and near wall field of the fluid domain, discussed earlier, remain frozen or independent of temperature variation in solid. In view of this, it is evident here that the leading edge non-uniform heat flux distribution would become promiment for experimental heat flux measurement mainly due to observed multidimensionality of heat transfer. Assumption of constant and uniform wall temperature, remain violated for long duration testing.

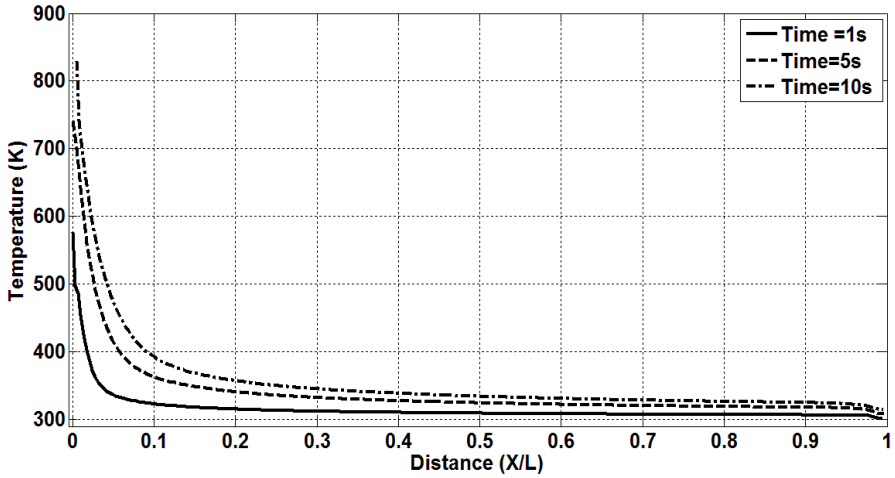

Fig. 4.10: Temperature distribution along the solid-fluid interface predicted using DC-CHT.

To ascertain this fact, temperature time history at three location on the plate are plotted in Fig. 4.11. Distances of these locations from the leading edge are X_1=0.003276 m, X_2=0.0107241 m and X_3=0.086035 m respectively**.** This figure re-asserts the earlier observation of higher temperature rise towards the leading edge due to higher heating rates and lower temperature rise downstream due lower heating rates. Temperature time history based on one dimensional heat transfer assumption, given by Eq. (3.20), is also plotted in the same figure based on corresponding heating rates. It is clear here that the one dimensional and two dimensional temperature traces show equivalence for locations X_2 and X_3. Almost

uniform heating rates in the neighborhoods of these locations are the major reason for those observations. This uniformity of surface heating rates in downstream locations observed in Fig. 4.8 forces one dimensionality. Therefore the temperature rise obtained from one dimensional assumption and two dimensional simulations show good agreement with each other. Moreover at the leading edge, strongly non-uniform heating rates provide sufficient internal temperature gradient along the x-axis which in turn leads to discrimination in temperature traces. In all, these simulations confirm the necessity of active or bi-lateral coupling between solid and fluid domain for accurate prediction of surface variations.

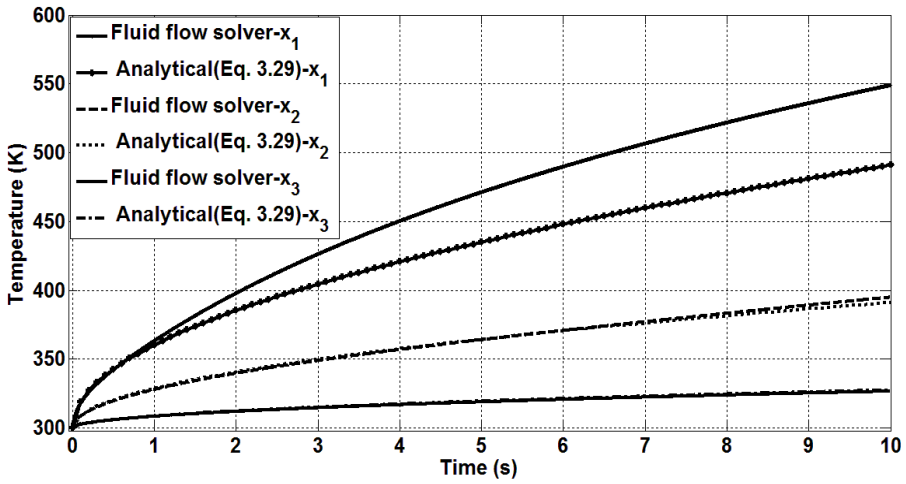

Fig. 4.11: Temperature traces at various locations predicted using DC-CHT.

4.4 Summary

Various coupling techniques are incorporated in the present solver. These techniques include strong and loose couplings between fluid flow and heat conduction solvers. The decoupled method of heat transfer analysis is also available with the present solver. In view of this, hypersonic flow over flat plate is simulated for freestream Mach number 9.0. The resulting heat transfer rates are given as boundary condition for conduction solver. The temperature contours of solid domain and the temperature traces at different locations clearly showed the necessity of multidimensional active coupling between fluid and solid domains for accurate prediction of surface properties. Moreover the decoupled analysis, although bears lesser computational cost, is found to have limitation in the presence of non-uniform surface heating rates. This observation demands for the application of strong and loose coupling techniques for heat transfer analysis.

CHAPTER 5

CONJUGATE HEAT TRANSFER STUDY IN HYPERSONIC FLOW OVER A FLAT PLATE

5.1 Preface

Higher surface heating rate is the major design constraint in hypersonic flow regime. Hence prediction of wall heating rates is always a challenging task for the design engineers. Flight testing or ground based testing are the two possible avenues apart from the computational means to achieve the required objectives. However either of these experiments is costly and hence prior ground work is essential for design of these experiments. Therefore, dedicated pre-processing for the actual experiments includes choice of thermal sensor, prediction of strength of signal, optimization of sensor location to capture the physical phenomenon and best data acquisition settings. In view of reduction of experimental cost, conjugate heat transfer analysis can be performed to simulate the experimental heat transfer measurement. Simulations carried out for such application would be very useful to get the strength temperature signal based on its location, appropriate location of thermal sensor and effective data acquisition setting. Establishment of this procedure would in turn reduce the experimental cost by enhancing the success rate of the experiments.

In view of the afore said advantage , CHT studies are planned to demonstrate a typical heat transfer measurement from acquisition of the temperature signal to the post processing of the same to get the heat transfer rate signal. This demonstration is planned for the test case of hypersonic flow over finite thickness flat plate. Various locations on the plate are considered here to extract the temperature signals which in turn represent the thermal sensor locations. Such considerations provide the necessary input to the experimentalist as change in strength of the temperature signal due to change in location. The wall material change has also been incorporated during these studies which accounts for the choice of different model materials and also the materials used for fabricating the thermal sensor. Variation of freestream Mach number is also part. To account for change in strength of the temperature signal at a location due to change in freestream conditions is the objective behind this parametric variation. These simulations are carried out for the duration of 1 ms pertaining to shock tunnel test duration. Coupled and decoupled strategies are employed for these simulations. The temperature signals are then used to recover the heat flux using the

techniques discussed in Chapter 2. Therefore, the adopted computational strategy can completely imitate the heat transfer rate measurement experiments. Simulations are also performed on the same configuration for larger duration of 0.1 ms to understand the effect of wall heating on the fluid domain.

Simulation for heat transfer measurement experiments using conjugate heat transfer methodology is the central theme of this chapter. Coupled and decoupled CHT techniques are used to demonstrate this theme for hypersonic flow over finite thickness flat plate. Both the strategies are seen to be equally useful for prediction of local temperature and heat flux signals for short duration experiments (~1ms). Effect of wall property variation on the fluid flow has also been studied for comparatively large time scale (~0.1s) using loosely coupled CHT technique. Thermal boundary layer and velocity boundary layer thicknesses are used to understand the interaction between wall heating and hydrodynamic boundary layer. Details of the test case, boundary conditions and results are discussed in the following sections.

5.2 Computational Methodology for CHT studies

The conjugate heat transfer analysis for the hypersonic flow over a flat plate involves both fluid as well as solid domain. Typical computational domain describing the boundary conditions is given in Fig.5.1. The plate of length 100 mm and thickness 5 mm has been considered as the solid domain. The methodologies of coupled and decoupled CHT analysis explained in earlier chapter are used for present studies. Stretched grid is used at the interface in fluid as well as solid domains to compute the interface fluxes correctly. Mesh independence studies have been performed and the final mesh size is selected as, 300x250 for fluid domain and 300x180 for the solid domain. Details of these results are mentioned in the following sections.

5.2.1 CHT simulation for short time scale applications (shock tunnel)

Strongly coupled and decoupled conjugate heat transfer analyses have been carried out for different freestream conditions pertaining to typical test conditions of a shock tunnel (Kulkarni et al. 2010). Freestream Mach numbers considered for the present studies are 6, 7 and 8 with Reynolds number of 85,000 while the freestream temperature and the initial wall temperature are taken as 113 K and 300 K, respectively. Wall materials such as Macor, aluminum and silicon carbides (SiC) are chosen for the solid domain. The major reason for this choice is that these materials are most commonly used either as backing materials for making thermal sensors or for model making during ground testing experiments. The

properties of these wall materials used are given in Table 5.1 while the notations used in the subsequent figures are mentioned in Table 5.2. All the simulations are performed for 1ms time-scale which corresponds to the duration of experiments in the high enthalpy impulse facilities.

Table 5.1: Material properties used in the simulation by (Holman, 1989)

Material	Thermal conductivity (k) $(W/m.K)$	Density (ρ) (kg/m^3)	Specific heat (C) $(J/kg.K)$	Thermal diffusivity $(k/\rho C)$ (m^2/s)
Aluminum	204	2704	896	8.4×10^{-5}
Silicon Carbide(SiC)	120	3100	750	5.1×10^{-5}
Macor	1.46	2520	790	7.3×10^{-7}
D	204	1000	10	2.04×10^{-2}
E	1.46	1000	10	1.46×10^{-4}
Thermal Insulation	0.0258	73.0	729	4.8×10^{-7}

Table 5.2: Notations used in figures

Notations	Remarks	Notations	Remarks
SC-CHT	Strongly coupled CHT	B	Aluminum
DC-CHT	Decoupled CHT	C	Silicon carbide (SiC)
LC-CHT	Loosely coupled CHT	D	Arbitrary Material 1
Eq. (2.10)	Piece-wise linear fitting	E	Arbitrary Material 2
Eq. (2.12)	Polynomial fitting	F	Thermal Insulation
Eq. (2.15)	Cubic-spline method	x_1	Location 0.3mm from the leading edge
A	Macor	x_2	Location 3mm from the leading edge

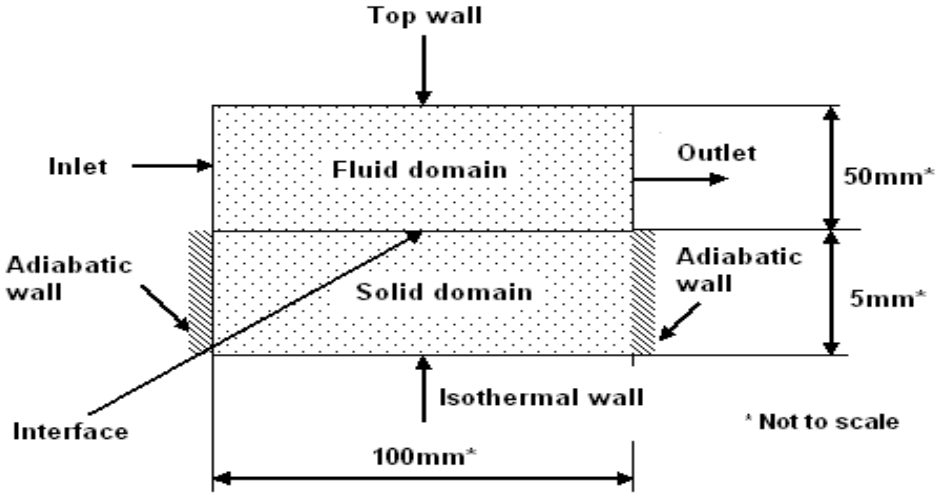

Fig. 5.1: Schematic diagram of computational domain for CHT analysis.

Temperature histories for two locations on the plate, viz. 0.3 mm and 3 mm from the leading edge of Macor plate, are shown in Fig. 5.2 for freestream Mach number 6.0. The temporal variation of heat flux at these locations of the plate is also shown in Fig. 5.3. It is seen here that prediction of temperature and heat transfer signals from both the methodologies are in good agreement with each other for both the locations. Similar matching of the heat flux history can be expected since prediction of temperature rise and rate of temperature are same for both the locations by both the methods. As seen in Fig. 5.3, location x_1 represents higher value of heat flux in comparison with location x_2 since boundary layer thickness at this location is comparatively lower. It attributes a higher rise in surface temperature of around 7.5 K (as seen in Fig. 5.2) during simulation time of 1ms, at location x_1.

Surface temperature history obtained from strongly coupled and decoupled CHT solvers at x_1 for freestream Mach number 6 with different wall materials is shown in Fig. 5.4. For all the cases, both the CHT techniques have predicted similar trend and magnitude for the temperature signal. Temperature rise of 7.5 K has been observed with Macor as wall material while the same is 0.15 K with Aluminum and 0.25 K Silicon carbide (SiC) as wall materials. Higher temperature rise with Macor is accounted due to its lower thermal diffusivity. Heat flux obtained from coupled and decoupled CHT solvers at location x_1 for the same freestream condition in case of three wall materials is also shown in Fig. 5.5. Here, it should be noted that the heat flux obtained from the decoupled CHT method is necessarily through the fluid flow solver with isothermal wall boundary condition and thus it is independent of the wall material. Moreover, one can predict the heat flux for different wall material using coupled CHT solver. However, thus computed time history of wall heat flux for location x_1 is seen to be constant and same for different wall materials for the simulation time of 1ms. Surface variation of heat flux at the end of simulation represented by Stanton number and expressed by Eq. (5.1) is also plotted in Fig. 5.6 for all the materials.

$$s_t = \frac{q_t}{\left\{\rho_\infty u_\infty [C_p (T_0 - T_w)]\right\}} \tag{5.1}$$

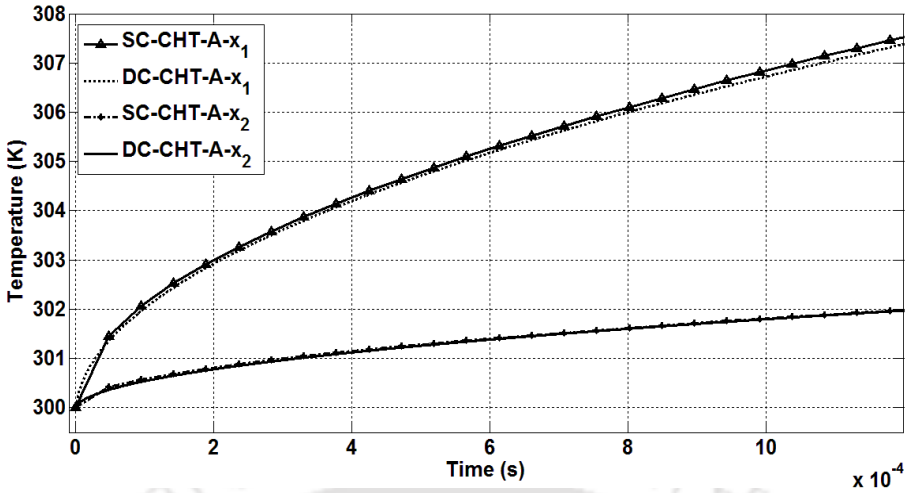

Fig. 5.2: Predicted temperature traces at locations close to the leading edge with freestream Mach number of 6.

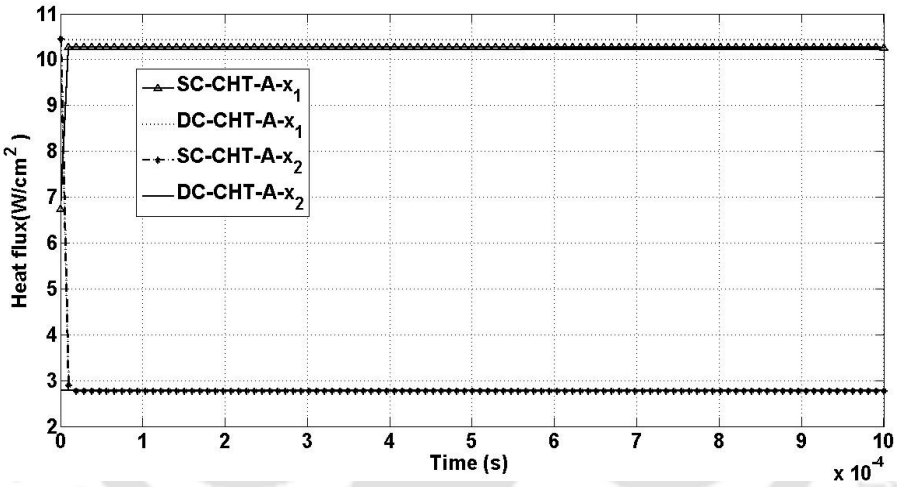

Fig. 5.3: Variation of Surface heat flux with time at locations close to the leading edge with freestream Mach number of 6.

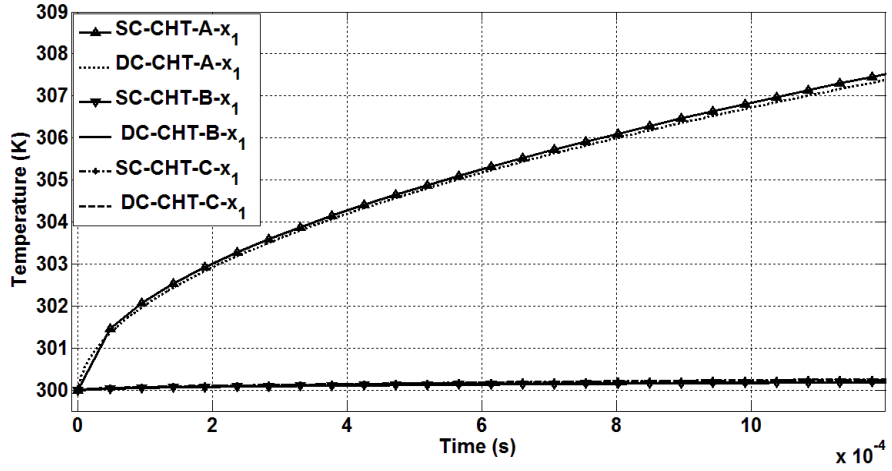

Fig. 5.4: Comparison of surface temperature rise at location x_1 =0.33 mm for three different materials at Mach 6 conditions.

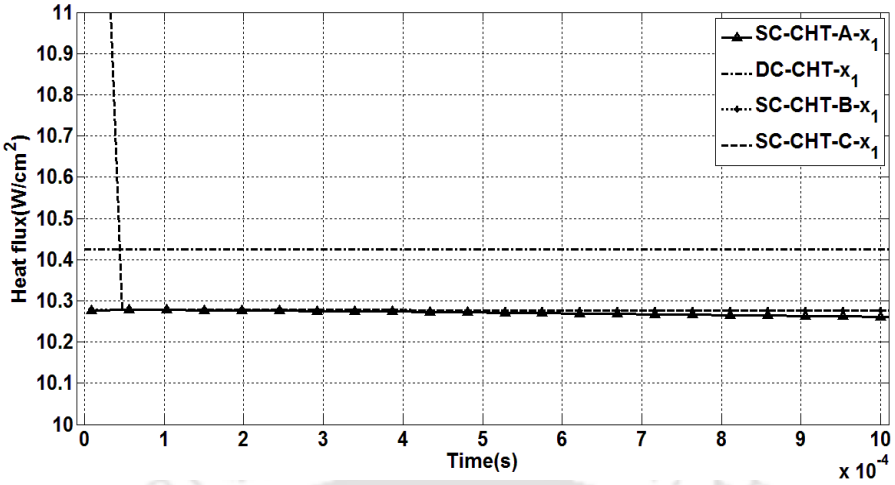

Fig. 5.5: Comparison of surface heat flux at location x_1 =0.33 mm for three different materials at Mach 6 conditions.

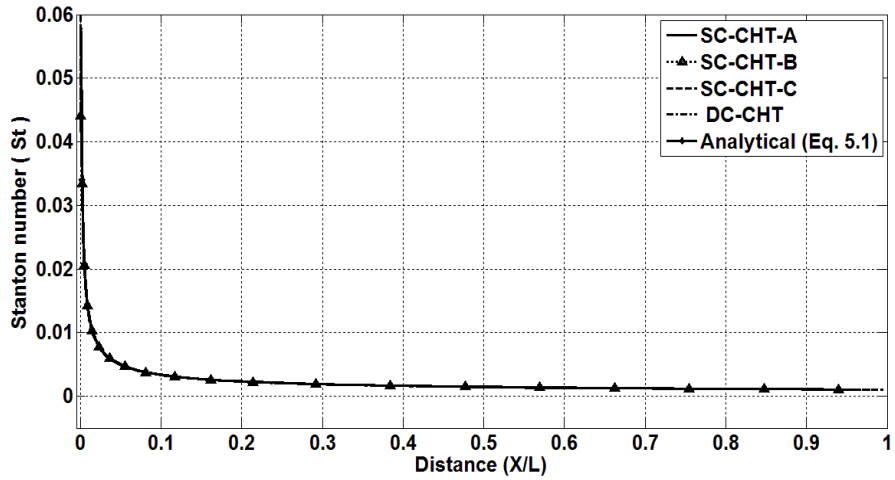

Fig. 5.6: Stanton number variation along the length of the plate.

This figure also includes the theoretical variation for the surface heat flux along the length of the flat plate for hypersonic freestream conditions [Anderson, 2006]. From this figure it can be concluded that any technique, either coupled or decoupled way of heat transfer analysis, can be used to infer the transient temperature and heat fluxes for the simulation time of 1ms, which is typical run time of any short duration impulse facilities. Further comparisons of temperature and heat flux history for freestream Mach numbers 7 and 8 with Macor as wall material has also been estimated for location x_1 in Figs. 5.7 and 5.8. These figures show a clear agreement between the predictions made from coupled and decoupled CHT solvers. Increase in local wall heat flux with increase in freestream Mach number is clearly evident because of higher temperature rise. Heat flux which is 1.042 x 10^5 W/m^2 for Mach 6 flow conditions increases by 61% for Mach 7, while the same increases by

1.5 times for Mach 8 conditions. The major reason for this enhancement is the increase in total enthalpy of the flow due to increase in freestream Mach number for the same freestream static temperature.

The heat flux recovery techniques discussed in Chapter 2 are considered herein to post process the temperature signals obtained from both the CHT strategies. Since coupled as well as decoupled methodologies are seen to be useful for temperature and heat flux prediction, an attempt has been made to recover the time history of surface heat flux from the know temperature history and wall material properties using the established techniques. Heat flux recovered for location x_1 is shown in Fig. 5.9 for freestream Mach number 6 for Macor as wall material. Heat flux signals recovered using the reported techniques are seen to be in good agreement with the heat flux predicted using coupled and decoupled CHT methodologies.

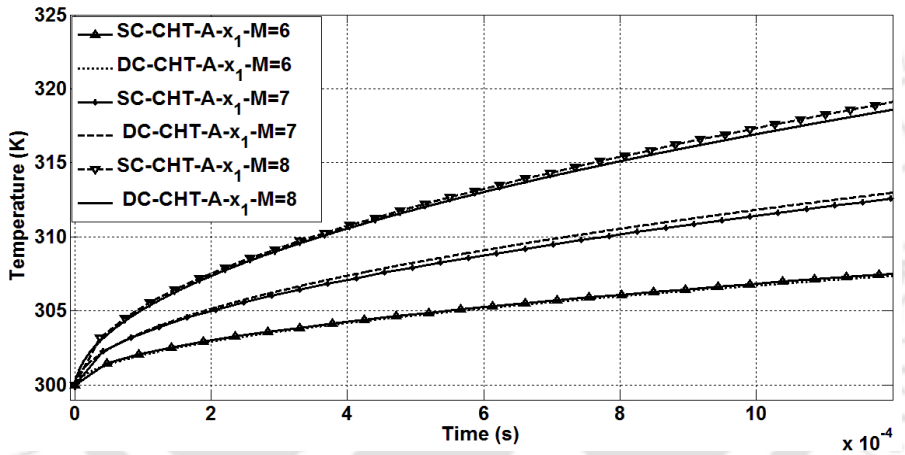

Fig. 5.7: Comparison of surface temperatures at location x_1=0.33 mm for different Mach numbers.

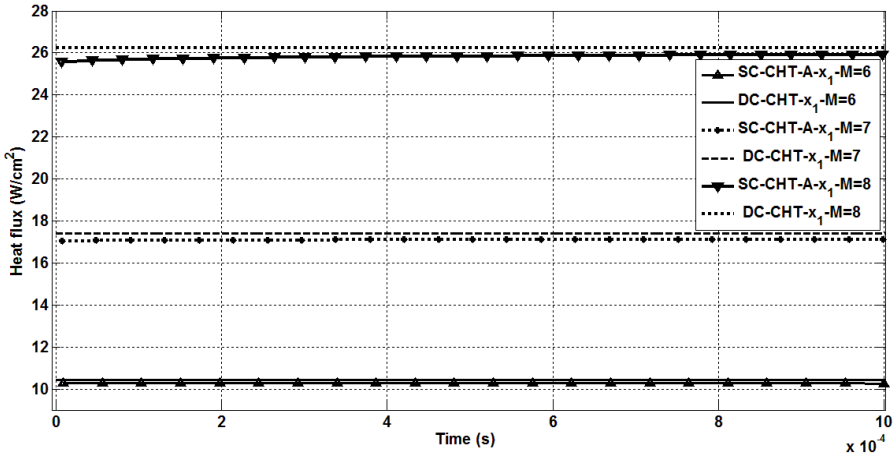

Fig. 5.8: Comparison of Surface heat flux at location x_1=0.33 mm for different Mach numbers.

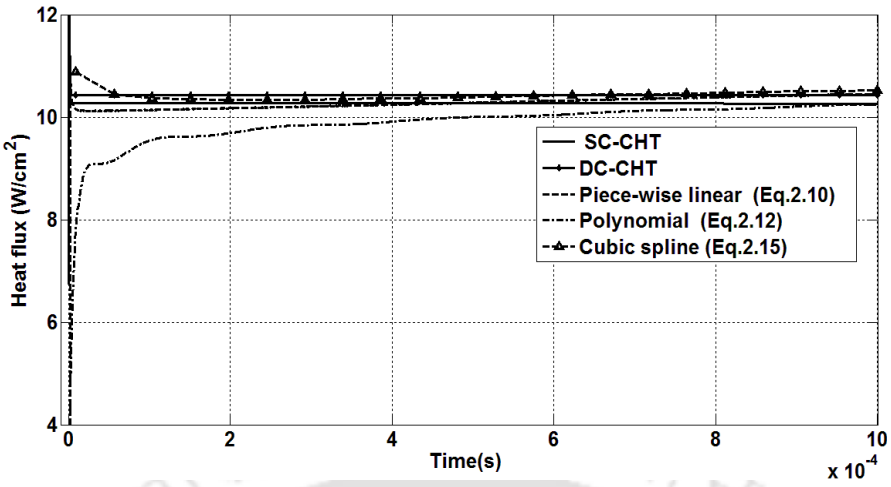

Fig. 5.9: Surface heat flux recovered by various methods for the location x_1=0.33 mm at Mach 6 with Macor as wall material.

The recovered heat flux signal has assumptions like unidirectional heat transfer and semi-infinite depth of the backing material. The encouraging match among the heat flux signals necessarily portrays two things. First one is about the depth of the plate which is seen to be much higher than the depth of penetration of heat in the experimental duration. Second one is uni-directionality of the heat transfer in the solid which is evident from the match among the two dimensional computations and heat flux recovery from literature reported techniques with uni-directional assumption. It can also be viewed that, the depth of heat penetration in the plate, for the non-uniform surface heat flux distribution, is very small so that the heat transfer in the solid can be treated locally along the depth of the plate. Complete solid domain has been observed to be undisturbed by retaining the initial temperature in both the techniques. Hence it is evident here that, the assumption of semi-infinite depth of the backing material which leads to uni-direction heat transfer, is appropriate pertaining to very small test duration. Therefore, this figure reasserts the benefit of coupled and decoupled techniques for design of shock tunnel heat transfer measurement experiments by verifying the associated assumptions.

5.2.2 CHT simulation for large time scale applications

CHT studies are also carried out for the test conditions of free piston shock tunnel experiment. These conditions are as Mach number 9.2, pressure 690 Pa, temperature 155 K and initial wall temperature is 300 K (Samuel and John, 1995). The wall materials used for these studies are non-real. The properties of those materials used in the present investigations are given in Table 5.1. All the simulations are performed for a maximum duration of 0.1s.

The major objective of this study is to analyze the effect of aerodynamic heating on fluid domain and associated change in the same with change in wall material. The configuration shown in Fig. 5.1 is employed for this study. These computations are carried out using loosely coupled CHT technique.

The temperature and velocity profiles, at selective locations, in the fluid domain along with the temperature contour in case of material 'E', for 0.01s and 0.1s, are shown in Figs. 5.10-5.11 respectively. Streamwise increase in velocity boundary layer and thermal boundary layer thicknesses is evident in both the cases. Apart from this, velocity boundary layer can be seen always thinner than the thermal boundary layer. These figures clearly demonstrate the presence of large velocity and temperature gradients at the wall which decrease in the direction of flow. In line with this, higher value of heat transfer rate is expected at the leading edge of the plate in comparison with the same at downstream location. As a result of this, highest wall temperature of 1057 K for 0.01s and 1544.9 K for 0.1s are noticed at the leading edge. Thus these figures display enhancement in maximum temperature by 2.5 times (252.3%) for 0.01s and 4.14 times (414.9%) for 0.1s from its initial value (300 K). It is also evident from these figures that the heat which penetrated for ~9% of the depth of solid domain in 0.01s has disturbed 26.3 % of the solid domain in 0.1s.

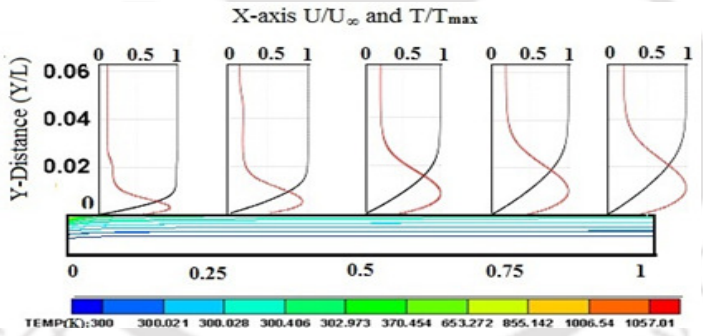

Fig. 5.10: Temperature and velocity profile along the length and temperature contour at time=0.01s for wall Material E.

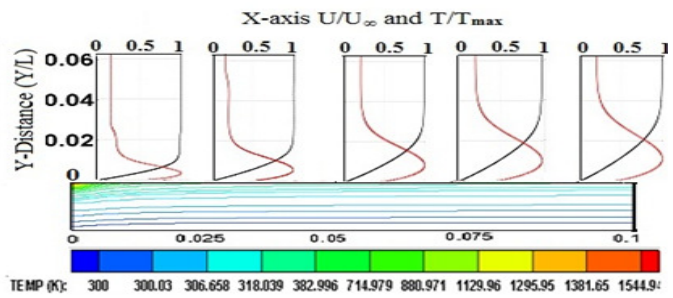

Fig. 5.11: Temperature and velocity profile along the length and temperature contour at time=0.1s for wall Material E.

Quantitative variation of thermal and velocity boundary layer thicknesses along the length of at the end of simulation (0.1s) are plotted in Fig. 5.12. Here thermal and velocity boundary layer edges are considered where the flow variables attain 95% of their freestream value. Precise values of the thicknesses can be obtained from this figure. Here, relative comparison of thickness shows that the hydrodynamic or velocity boundary layer has around 30% less thickness than the thermal boundary layer.

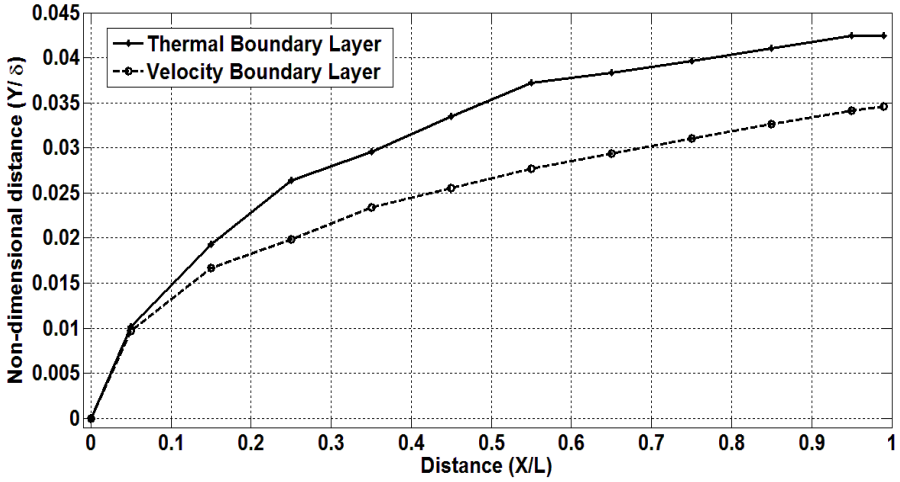

Fig. 5.12: Variation of thermal and velocity boundary layer along the plate of Material E.

The variation in temperature and velocity profiles at locations 0.01m and 0.09 m from the leading edge, for various time levels of CHT simulations, are as shown in Fig. 5.13 – 5.16. The temperature profiles shown in Fig. 5.13 and Fig. 5.14 portray inversion in trend. The temperature of the fluid increases in the normal direction to wall and attains a maximum. Upon this maximum, temperature decreases and reaches to the freestream value. Such profile is commonly experienced for isothermal cold wall conditions of conventional CFD. In the same figure, temperature profile for the adiabatic wall condition in conventional CFD shows monotonic decrease from wall temperature to the freestream value. Hence the maximum temperature point remains at the wall for adiabatic case which is 2480 K for both the locations. The maximum temperature obtained from CHT studies for 0.01 m case is 960 K and 1024 K corresponding to 0.01s and 0.1s while the same is 850 K and 875 K for 0.09 m respectively. Thus, the maximum temperature in the thermal boundary layer at 0.01 m increases by times 2.2 (220%) initially for 0.01s and then by 2.41 times (241 %) for 0.1s from its base value corresponding to isothermal simulation. The increment for the maximum temperature corresponding to same time intervals is 1.8 times (183%) and 1.91 times (191%) for 0.09 m location. Thus increase in maximum temperature is more towards the leading edge. Moreover temperature at all locations increases with time in the presence of Material

'E'. It's effect on velocity profiles is shown on Fig. 5.15 and 5.16. Besides, thicker velocity profile at any time instance, as an indication of higher boundary layer thickness at 0.09 m in comparison with the same at 0.01, is evident from those figures. The leading edge shock which is clear in the velocity profile near to the edge (Fig. 5.15) has been observed in temperature profile as well (Fig. 5.13). However shock is seen to be absent in the downstream station as shown in Fig. 5.16. As observed earlier, increase of velocity boundary layer thickness downstream of the leading edge is also clear from Fig. 5.15 and Fig. 5.16. Apart from this, inflation of the velocity profile with time is observed as its characteristic feature. This inflation can be accounted to the enhanced temperature at all locations. Such temperature increment increases the viscosity which in turn increases the boundary layer thickness. Therefore the expected increment in boundary layer thickness with time at various locations is plotted in Fig. 5.17. This figure clearly demonstrates the role of wall material 'E' in the boundary layer thickness increase which is around 29% at 0.01 m and 20% at 0.09 m from the leading edge in comparison with the conventional isothermal wall boundary condition.

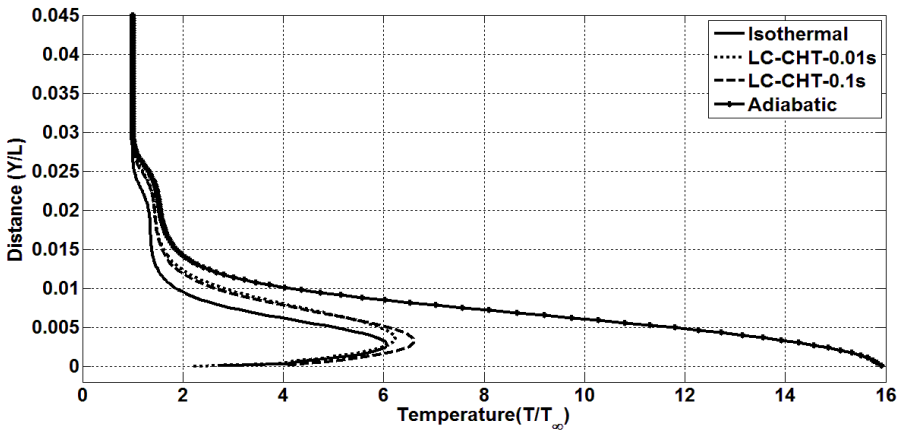

Fig. 5.13: Temperature profile normal to the wall at x=0.01 m for 'E' as wall material.

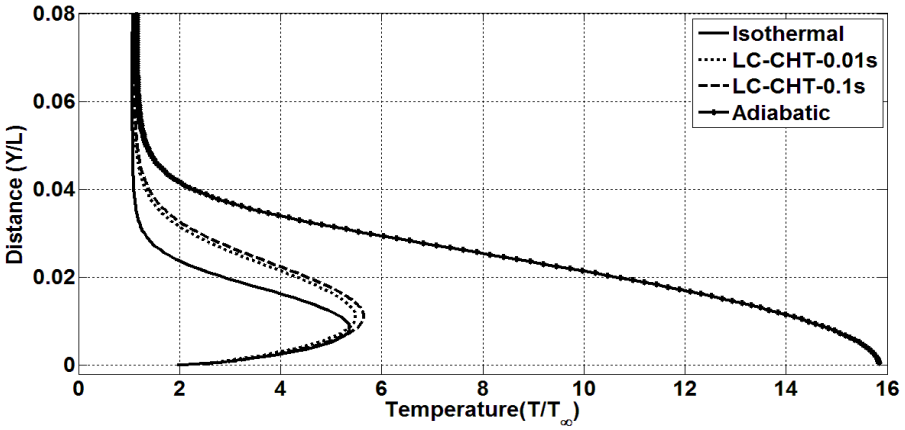

Fig. 5.14: Temperature profile normal to the wall at x=0.09 m for 'E' as wall material.

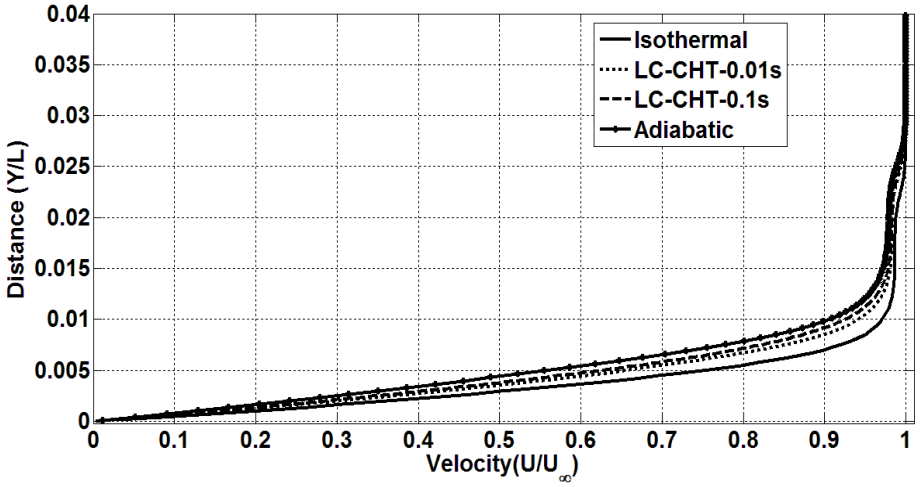

Fig. 5.15: Velocity profile normal to the wall at x=0.01 m for 'E' as wall material.

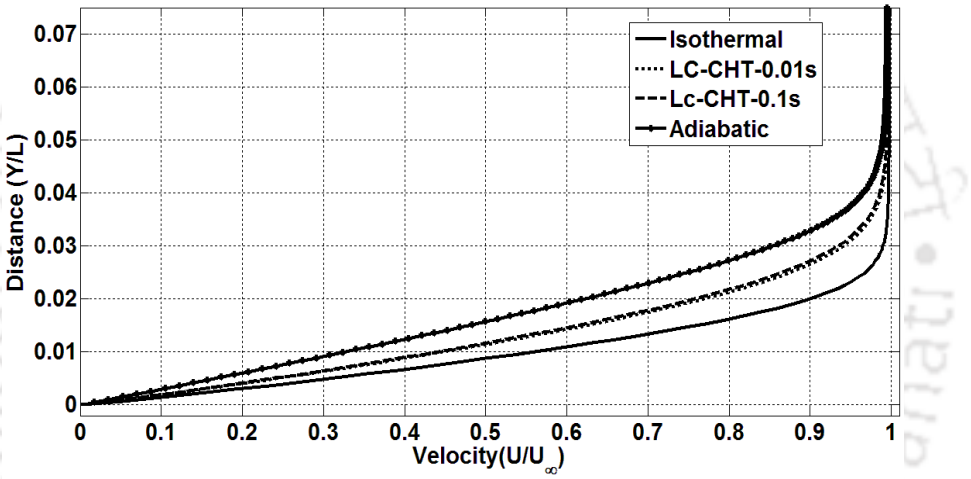

Fig. 5.16: Velocity profile normal to the wall at x=0.09 m using 'E' as wall material.

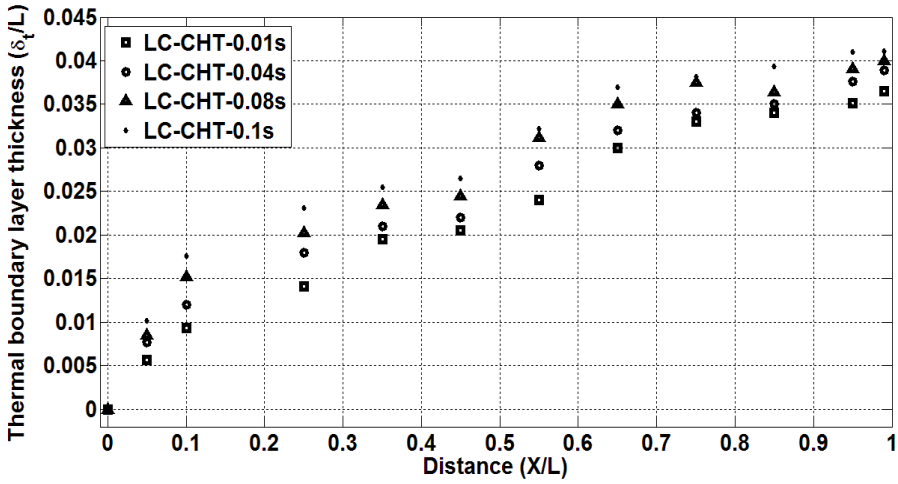

Fig. 5.17: Thermal Boundary Layer along the flat plate at various times scales of CHT studies using 'E' as wall materials.

Similar exercise has also been performed for the wall material D. As a result of this, the thermal boundary layer thickness at various streamwise locations is plotted in Fig. 5.18 for various time instances. No significant alteration in thermal boundary layer thickness is evident from this figure. Similar observation has been drawn for the velocity boundary layer thickness. Therefore material 'D' is seen to have lesser effect on the fluid flow in the duration of 0.1s. Two orders of higher thermal diffusivity in comparison with material E is the major reason for this disparity. The thermal and velocity boundary layers are plotted for all the wall conditions in Fig. 5.19 and Fig. 5.20 respectively. Here, adiabatic wall boundary condition corresponds to highest thermal and velocity boundary layer thicknesses while the minimum corresponds to the isothermal (300 K) wall boundary conditions. These figures reassert the advantage of CHT over the conventional CFD which corresponds to extreme wall boundary conditions.

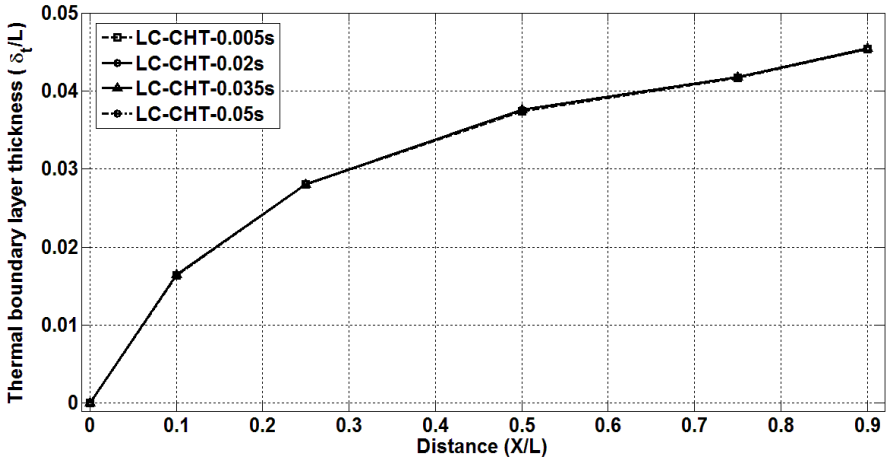

Fig. 5.18: Thermal boundary layer along the flat plate at various times scales of CHT studies using 'D' as wall materials.

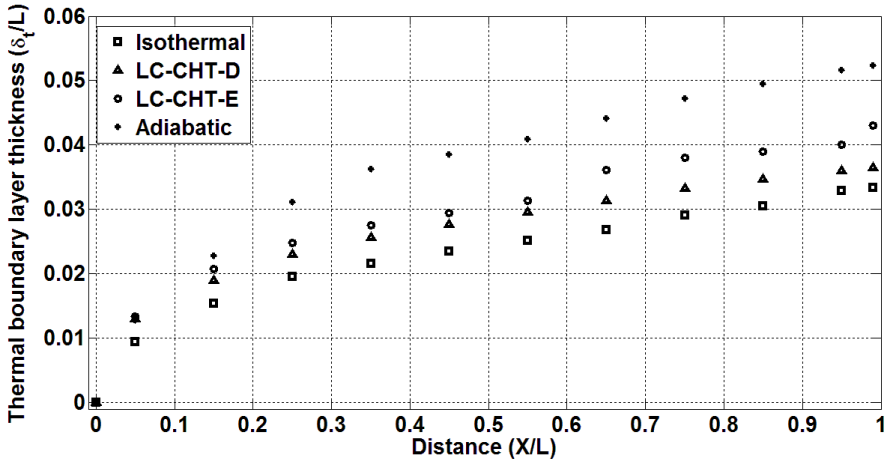

Fig. 5.19: Thermal boundary layer thickness along the flat plate using various wall materials.

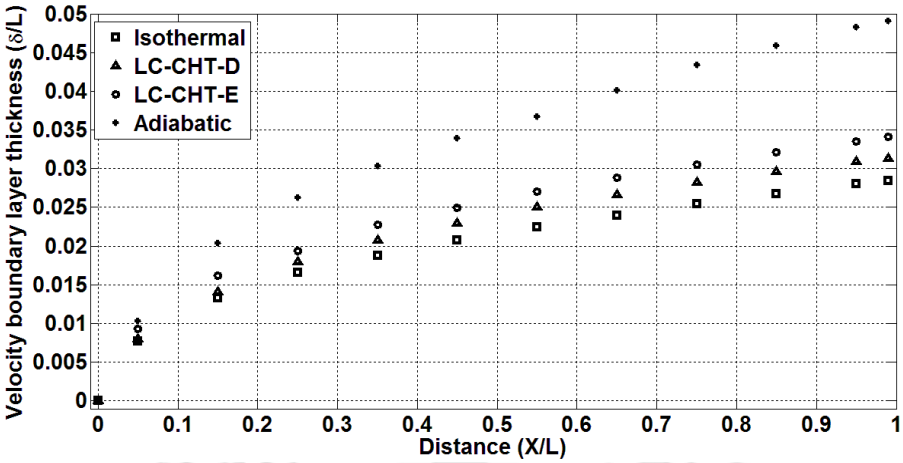

Fig. 5.20: Velocity boundary layer along the flat plate using various wall materials.

The CHT based boundary layer thicknesses are seen to be placed between the extreme wall conditions. Apart from this, the thicknesses approach the adiabatic wall condition from their initial value of isothermal wall with increase in time. Boundary layer thickness is higher for material 'E' due to its lower thermal diffusivity in comparison with the material 'D'. Change in wall properties for different wall conditions at time instance of 0.1s are plotted in Fig. 5.21 and Fig. 5.22. Presence of wall material is seen to have lesser impact on the heat flux at the leading edge which otherwise decreases slightly towards the trailing edge. Major change has been noticed in skin friction coefficient which increases in case of finite thermal conductivity. Increase in viscosity with temperature is seen to dominate the decrease in velocity gradient for increment of wall shear. Therefore higher wall shear at all locations is the result of presence of wall material.

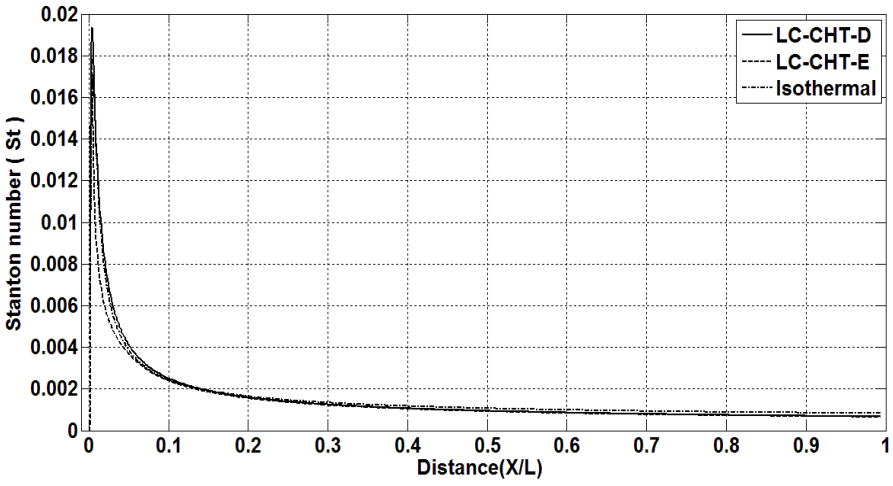

Fig. 5.21: Stanton number along the length of the plate.

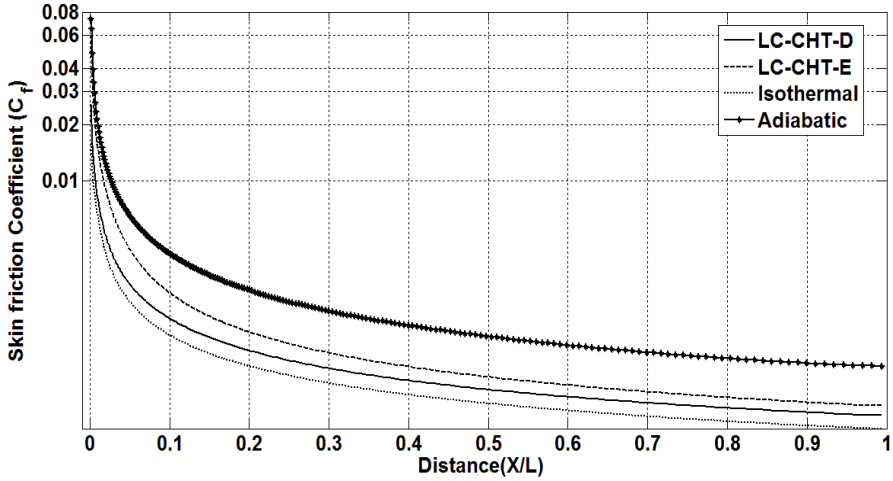

Fig. 5.22: Variation of skin friction coefficient along the length of the plate.

5.3 Summary

Flow over finite thickness flat plate has been studied successfully using all the coupling techniques. Initially these CHT studies are performed to imitate the heat transfer rate measurement for short test duration of 1ms which relates with shock tunnel testing. Decoupled strategy is found equally effective as the strongly coupled technique to employ for simulating the heat transfer rate measurement. Usefulness of such simulations is thus demonstrated for designing the experiment which in turn would be useful for selecting the sensor and its mounting location along with data acquisition settings. Extended study using loosely coupled CHT technique on the same configuration showed significant effect of wall material on the fluid flow at moderately large time scales. This effect is noticed to be dependent on thermal diffusivity of the wall material. Material with lower thermal diffusivity is found to get disturbed more keeping the fluid domain relatively undisturbed. In line with this, the material with lower diffusivity is noticed to alter the boundary layer thickness and interface properties with lesser heat penetration in itself.

CHAPTER 6

CONJUGATE HEAT TRANSFER ANALYSIS FOR A FINITE THICKNESS CYLINDER IN A HYPERSONIC FLOW

6.1 Preface

Presence of high temperature decelerated fluid in the vicinity of the spacecraft is major concern for hypersonic flights. Higher surface heating rate is the drawback of this incidence. However, the stagnation point heat transfer rate is inversely proportional to the square root of bluntness radius. Therefore hypersonic vehicles are invariantly configured as blunt nosed to reduce the surface heating rates. In view of this, blunt nosed configurations are invariantly considered for understanding the external aerodynamics in hypersonic flow regime. Prediction of wall heating rates and surface temperature remains as the central theme for such investigations. Flat plate has been considered in earlier chapter for similar objective. However the downstream surface heat flux uniformity introduces the limitations on the conclusions as specific to those studies. Therefore cylindrical geometry is the most eligible configurations to undertake such studies. Formation of strong bow shock ahead of the cylinder and larger surface property variation are the major reasons for cylinder to be a choice for simulation. Apart from this, all the coupling techniques implemented in the solver can be assessed for their implementation and computational cost for heat transfer studies for a finite thickness cylinder. This examination of the coupling techniques is essential to correlate the usefulness of a particular coupling technique and maximum simulation time. Outcome of such studies is helpful to build the compromise between computational cost and accuracy. In view of this literature reported configuration and test conditions are considered for present studies.

The present chapter addresses the conjugate heat transfer analysis of hypersonic flows over a thick cylinder. These studies mainly focus on defining a computationally cheaper CHT algorithm for the above mentioned application. Since prediction of the surface heating rates and temperature is of prime importance for the hypersonic applications, CHT studies are carried out by adopting various coupling techniques to examine their implementation abilities. Three types of solution methodologies are adopted, namely, decoupled, strongly coupled and loosely coupled analysis. The study also focuses on the effect of hypersonic flow field on wall heat flux for a finite thickness insulating cylinder at moderately large time

scales. Increase in wall temperature and decrease in surface heat flux have been noticed by using strong and loose coupling techniques when simulation time is increased. Decoupled fluid and solid domain analysis is found to be useful for typical shock tunnel test durations (~1ms) while investigations with loose coupling technique are advisable for time scales corresponding to flight testing (~1s). Efforts are also made to reason the discrimination in prediction of stagnation point heat flux using conventional computational and experimental analysis.

6.2 Computational Strategy for Finite Thickness of Cylinder

The present CHT solver employed with various coupling techniques is used for the proposed objectives. Schematic of the computational domain and associated boundary conditions for hypersonic flow over finite thickness cylinder are shown in Fig. 6.1. Solid cylinder of diameter 76.2 mm, considered by Wieting (1987), is used for current simulations as well. Thickness of the cylinder is taken as 12.1 mm. Quarter cylinder is considered for simulation to account for the symmetry of the geometry about its axis. Stretched grid is used at the interface in the fluid as well as solid domains to accurately compute the interface fluxes. Mesh independence studies have been performed and the final mesh size of 400x180 is selected for both fluid and solid domains (Fig. 6.2). The freestream parameters and boundary conditions are listed in the Table 6.1. These freestream conditions belong to the one considered by Wieting (1987) during experimental studies. The material considered for cylinder, Macor, is typically an insulating material for which density is 2520 kg/m^3, thermal conductivity is 1.46 W/m.K, and specific heat is 790 J/kgK. In order to understand the effect to experimental time scale on fluid domain and wall properties, the simulations are performed for different time scales in the range of 1ms to 1s.

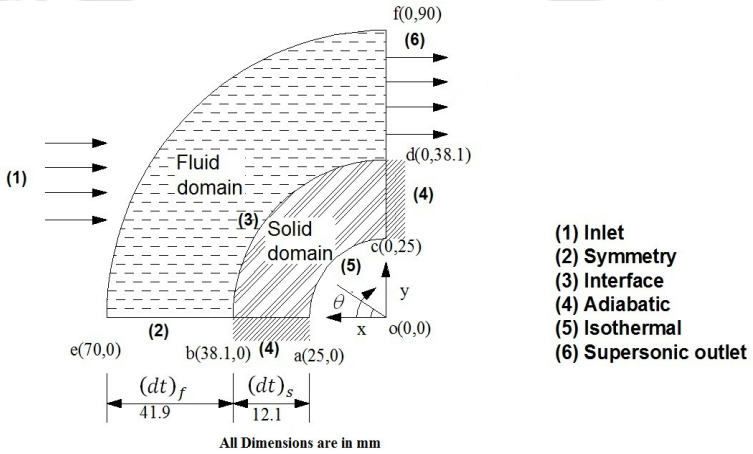

Fig. 6.1: Schematic representation of computational geometry for CHT analysis with appropriate boundary conditions.

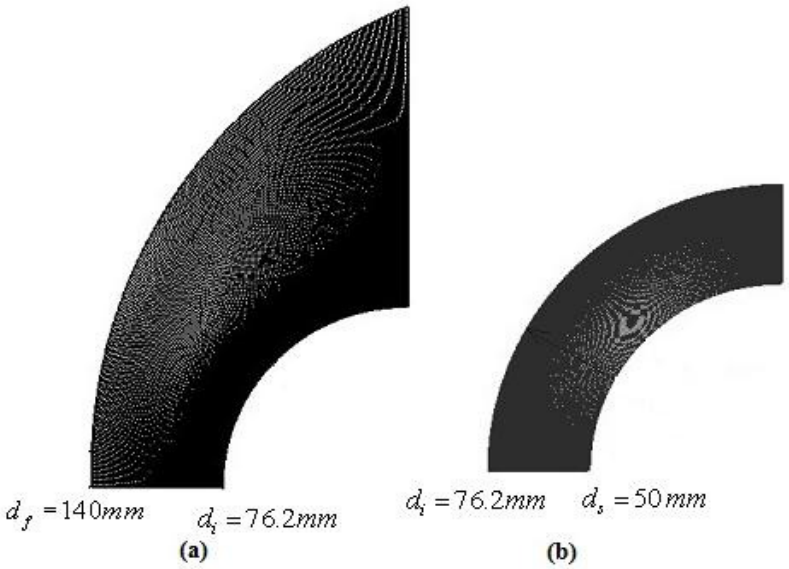

Fig. 6.2: Computational grid for CHT analysis: (a) Fluid domain; (b) Solid domain

Table 6.1: Parameters and properties used for CHT analysis

Boundary conditions	Explenesion of boundary conditions
Input	Freestream Properties parameters [Xiaoli et al. (2010) andWieting (1987)], are pressure $(p_\infty) = 0.6481$ kPa Temperature $(T_\infty) = 241.5\,K$ Mach number $(M_\infty) = 6.47$ Reynolds number $(\mathrm{Re}_\infty) = 1.3\times10^6$ m^{-1}
Symmetry	No flow across the boundary and no scalar flux across the boundary
Interface	Unity of temperature and "continuity in heat flux" boundary condition is considered. [Heat flux(x, interface, t)] $_{\mathrm{FLUID}}$ = [Heat flux (x, interface, t)] $_{\mathrm{SOLID}}$
Adiabatic	Wall heat flux is considered as zero
Isothermal	Wall Temperature is considered as constant (T=const)
Outlet	Supersonic outlet boundary

6.3 Results and Discussion

The pressure distribution along the surface of the cylinder (interface) is represented in non-dimensional form (c_p) and is given by the following equation;

$$c_p = \frac{1}{2}\left(\frac{p - p_\infty}{\rho_\infty V_\infty^{\ 2}}\right) \tag{6.1}$$

The variation of pressure coefficient along the surface of the cylinder is plotted in Fig. 6.3. Encouraging comparison among all the techniques and at different time scales are noticed from Fig. 6.3. The inviscid shock stand-off distance is calculated using the billing correlation [Anderson, 2006] which is given by the following expression.

$$\frac{\delta}{r_0} = 0.386 \exp\left[\frac{4.76}{M_\infty^2}\right] \tag{6.2}$$

Further, the pressure variations $\left(c_p\right)$ are plotted against non-dimensional distance $\left(x/d_i\right)$ along the stagnation streamline at various time instances (Fig. 6.4). The shock stand-off distance with inviscid assumption given by Eq. (6.2) has also been marked in the same figure. Effect of viscosity has seen to increase the shock stand-off distance in the presence of boundary layer on the cylinder wall. Among all the present computations, least shock stand-off distance is obtained for the isothermal wall boundary condition because the boundary layer thickness is the lowest. The shock stand-off distance for the time scales of the order of few milliseconds is almost equal to the one obtained for isothermal wall boundary conditions. This distance is clearly seen to increase with increase in time due to increase in wall temperature and hence the thickness of the boundary layer. For the simulation time of 1s, it approaches same as the adiabatic wall boundary condition for which maximum boundary layer thickness can be expected.

Stagnation point heat flux histories obtained from all the strategies are shown in Fig. 6.5. Stagnation point heat flux can also be evaluated analytically from the Fay and Riddell correlation expression (Anderson, 2006).

$$q_0 = 0.57 \times \mathrm{Pr}^{-0.6} \times (\rho_\infty \times \mu_\infty)^{0.5} \times \sqrt{\frac{du}{dx}} \times C_p \times (T_S - T_W); \quad \frac{du}{dx} = \frac{1}{r_0} \times \sqrt{\frac{2 \times \left(p_S - p_\infty\right)}{\rho_\infty}} \tag{6.3}$$

The stagnation point heat flux value obtained from (Eq. 6.3) deviates only by 0.5% in magnitude with the same one obtained from the present solver with isothermal wall boundary condition.

It is seen that magnitude of heat flux at the stagnation point, obtained from strong and loose coupling techniques, decreases initially over the time period of 200μs and subsequently attains the steady value. This time can be accounted for the development of thermal and hydraulic boundary layers on the body which commonly referred to as the flow establishment time. The heat flux for the DC-CHT method is constant with time because it is obtained from the established flow field and subsequently used as the boundary condition to solve the heat conduction equation in solid domain. The stagnation point temperature-time trace obtained from DC-CHT method is compared with the others in Fig. 6.6. Both, loose and strong coupling techniques portray agreement in this figure while the reason for initial deviation of the trace from the decoupled technique is mainly due to flow establishment time. Moreover, the rate of change of temperature can be seen to be identical for all the techniques after flow establishment (~200μs) which necessarily proves the alike surface heat fluxes as seen in Fig. 6.5. It shows around 55 K temperature rise at the stagnation point during 1ms which is about 16% of the initial wall temperature. However, this temperature rise, which corresponds to maximum value in the solid domain, is inadequate to alter the flow field. Hence, the cylinder wall at the interface can be treated as the isothermal wall for the simulation duration of 1ms, which corresponds to the test duration of a typical shock tunnel application. Moreover, it can be noticed that the prediction of temperature at the stagnation point using various methodologies is in good agreement with each other for the simulation time of 1ms after the establishment of flow field. Therefore, the DC-CHT methodology can be used to evaluate the steady state results due to requirement of lesser computational time in comparison with the LC/SC CHT solvers.

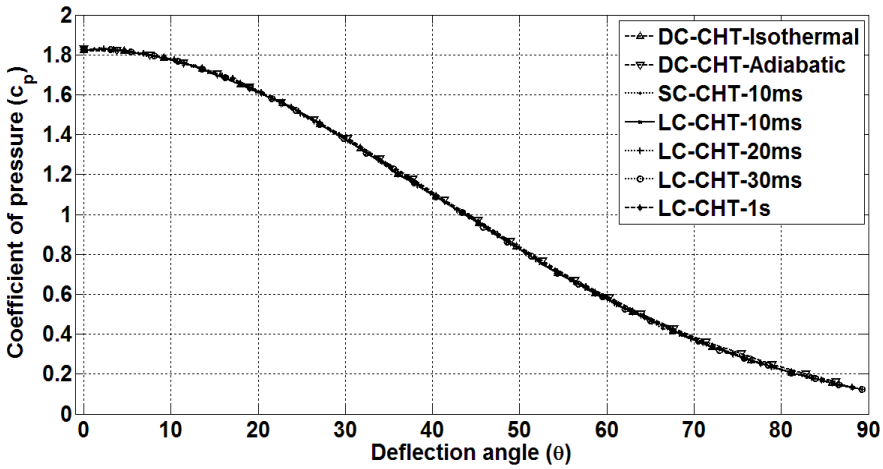

Fig. 6.3: Comparison of coefficient of pressure distribution along the cylinder surface.

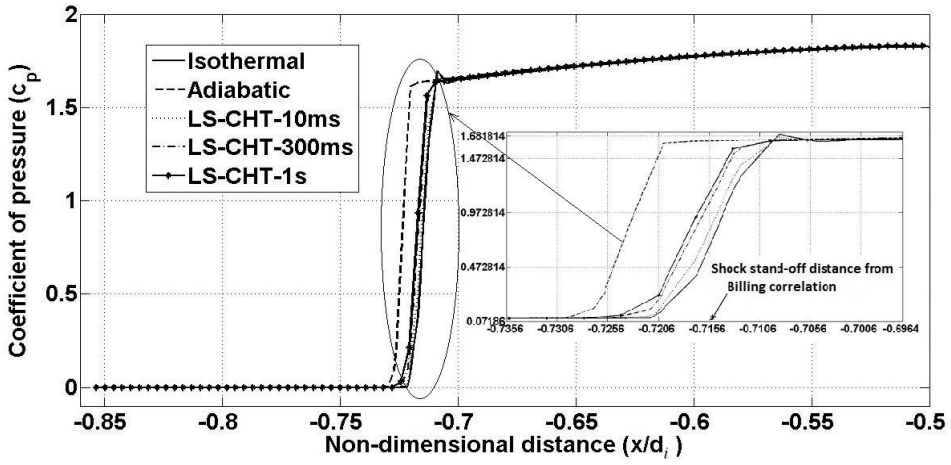

Fig. 6.4: Coefficient of pressure variation along a stagnation line.

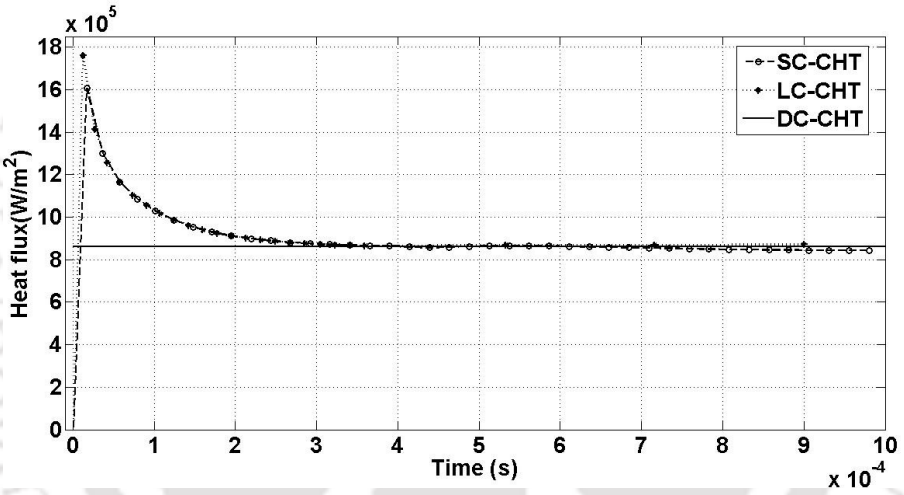

Fig. 6.5: Time variations of stagnation heat flux for simulation time of 1ms.

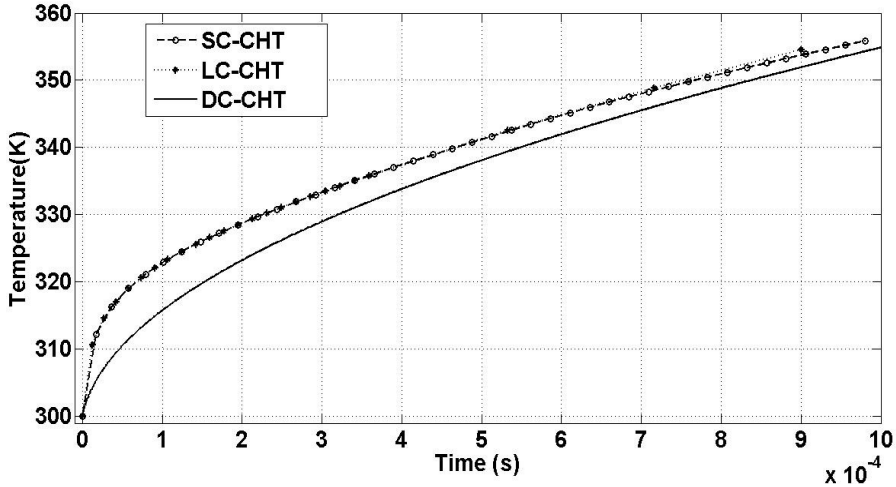

Fig. 6.6: Time variations of stagnation point temperature for simulation time of 1ms.

The temperature history and the time trace of wall heat flux at the stagnation point for the simulation duration of 10ms are shown in Fig.6.7 and Fig. 6.8, respectively. The SC and LC CHT based results are seen to under-predict the temperature rise after 5ms which lead to prediction of 15 K lesser temperature at the end of the simulation in comparison with the same obtained from DC-CHT strategy. Prediction of increased wall temperature and decreased rate of temperature rise exhibit marginal decrease in stagnation point heat flux after 5ms. The under-prediction of stagnation point heat flux using strong and loose coupling techniques can be justified from temperature contours of the solid domain shown in Fig. 6.9. Negligible depth of penetration of heat in solid during 10ms, introduces directionality in the heat transfer which in-tern leads to minor discrimination in the prediction by different techniques. Therefore, implementation of decoupled CHT method and isothermal wall boundary condition can be stretched comfortably till 50% increase in maximum temperature of the solid domain from its initial value. The wall heat flux distribution is obtained from all the techniques are compared with reported literature results (Fig. 6.10). It reconfirms the encouraging match of present methods with the literature reported predictions. In order to compare the relative advantages of present CHT methodologies, the simulation times are compared for strong and loose coupling techniques in Fig. 6.11. The SC-CHT based solver completes the computations for 10ms of simulation time in 110 hours which is around 11 times more than that taken by the loose coupling technique. Hence, the computations using strong coupling are seen to overshadow its accuracy due to intense time requirement. Therefore, it is advisable to carry out the CHT investigations involving higher simulation duration using loose coupling technique.

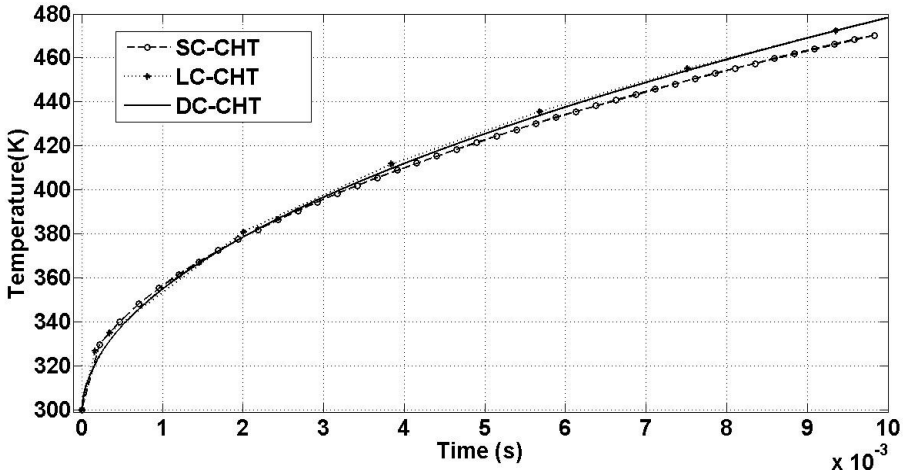

Fig. 6.7: Time variations of stagnation point temperature for simulation time of 10ms.

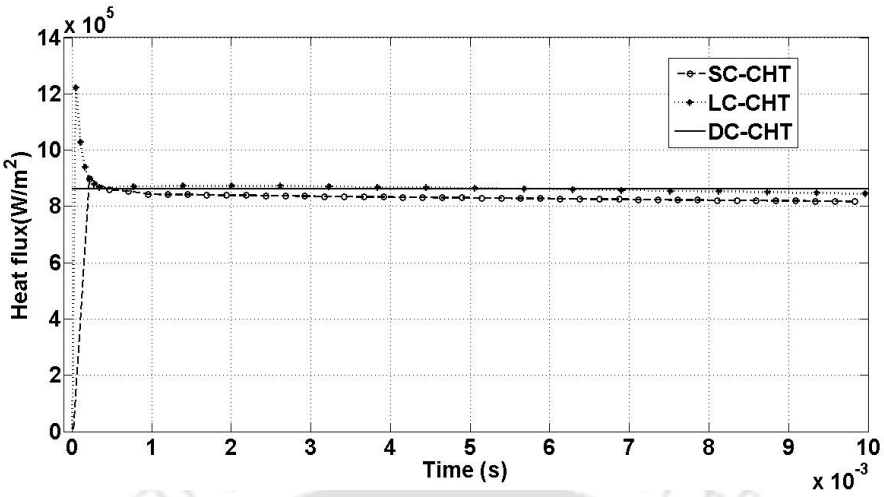

Fig. 6.8: Stagnation heat flux history for simulation time of 10ms.

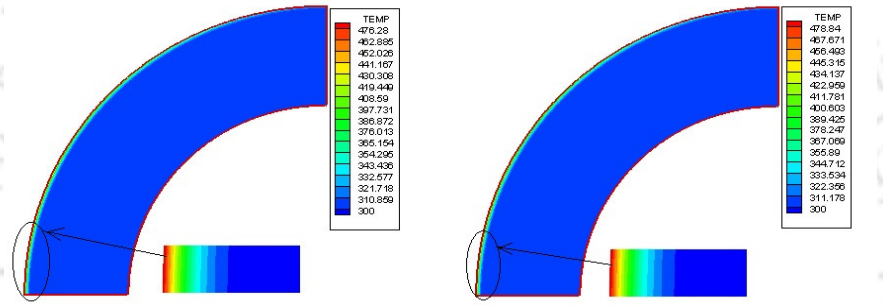

Fig. 6.9: Comparison of solid domain temperature contours obtained for simulation duration of 10 ms: (a) SC-CHT; (b) LC-CHT.

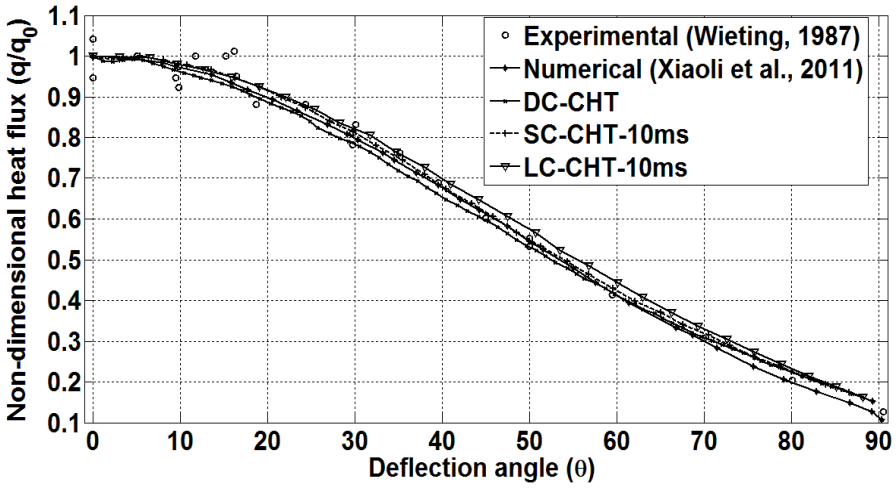

Fig. 6.10: Non-dimensional surface heat flux distribution along the surface of the cylinder.

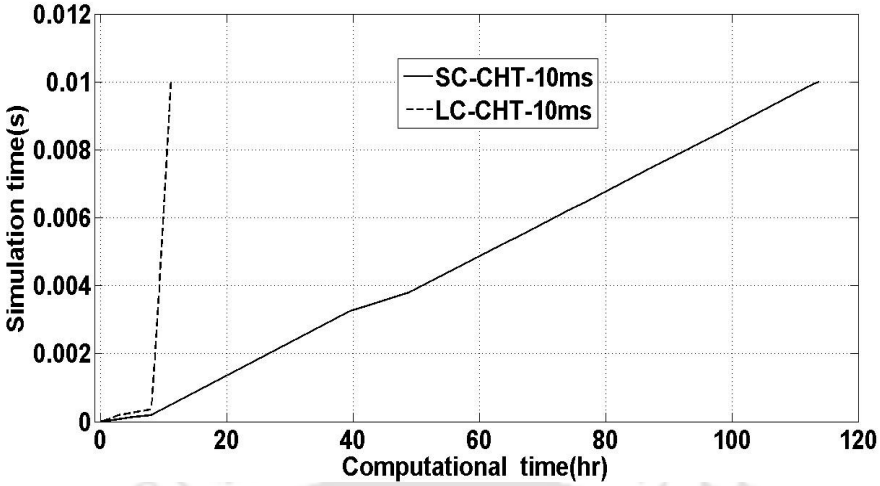

Fig. 6.11: Comparison of computational time with simulation time using various CHT techniques.

When the simulation is carried out for test duration of 1s, the results exhibit higher degree of discrimination between (DC & LC) CHT methodologies. The predictions of time trace of stagnation point temperature and heat flux are shown in Fig. 6.12 and 6.13, respectively. It clearly shows that DC-CHT method over predicts heat flux and temperature for large time scale applications. In other words, isothermal wall boundary in DC-CHT method is not valid for large time scale applications. In actual experiments (typically in flight tests), solid and fluid interface properties change with respect to time which is not incorporated in DC-CHT method. In such cases, the LC-CHT method shows increase in wall temperature and decrease in surface the heat flux while the mean flow properties changes are small compared to the wall properties.

The comparison of surface heat flux distribution on the surface of the cylinder compared by all CHT methodologies and different time scales (Fig. 6.14). The bell shape distribution of wall heat flux is seen to be valid for all the time scales considered for present studies. However, decrease in heat flux is noticed with increase in simulation time at all points. For simulation time of 1s, the maximum discrimination at the stagnation point is seen for LC-CHT method where the heat flux is under-predicted by 65% as compared to DC-CHT technique. Moving along the surface of the cylinder from stagnation point, at the angle 90º, the difference of surface heat flux reduces to 35%. However, interesting comparison in surface heat flux is observed among all the techniques when the simulation is performed for time scale of 1ms. Hence, LC-CHT technique can be considered as a better approach with less computational time of simulation. Referring to Fig. 6.15, the increased heat penetration depth (around 50%) and corresponding multidimensionality of heat transfer in the solid is

obvious. Hence, the assumption of uni-directionality used for recovery of wall heat flux from experimentally obtained temperature signal remains invalid for large simulation durations. Highly non-uniform distribution of surface heat flux, choice of insulator as wall material and large simulation durations are the major factors of multi-dimensional heat transfer rate. In contrast, choice of heat conductor as the wall material would lead to violation of semi-infinite wall material assumption by the virtue of completely disturbed solid domain. Therefore, the prediction of wall heat flux and surface temperature remain a difficult task due to violation of fundamental assumptions considered for experimental data reduction and also due to in-appropriate choice of wall boundary conditions for the conventional CFD simulations. Moreover proper choice of critical parameters of loose coupling CHT technique makes it accurate and convenient to predict the wall heat flux and temperature simultaneously.

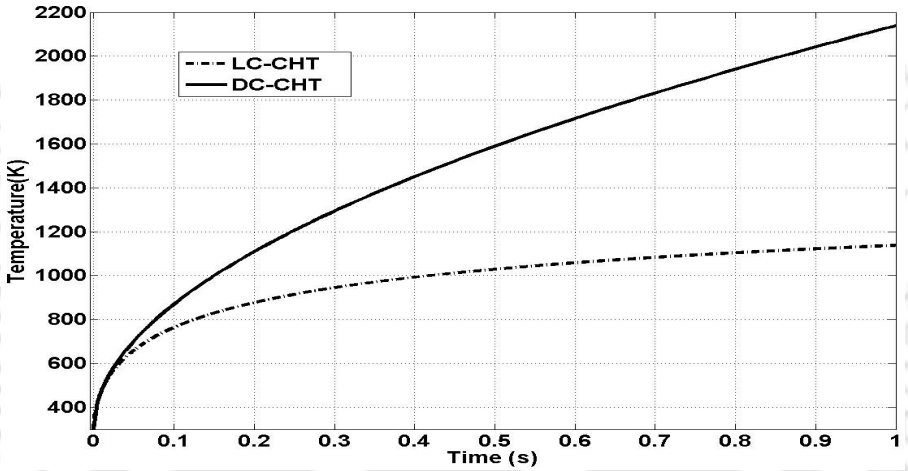

Fig. 6.12: Variations of temperature history at stagnation point for simulation time of 1s.

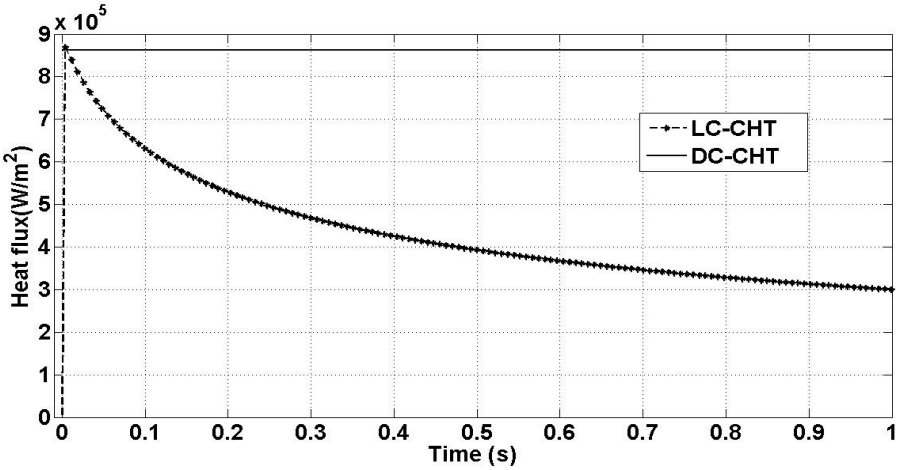

Fig. 6.13: Time traces of stagnation heat flux for simulation time of 1s.

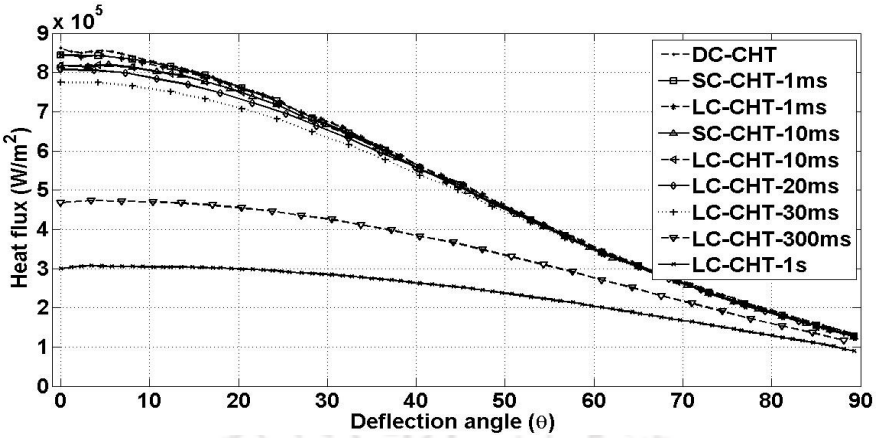

Fig. 6.14: Heat flux distribution along the surface of the cylinder at various time scales.

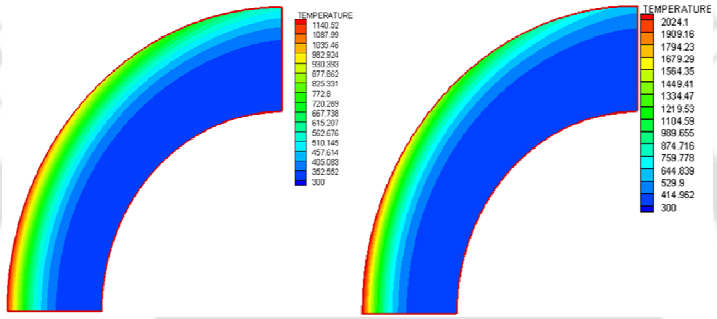

Fig. 6.15: Comparison of solid domain temperature contours obtained for simulation duration of 1s: (a) LC-CHT; (b) DC-CHT.

6.4 Summary

Research in the field of hypersonic flow regime is centered on prediction and minimization of surface heating loads. In view of importance to the basic heat transfer studies in communication with the fluid flow over the finite thickness cylinder, investigations are carried out for the conjugate heat transfer analysis at hypersonic speeds. Various coupling techniques are successfully implemented and assessed for their applicability for CHT analysis at various time scales. Decoupled CHT analysis is seen to be adequate for the simulation time during which wall temperature rises by 50% from its initial value. Strong coupling is found to be accurate but the requirement of intense computations is seen to limit its implementation for lower simulation times as per the computational capabilities. Loose coupling technique retains the advantage of its implementation for large time scales for accurate prediction subject to the choice of critical parameter. Decrease in wall heat flux for the same free stream parameters with increase in simulation time has been noticed using all the techniques. Stagnation point heat flux is seen to be largely decreased due to maximum rise in the wall temperature in that region.

CHAPTER 7

CONJUGATE HEAT TRANSFER ANALYSIS FOR COMPOSITE SOLIDS AT HYPERSONIC SPEEDS

7.1 Preface

Design of light weight structures and thermal protection systems (TPS) for hypersonic cruise and re-entry vehicles depends on accurate prediction of the aerothermal loads due to rise in surface temperature. Traditionally, an aerodynamicist will predict the surface pressures and heating rates assuming rigid isothermal body. Such conventional approaches under-predict the surface properties. This analysis is inefficient in high speed and sensitive applications. To overcome the above drawback the present study is done using conjugate heat transfer analysis (CHT). This is considered as a potential means for prediction of heating rates. Moreover, hypersonic flow over the object of interest establishes a very strong surface heat flux. The regions of high heating rates are leading edge for planer configurations and stagnation point of the blunt ones. Hence, CHT based heat transfer studies are inevitable to understand the heat penetration around those critical regions. This information is vital for designing the heat shield in order to protect the inside pay load for analogous spacecraft configurations. Use of the composite material can be a solution to this problem. In this strategy, the material of low thermal diffusivity should be allotted the region of high heating rates. In view of this, composite solid domains comprised of insulators like Macor and conductor like aluminum are considered to understand the heat penetration for flat plate and cylindrical geometries. These simulations would also examine the capability of present CHT solver to undertake the studies of hypersonic flow over composite solids. Therefore the major objective of the present studies is to understand the effect of composite solid domain on the interface heat flux and temperature using the established CHT solver. Hence the investigations carried out for finite thickness composite flat plate and cylinder configurations are discussed in following sections.

7.2 Computational Strategy

Conjugate heat transfer analysis has been carried out for freestream conditions pertaining to typical test conditions of a shock tunnel (Kulkarni et al., 2010). Freestream Mach number and pressure considered for the present studies are 8.0 and 89 N/m^2 respectively while the freestream

temperature and the initial wall temperature are taken as 113 K and 300 K, respectively. Macor and aluminum are chosen in the solid domain (i.e. wall) because they are most commonly used as backing materials for thermal sensors during ground/flight experiments. The properties of the wall materials are mentioned in the Table 5.1.

7.3 Results and Discussion

Flow over a composite flat plate and cylinder are analyzed for finding heat flux and temperature along the surface. The heat penetration rate in various wall materials is studied, at different time scales, using fluid flow solver and CHT solver. The results are discussed in subsequent sections.

7.3.1 Fluid flow study with isothermal and adiabatic boundary

A reference test case has been considered as a first step for proposed CHT analysis using only fluid domain. In this case, compressible fluid flow solver is tested for hypersonic flow over flat plate with streamwise varying boundary conditions as shown in Fig. 7.1. Two test cases are performed and the boundary is divided into two portions i.e. first half isothermal and second half adiabatic (Case I) and vice versa (Case II) as shown in Fig. 7.1. Major reason to perform this test is to get the extreme results. Hence, consideration on part of the wall as isothermal will simulate for the infinite conductivity material in that part while the adiabatic boundary condition will imitate the material to be of zero conductivity. Hence, effect of extreme material properties or wall composition can be understood in these reference cases. Temperature contours shown for such cases are shown in Fig. 7.2. In Fig. 7.2-a. the leading edge half portion is adiabatic and the downstream half portion is isothermal boundary. It is clearly visible in both the figures that the adiabatic region has higher temperature rise in the vicinity of the wall in comparison with the corresponding ideal conductor (isothermal wall).

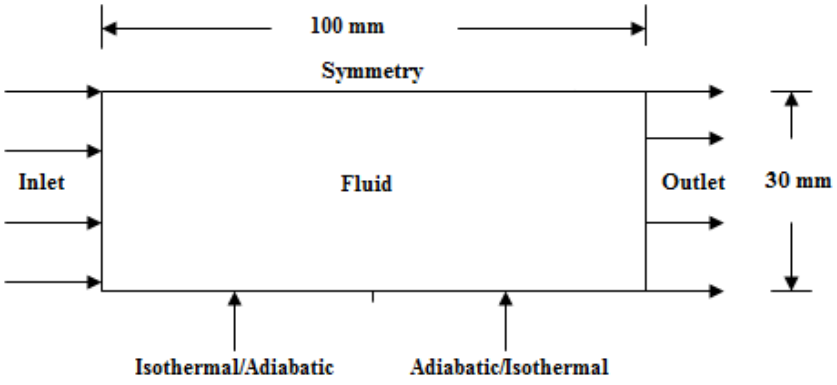

Fig. 7.1: Schematic representation of fluid domain computational geometry for Flat plate.

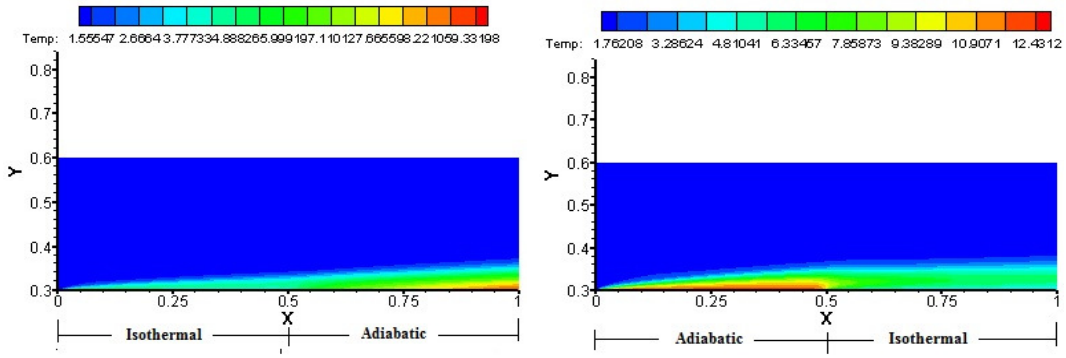

(a) Case-I (b) Case-II

Fig. 7.2: Temperature contours for fluid domain with different BC's at the bottom wall: (a) Case-I (Isothermal-Adiabatic); (b) Case-II (Adiabatic-Isothermal).

7.3.2 CHT analysis for flow over a composite flat plate

The fluid flow solver (N-S solver) is initially employed for the isothermal wall boundary at the first half and adiabatic wall boundary at the other half of the wall and vice versa. These results are compared with that of the results obtained for the different materials used here in CHT analysis to analyze the effect of composite domain. Computational domain shown in Fig. 7.3 has been considered for present CHT investigations. The composite solid domain analysis has two materials of different thermal conductivities. The effect on the variation of temperature at the surface of the solid is also of present interest. Apart from this, these simulations are also useful to understand the effect of heat interaction on fluid domain with various permutations of wall materials. Therefore, the wall materials viz. aluminum and Macor are chosen since these real materials have large difference in high conductivities. These composite CHT studies are carried out for two test cases as given below;

a) leading edge half portion as aluminum and trailing edge half as Macor.

b) leading edge half portion as Macor and trailing edge half as aluminum.

These results are compared with the fluid flow solver (N-S solver) results for isothermal-adiabatic boundary conditions. Such CHT studies are carried out for simulation duration of 0.1s, 0.5s and 1s.

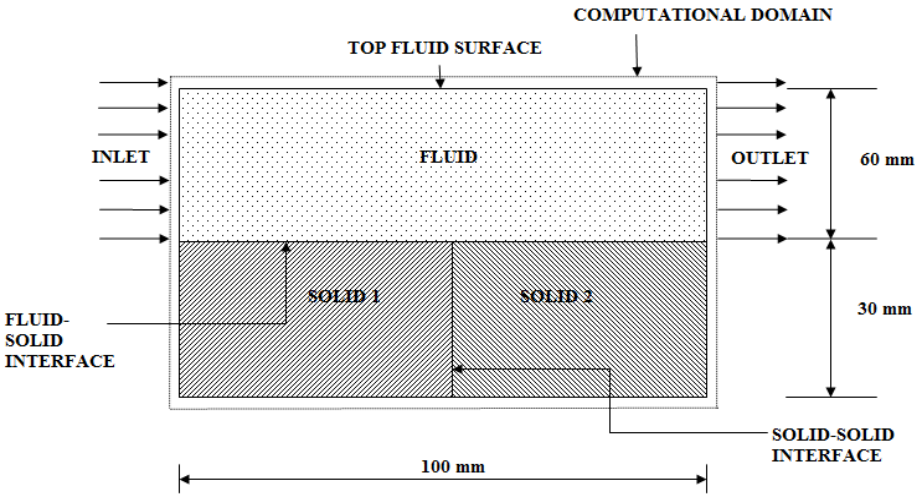

Fig. 7.3: Computational domain for the composite flat plate CHT analysis.

The surface heat flux variation at the fluid-solid interface in the normalized form using freestream parameters, expressed as Stanton number Eq. (5.1), is shown in Fig. 7.4 for various time intervals. This figure also accommodates the variation of Stanton numbers along the length of the plate using fluid flow solver (N-S solver). As seen in Fig. 7.4-a, Stanton number decrement along the length of the plate as observed in isothermal-adiabatic combination (case I) is in well agreement with the case-a. Marginal decrease, in leading edge Stanton number has been noticed when aluminum material is used in composite CHT studies at the leading edge. Such leading edge decrease of heat flux is attributed to the strong stream wise heat flux gradient and high thermal conductivity of Aluminum. Similarly variation of Stanton number along the length of the plate is seen (Fig. 7.4-b) with Macor as leading edge material.

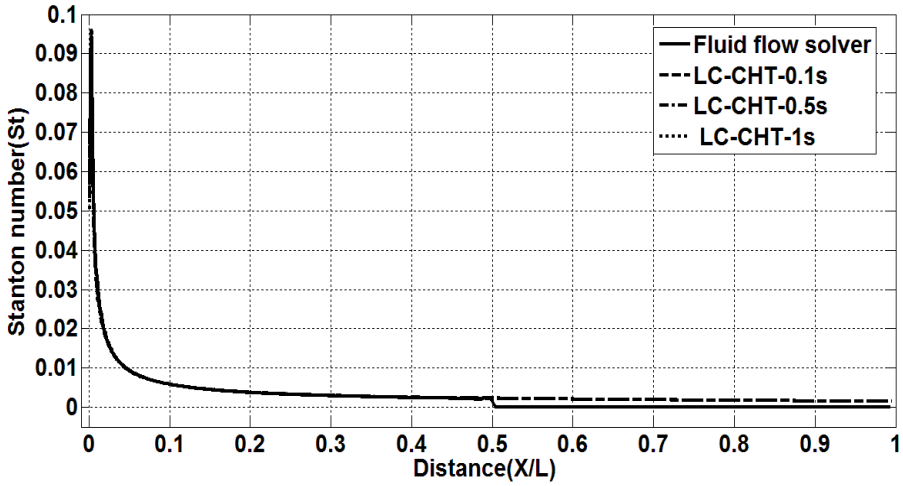

(a)

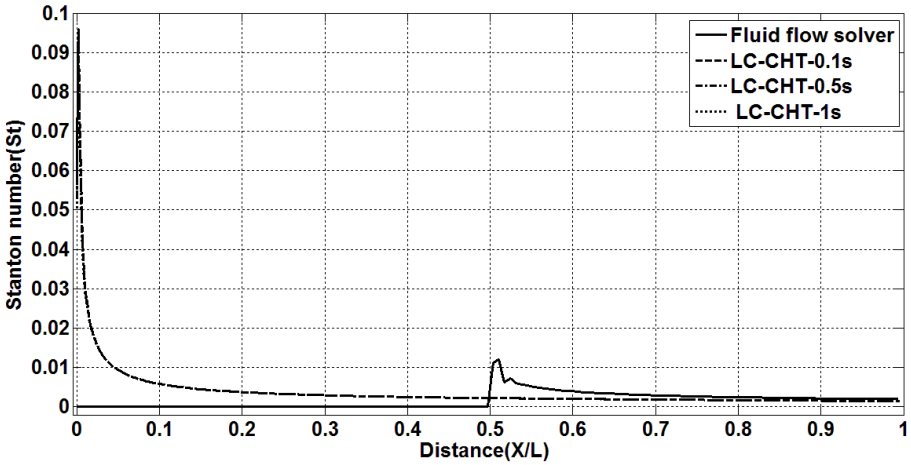

(b)

Fig. 7.4: Surface heat flux variation along the length of the flat plate; (a) Aluminum- Macor; (b) Macor- Aluminum.

Temperature variation along the solid-fluid interface is plotted for both the cases in Figs. 7.5 and 7.6. The comparison of case-I of fluid flow solver (N-S solver) and case-a of CHT simulations for temperature variation (Fig. 7.5) show temperature rise of 7 K at higher CHT simulation time of 1s. There is a sudden change in temperature at the solid-solid interface in CHT simulation and fluid flow solver (N-S solver) as well. As the CHT simulation time increases, temperature rise increases which is noticed to be around 700 K for fluid flow solver (N-S solver). It is due to lesser heat penetration for the trailing half due to an insulating material (Macor). Similarly, for the second test case (case-II and case-b), temperature variation along the solid-fluid interface is plotted for both the cases (Fig. 7.6). Results obtained from fluid flow solver (N-S solver) with adiabatic wall boundary at the first half and isothermal wall boundary at the other half are compared with CHT simulation (Macor-aluminum) in this figure. As the CHT simulation time increases, temperature raise increases at all locations which is marginal at the interface. Near the leading edge, temperature is higher with increase at around 500 K for 1s CHT simulation time. For the first half, fluid flow solver (N-S solver) (i.e. adiabatic wall boundary) based temperature rise is noticed to be more around 1750 K. The major reason for such increase is the presence of insulating wall boundary condition at the leading edge which when replaced by Macor in case of the CHT simulation shown around 500 K at 1s. There is a sudden decrease in temperature at the solid-solid interface in CHT simulation and fluid flow solver (N-S solver) (adiabatic-isothermal) at the interface for this case as well.

At this interface location, the temperature obtained from the fluid flow solver (N-S solver) decreases suddenly as the boundary condition changes from adiabatic to isothermal one. In the second half portion of the plate, material used is high conductivity material (Aluminum) in CHT simulation. Therefore, heat penetration is much faster inside the solid as compared to the Macor portion and hence surface temperature rise is less as shown in Fig. 7.6.

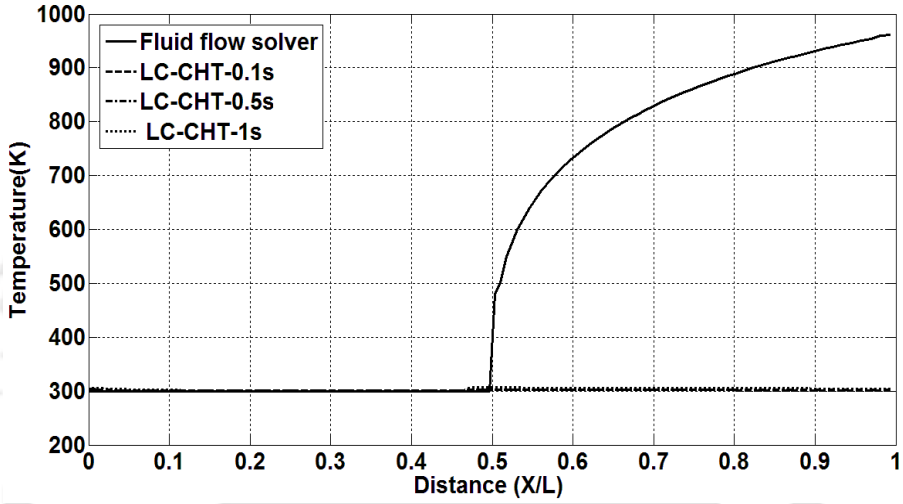

(a)

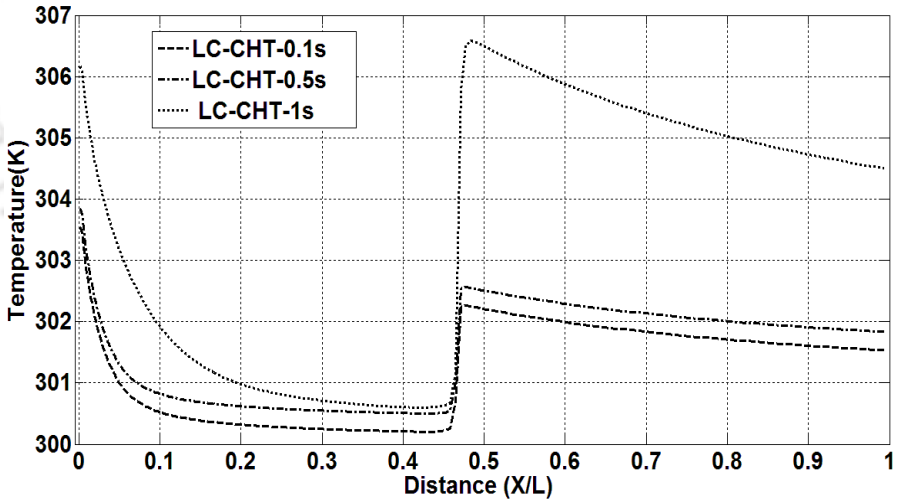

(b)

Fig. 7.5: Temperature variation along the length of the flat plate (Aluminum-Macor)
(a) Comparison of surface temperature with fluid flow solver (N-S solver); (b) Surface temperature rise in CHT.

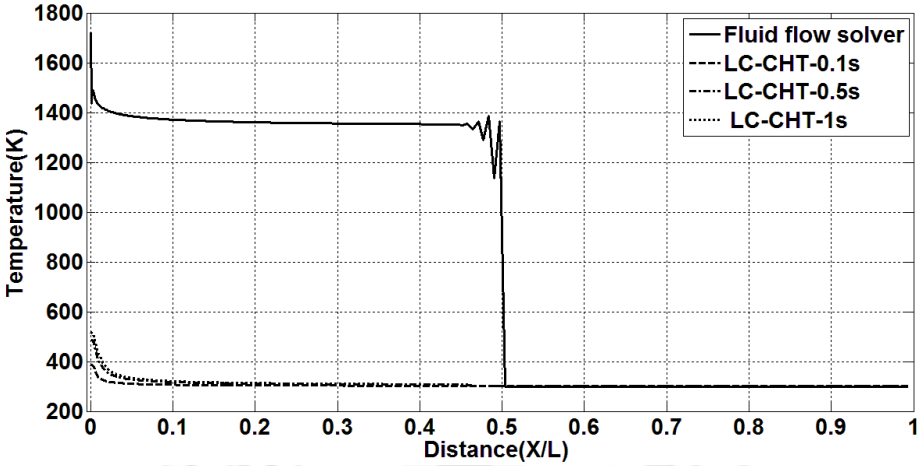

(a)

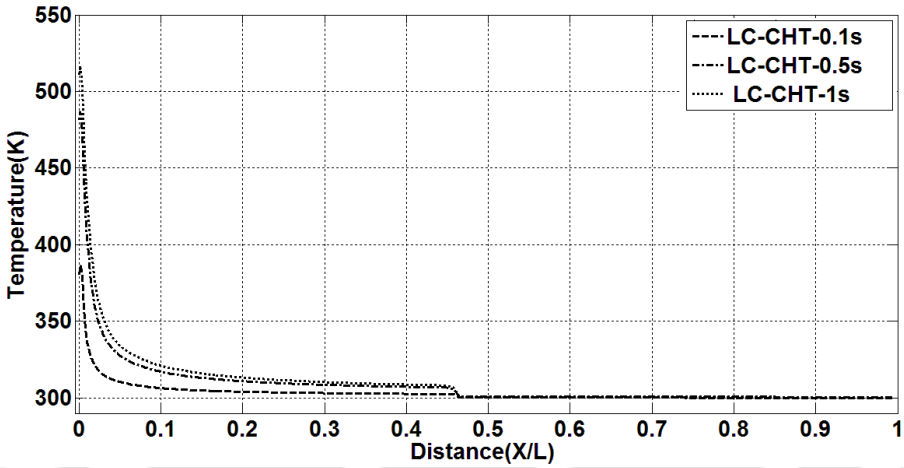

(b)

Fig. 7.6: Temperature variation along the length of the flat plate (Macor- Aluminum): (a) Comparison of surface temperature with fluid flow solver (N-S solver); (b) Surface temperature rise in CHT.

Typical temperature contours for fluid and solid domains corresponding to 1s are shown in Fig. 7.7 and 7.8. In both the cases for finite thickness flat plate, the maximum temperature rise in the solid domain is noticed at the Macor side. The low thermal conductivity of Macor material does not allow the heat to penetrate into the solid domain hence the temperature rise is more at the surface as compared to the aluminum side where heat penetration is more and hence temperature rise at the surface is less as seen in Figs. 7.5 to 7.6. Temperature and Velocity profiles at two selected locations are plotted in Fig. 7.9 and Fig. 7.10 respectively. These figures basically accommodate the case-I and II along with case-a and case-b. Fluid properties change with the change in wall temperature at location x=0.025 m and location x=0.075 m from the leading edge is shown in Fig. 7.9. At x=0.025 m location, the changes are less because wall temperature rise is less compared to the case II

(adiabatic-isothermal). Here, as expected, a slightly higher temperature rise is observed for the Macor material at the leading edge compared to the aluminum at the leading edge. At location x=0.075 m from the leading edge, the temperature rise not only depends on the wall material and boundary but it will also be affected by the heat diffusion from the preceding section of flow field. Here, for the extreme case of isothermal-adiabatic material (case I), the temperature rise is significant due to adiabatic boundary at this location. Whereas in the opposite case (case II), although there is an isothermal boundary at the location, the temperature rise is higher. This is due to the diffusion of heat from the flow field prior to it at the adiabatic boundary. For the other two cases the temperature rise is not so appreciable and is comparable. Similarly, velocity changes are noticed in Fig.7.10. Changes in the fluid domain with change in wall conditions are clearly evident from these figures.

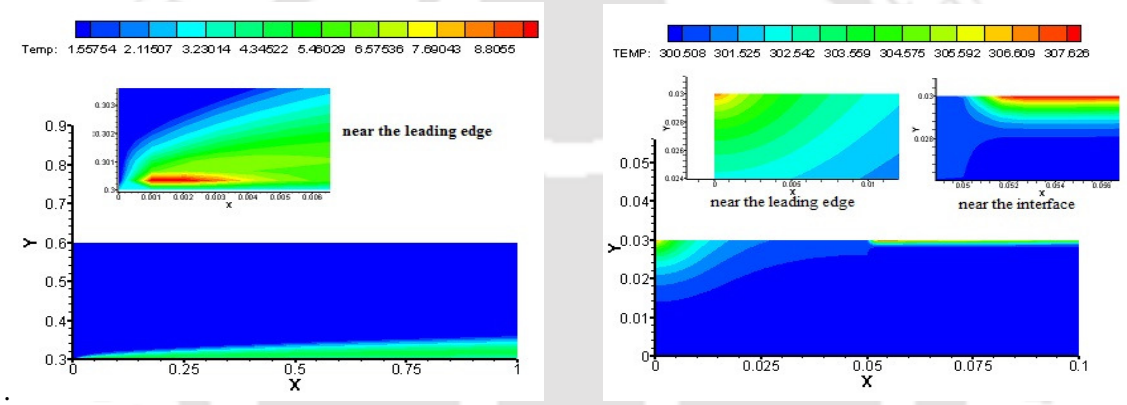

(a) (b)

Fig. 7.7: Temperature contour for flat plate fluid and solid domain for case-I; (a) Fluid domain; (b) Solid domain (Aluminum-Macor).

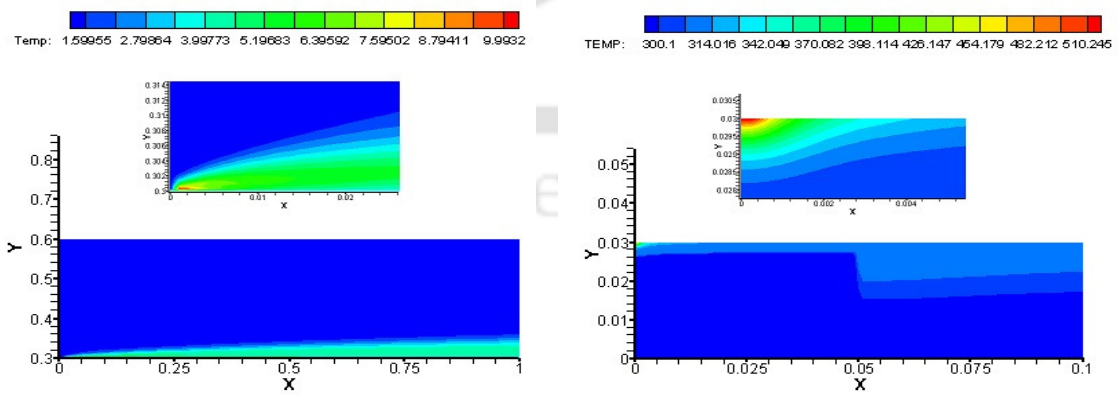

(a) (b)

Fig. 7.8: Temperature contour for flat plate fluid and solid domain for case-II; (a) Fluid domain; (b) Solid domain (Macor–Aluminum).

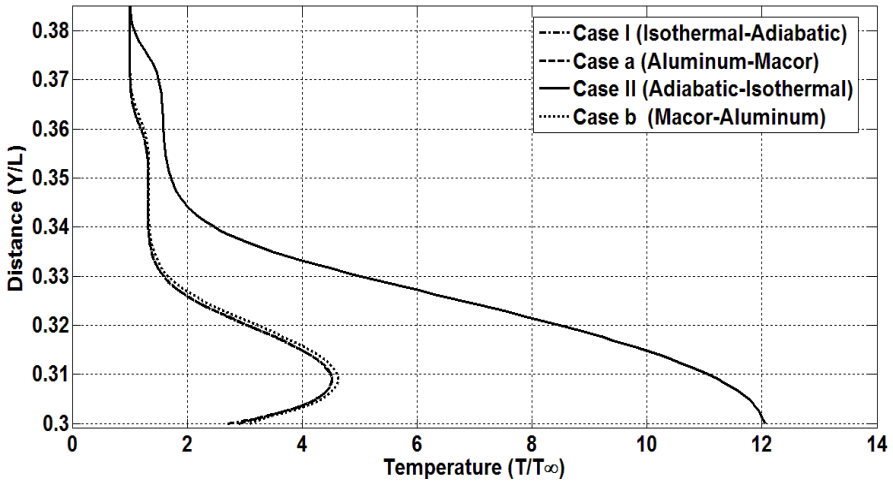

(a)

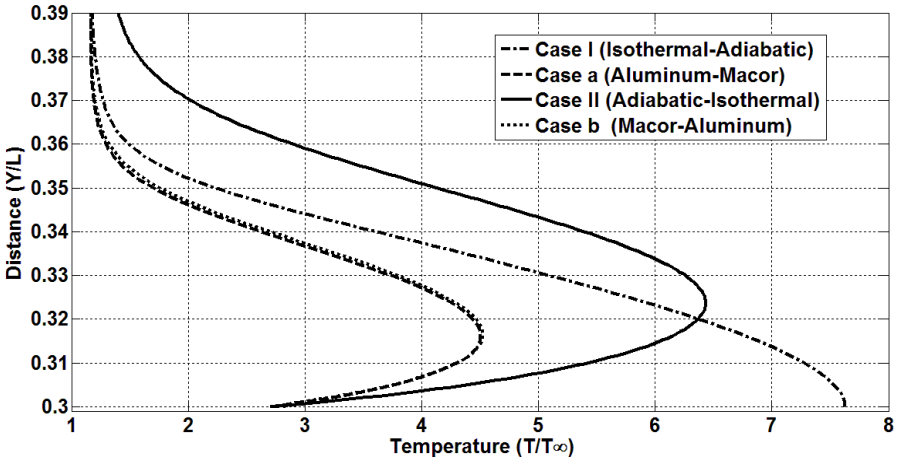

(b)

Fig. 7.9: Temperature profile at various locations using all the methods. (a) at x=0.025 m, (b) x=0.075 m.

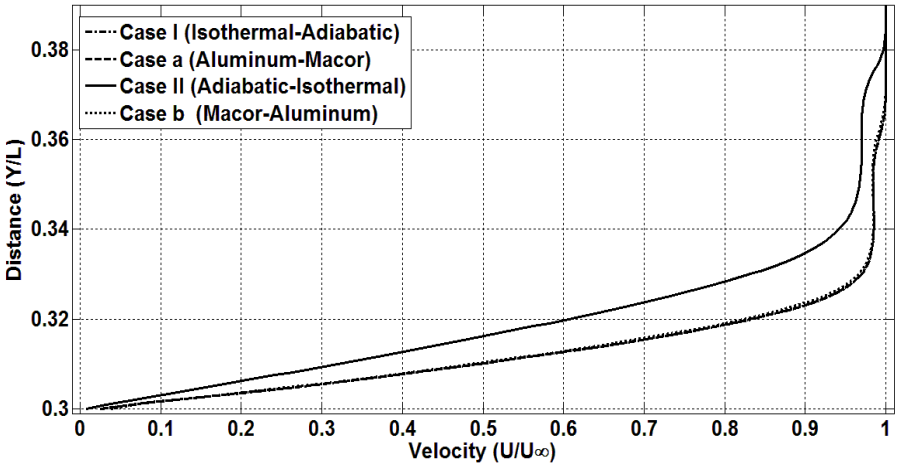

(a)

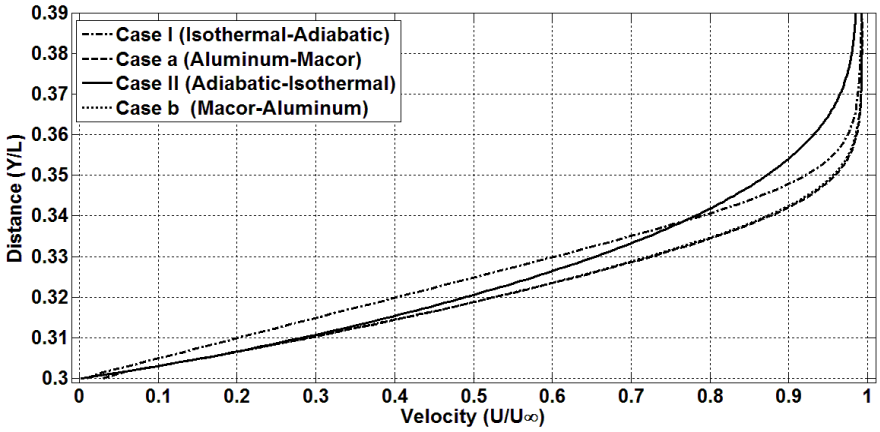

(b)

Fig. 7.10: velocity profile at various locations using all the methods.
(a) x=0.025 m, (b) x=0.075 m.

7.3.3 CHT analysis for flow over a composite cylinder

The composite cylindrical domain considered for CHT simulations is as shown in Fig. 7.11. The freestream conditions are mentioned in section 7.2. Again same two materials and their location based permutations are considered for this case. Hence here as well flow will encounter the change in wall material in the streamwise direction. The Stanton number and temperature variation is shown along the fluid-solid interface in Figs. 7.12 and 7.13 respectively. At the first half portion of cylinder, aluminum is used as the high conductivity material and at the second half portion of the cylinder, Macor is used as the insulating material for which results are shown in Fig. 7.12-a and Fig. 7.13-a. Stanton number decreases along the fluid-solid interface. In CHT analysis, no significant change in surface heat flux is observed in this figure near the stagnation region where aluminum is present. However, small decrement in Stanton number with simulation time increases (Fig. 7.12-a) is noticed in the downstream Macor portion. Again CHT simulations are carried out with the first half portion of solid material as Macor and second half portion of the solid material as aluminum. As the CHT simulation time increases Stanton number decreases in the first half portion as shown in Fig. 7.12-b. Similarly, here as well, no significant change in Stanton number is noticed in the downstream aluminum part. Hence these figures clearly portray that the presence of Macor decreases the wall heat flux with time. The reason for this is clear in Fig. 7.13 which displays surface temperature variation with time. The maximum temperature for aluminum increases from 300.5 K at the solid-solid interface at 0.1s to 306.5 K at 1s due to higher thermal diffusivity of aluminum (as shown in Fig. 7.13-a). However the maximum temperature for Macor increases from 315 K at the solid-solid interface at 0.1s to 360 K at 1s due to lower thermal diffusivity of Macor (as shown in Fig. 7.13-b). Hence, although aluminum has faced

stagnation point high heat flux, the temperature rise is only 6.2 K in 1s. But the Macor portion shows around 60 K raise in temperature in the same duration for 8% lesser heat flux. Thus increase in wall temperature is though prominent in CHT, it is more significant in Macor portion. This fact can be cross verified when Macor is present in the stagnation region. In this case, as per Fig. 7.13-b, stagnation point temperature rise is 80 K where maximum temperature in the aluminum region is hardly 6 K at 1s.

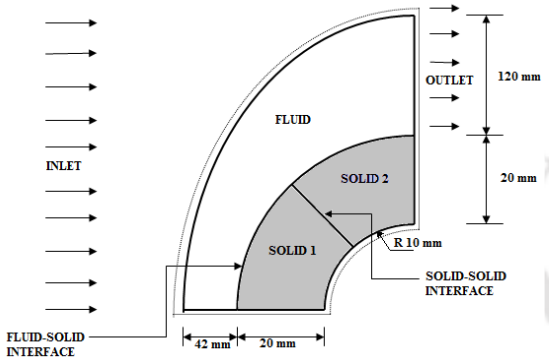

Fig. 7.11: Computational domain for the composite cylinder CHT analysis.

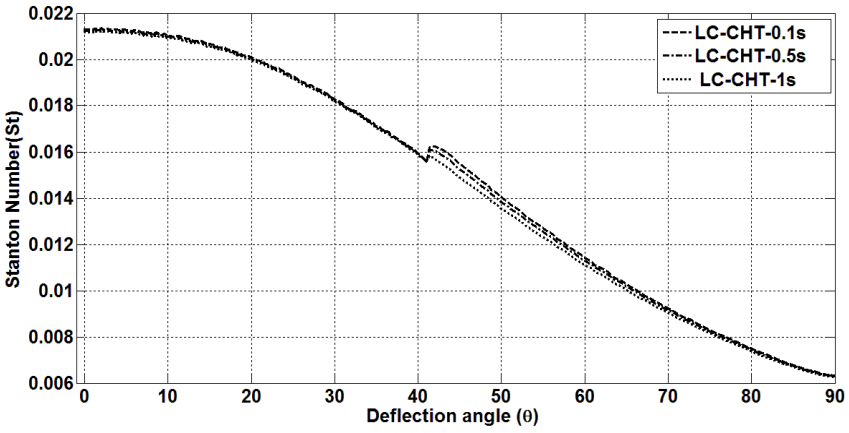

(a)

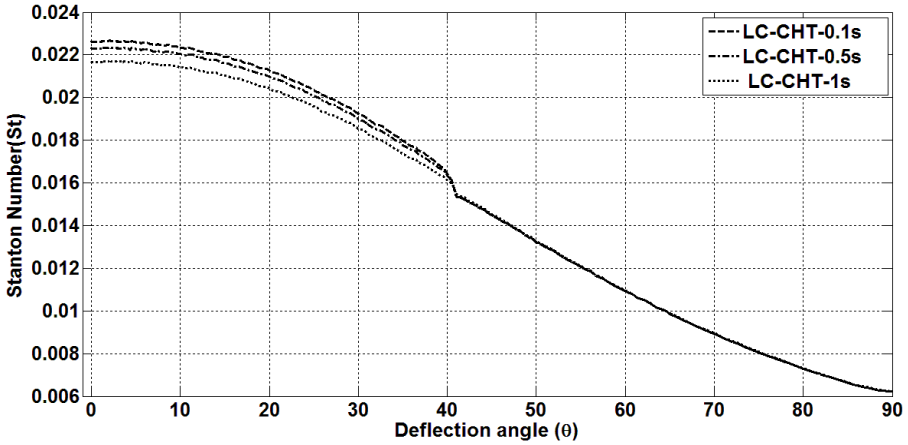

(b)

Fig. 7.12: Surface heat flux variation along the surface of the cylinder; (a) Aluminum-Macor; (b) Macor-Aluminum.

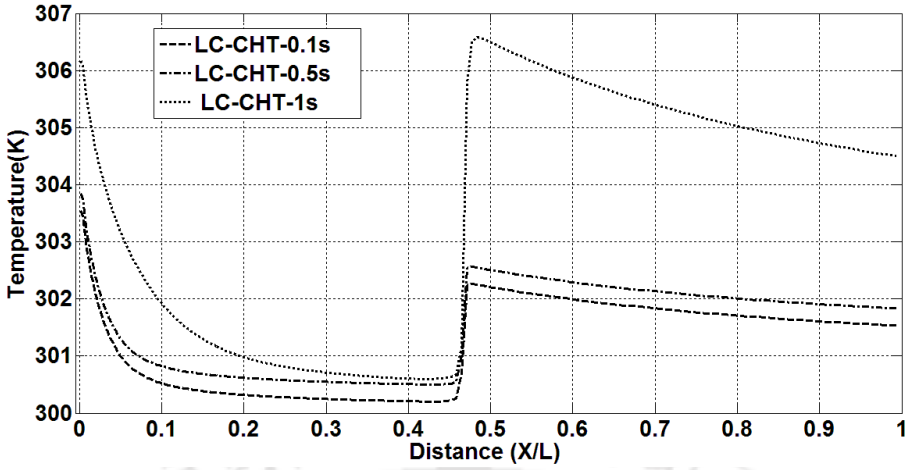

(a)

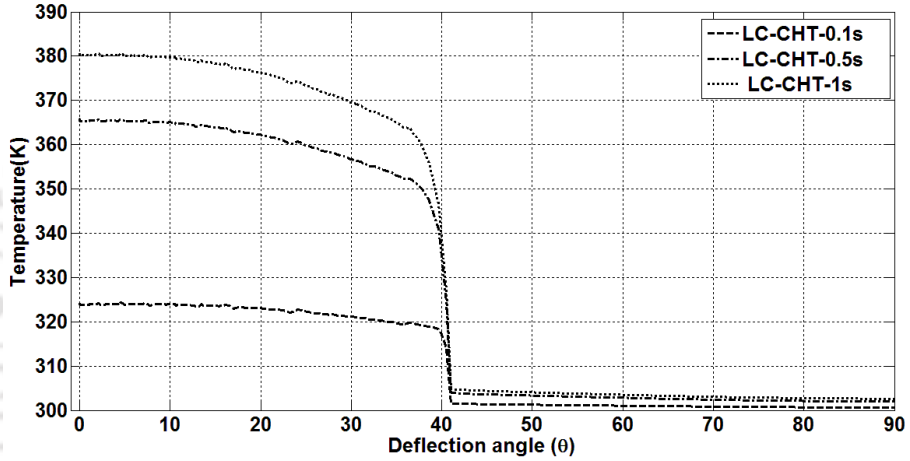

(b)

Fig. 7.13: Temperature variation along the surface of the cylinder; (a) Aluminum- Macor; (b) Macor- Aluminum.

The heat penetration in solid and fluid domain and associated temperature variations are shown in Fig. 7.14 and Fig. 7.15 respectively. For the fluid domain, at the stagnation point, kinetic energy is converted into heat energy due to which high temperature fluid is present in the stagnation region as observed in both the figures. Hence higher heat transfer rates are expected and observed (Fig. 7.14) in the vicinity of stagnation region. The temperature contour shows the high temperature area for the material with low conductivity material i.e. Macor. There is a larger penetration of heat on the other side as a higher thermal conductive material used (i.e. Aluminum). Thus use of insulating material in the stagnation region does not allow heat penetration inside the solid. However presence of heat conducting material in this region thermally disturbs the solid domain. In view of this, CHT studies are essential to predict the depth of heat penetration and effect of wall material on fluid domain in designing the thermal protection system.

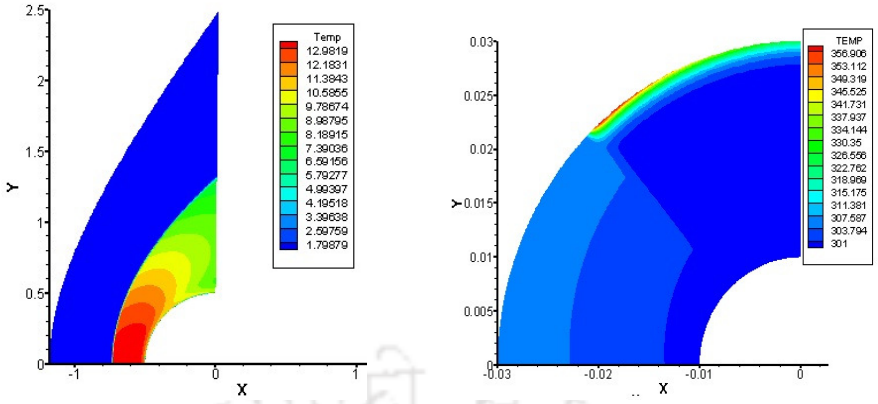

(a) (b)

Fig. 7.14: Temperature contour for cylindrical fluid and solid domain for case-I; (a) Fluid domain; (b) Solid domain (solid1-Aluminum, solid2-Macor).

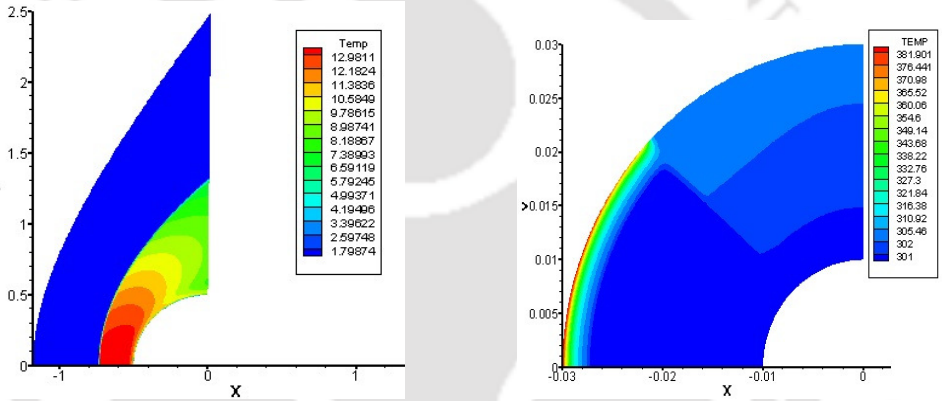

(a) (b)

Fig. 7.15: Temperature contour for cylindrical fluid and solid domain for case-II. (a) Fluid domain; (b) Solid domain (solid1-Macor, solid2- Aluminum).

7.4 Summary

A CHT solver for the composite solid domain analysis is developed and successfully implemented to understand the heat transfer at hypersonic speeds. It is observed that when insulating material is used in solid domain, the heat penetration and the magnitude of temperature rise is very less within the solid domain and is limited to the surface only. The surface temperature rise is very high for the low thermal conductivity material and it reaches the stagnation temperature at much faster rate. For the high thermal conductivity material there is larger depth of penetration of heat inside the solid domain and the surface temperature rise is comparatively very less. The idea of using lower conductivity material at the leading edge and other such regions where there is higher heat flux generation will prominently help in thermal protection of vehicles. Thus solver can be useful for design of thermal protection systems for hypersonic vehicles.

CHAPTER 8

CONJUGATE HEAT TRANSFER ANALYSIS OF HYPERSONIC FLOWS OVER DOUBLE WEDGE

8.1 Preface

The phenomenon of shock wave/boundary layer interactions (SWBLI) in supersonic and hypersonic flows has been studied for last five decades. It has its direct application in various configurations such as re-entry vehicles, spacecraft and missiles etc. In these configurations SWBLI has a strong influence in the following parameters: the levels of heating, the size of the recirculation regions, the loss of efficiency of control surfaces and the oscillation of transient pressure loads. Thus alterations in aerodynamic heating and aerodynamic coefficients can be expected in the presence of SWBLI. Therefore, exact prediction of wall temperature, pressure, separation bubble length, wall skin friction and heat transfer in hypersonic applications is essential for successful design of the space vehicle.

Flow over double wedge represents many parts of hypersonic vehicle geometries. Such configuration is invariantly considered to study the SWBLI. In such flow fields, the hypersonic flow gets decelerated in the presence of first standing shock of the first wedge. This shocked flow develops the boundary layer on this wedge which approaches the second wedge. Therefore shock wave should be expected from the seconds wedge due to supersonic or lower hypersonic Mach number of the flow in the shock layer. This shock offers the adverse pressure gradient to the approaching boundary layer which at least gets disturbed or gets separated. This interaction dynamics depends on the freestream Mach number, Reynolds number, wedge angles and viscous interaction parameters. Both the shocks from the wedges interact with each other to generate a shock-shock interaction region. Field and wall properties are dependent on the strength of this interaction. Due to such interaction, pressure and heat flux are locally increased the body surface Anderson, (2006). A shear layer generated from the two shocks approaches the body surface, and results in locally anomalous increase in pressure and aerodynamic heating of the hypersonic flow field over a double wedge, Olejniczak et al. (1999). However, Davis [Davis, (1999)] concentrated on predictive methods for separation length and reattachment heating in high enthalpy flows. Numerous researchers [Olejniczak et al. (1997), Mallinson, (1996), Boyce and hillier (2000), Arnal and Delery, (2004), Bibin et al. (2014), Bibin and Kulkarni (2014)] studies various aspects of the

shock wave boundary layer interaction through experimental measurements or numerical simulations. However these studies were carried out with adiabatic or isothermal wall boundary conditions. But the heating in the presence of SWBLI significantly alters the surface temperature over a period of time [Kolodziej, (1997), Quinn et al. (2000)]. Thus wall material properties and wall thickness largely decides the accurate estimation of temperature distribution of the vehicle structure. Therefore, for the prediction of aerodynamic load and aerothermal effects of high speed vehicle, it is necessary to consider the fluid flow and heat conduction in the structure simultaneously. Such consideration of unsteady or transient effects is necessary to predict the aerodynamic heating loads accurately. Hence CHT studies should be initiated to understand the shock wave boundary layer interaction. Along these terms, the prediction of interaction parameters like separation bubble length, surface heating rates, skin friction, flow properties, surface pressure and temperature can be improved through CHT studies. In view of this literature reported configuration and freestream conditions are considered along with the earlier choice of wall materials to undertake the CHT studies for SWBLI.

8.2 Computational Strategy for Double Wedge

The typical computational domain considered for present CHT analysis is shown in Fig. 8.1. This configuration was considered by Yang et al. (2012) during their experimental studies. The details of this configuration include first wedge length (L_1) of 50 mm, second wedge length (L_2) of 30 mm, first ramp angle (θ_1) of 12^0 and the second ramp angle (θ_2) of 22^0. Hypersonic wind tunnel experimental freestream conditions are as M_∞=5, T_∞=62.5 K, and P_∞=1.22 kPa. These conditions are considered at the inlet while the fluid domain outlet is considered as supersonic. Wall materials Silicon Carbide (SiC), Thermal Insulation (Adam and Jack, 2010) and Macor are considered for present simulations are given in Table 8.1. For the solid domain, the two side walls are assumed to be adiabatic and the bottom wall of the solid domain is considered to be an isothermal wall. Interface boundary condition is employed at the boundary between solid and fluid boundaries. Loosely coupled technique is used for fluid flow and conduction solvers analysis. Simulation has also been carried out with isothermal wall boundary condition with wall temperature of 300 K as experienced during the actual hypersonic wind tunnel experiments. These simulations are carried out for different time scales for different materials based on their thermal diffusivities. The final time for Silicon Carbide (SiC) is 0.1s, Thermal Insulation is 0.4s and Macor is 3s. Mesh independent

studies have been carried out for the present test case and the final mesh for the fluid and solid domain is of size 300x180.

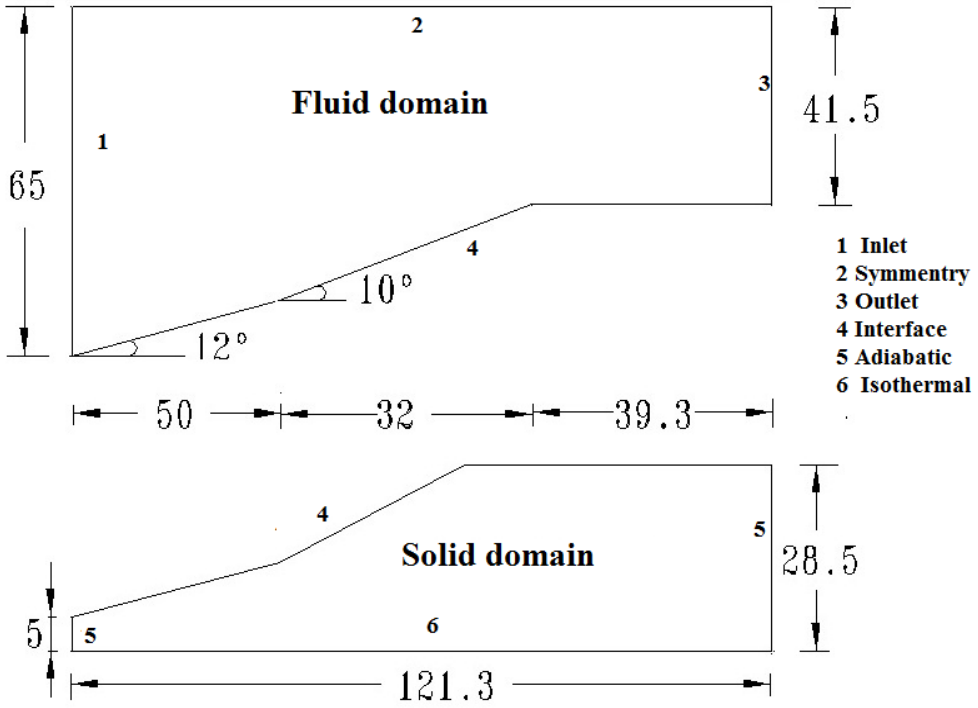

Fig. 8.1: Dimension of the double wedge model, all dimensions are in mm

8.3 Results and Discussion

Typical Mach number contour obtained from present simulations with isothermal wall boundary conditions and CHT simulation at various time instances for different wall materials are shown in Fig. 8.2. These contours clearly display the expected flow field with two shocks. Here the low Mach number flow behind the first wedge shock experiences the second shock in the presence of second wedge. The details of the interaction of this shock and approaching boundary layer are not clear from this figure. Hence surface pressure variation is plotted in the Fig. 8.3. Excellent agreement of the wall pressure trace with the present simulations can be experienced from this figure. In all the cases included in this figure, the distribution displays decrement in pressure on the first wedge which is followed by sudden increment. This location of pressure rise is the typical characteristic of separated flow. A small constant pressure region is also evident in this figure. Downstream of this constant pressure region further increment in pressure takes place which includes the highest pressure value attained along the second ramp surface. This is because the flow in this region has been compressed twice, first by the leading edge shock and then by the

reattachment shock. The lowest value of pressure is recorded along the shoulder due to the acceleration of the flow across the expansion fan. It is well in agreement, for all cases, with the experimental results as shown in Fig. 8.3. It clearly shows that even though the CHT simulation time increases, the wall pressure doesn't change much.

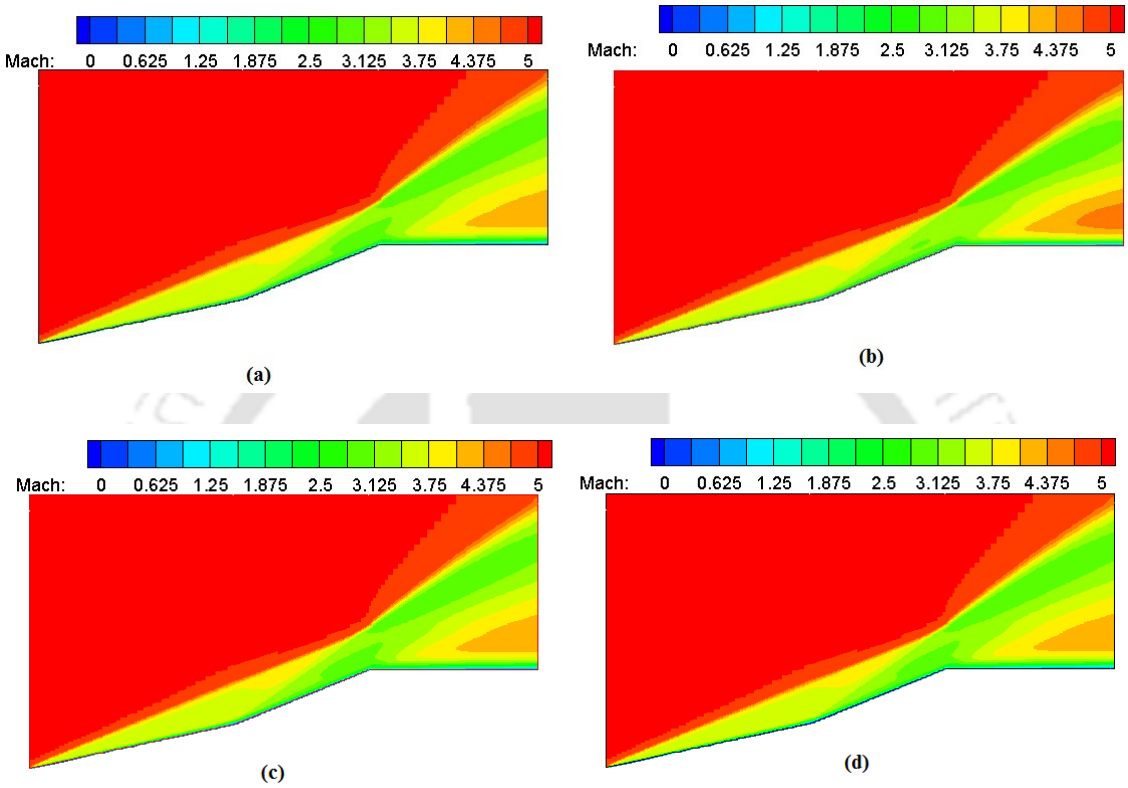

Fig. 8.2: Mach contour for isothermal with CHT studies with various wall materials. (a) Isothermal; (b) Silicon Carbide (SiC); (c) Macor; (d) Thermal insulating material.

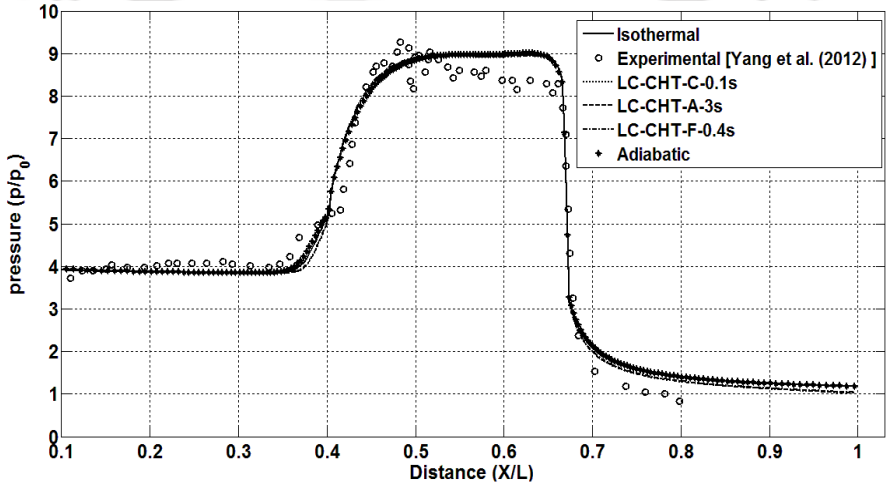

Fig. 8.3: Wall pressure distribution along the length double wedge.

For better understanding of the interaction, surface heat flux variation along the length of the double wedge is plotted in Fig. 8.4. In case of isothermal wall condition, local heat transfer gradually decreases downstream in the first wedge due to the spatial development of the boundary layer. At the expected location of boundary layer separation or constant pressure region location of Fig. 8.3, the heat transfer rate profiles exhibits a unique trend of 'V' shape where the heating rate initially decreases to minimum value and then starts increasing. However this increment continues on the second ramp which is in contact with very high temperature fluid. Therefore the heat transfer attains its maximum on the second ramp and later on decreases downstream due to expansion of the flow at the shoulder. Excellent agreement of this trace with the measured heating rates is also clear from this figure.

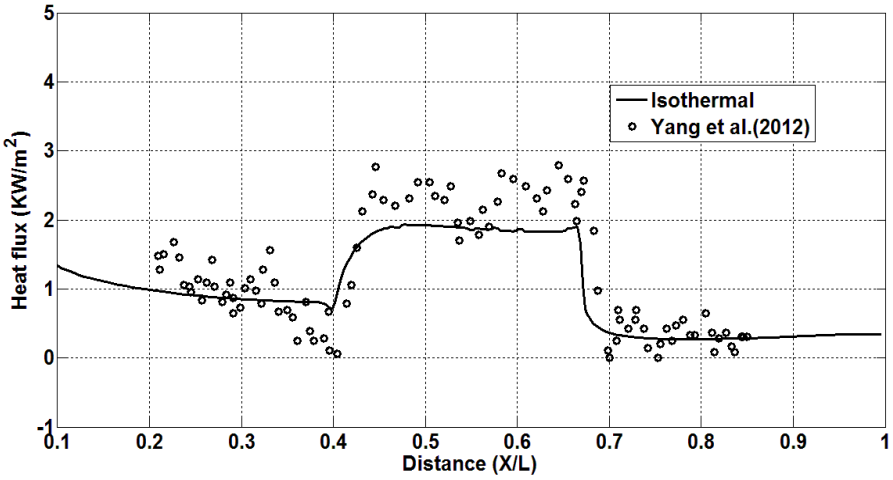

Fig. 8.4: Wall heat flux distribution along the length double wedge.

In case of the CHT simulations with different wall materials, as seen in Fig. 8.5, local value of wall heat transfer rate decreases with increase in time. The value at the leading edge decreases by 47% for Macor in 3s 96 % for Insulating material in 0.1s and 3% for SiC in 0.1s. Similarly, the minimum value of heat transfer rate which is attained in the expected separation region, gets lowered during the corresponding time intervals from 0.655 kW/m^2 to 0.2823 kW/m^2 for Macor, 0.75 kW/m^2 to 0.0241 kW/m^2 for insulating material, and 0.7359 kW/m^2 to 0.6189 kW/m^2 for SiC. In line with time, the maximum heating rate is also seen to be lowered for all materials under consideration. The maximum decrement of 96% has been observed for insulating material while minimum of 7% is recorded for SiC.

The heat transfer rate traced for all the materials at 0.1s time are as shown in Fig. 8.6. The value at the leading edge is 1.29 kW/m^2 for SiC, 1.13 kW/m^2 for Macor, and 0.6337 kW/m^2 for Insulating material in 0.1s. At the expected separation region, heat flux values are 0.7135 kW/m^2, 0.608 kW/m^2, and 0.436 kW/m^2 for SiC, Macor, and Insulating materials respectively. At the second wedge region, shock-boundary layer interaction takes place and in that region wall heating rates increase drastically. The values of heat flux are 1.925 kW/m^2, 1.541 kW/m^2, and 0.9713 kW/m^2 for SiC, Macor, and Insulating materials respectively.

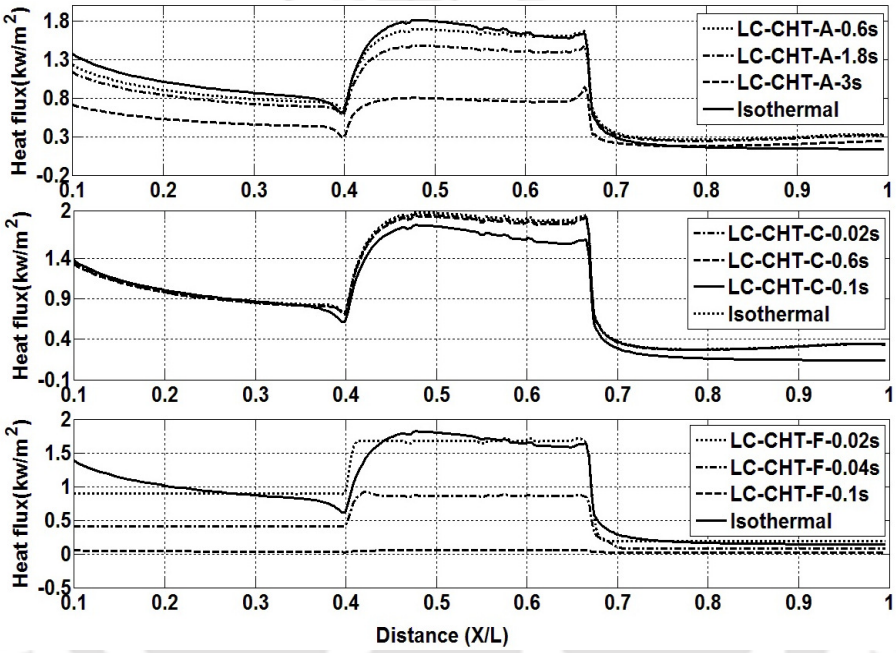

Fig. 8.5: Surface heat flux distribution along the length for different wall materials.

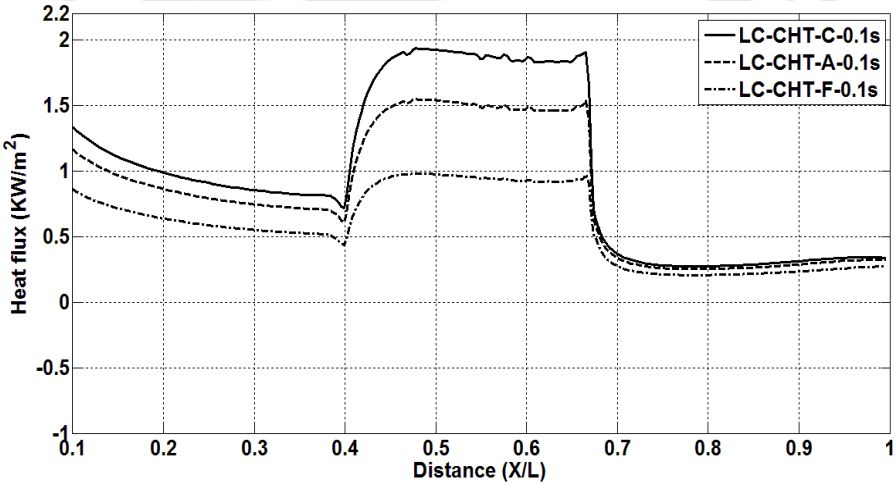

Fig. 8.6: Surface heat flux distribution along the length for different wall materials at 0.1s.

The major reason for decrement in wall heating rate with time is the local increment in wall or interface temperature. Therefore interface temperature profile is plotted in the Fig. 8.7at the same time instances which are considered in Fig. 8.7 for corresponding materials. Highest temperature rise has been observed at the leading edge and on the second wedge for all the material at all the times. These temperature traces exhibit same trend as that of the heat transfer profile except that the local temperature increase with time unlike local heat transfer rate which decreases with time.

The local value of wall temperature increases with time. The value at the leading edge increased by 3% for Macor in 3s, 4.5% for Insulating material in 0.1s and 0.08% for SiC in 0.1s. Similarly the minimum value of temperature rise, which is attained in the expected separation region, gets lowered during the corresponding time intervals from 301 K to305 K for Macor, 302.5 K to 310 K for insulating material and 300.09 K to 300.25 K for SiC. In line with time, the maximum temperature rise also lowered for all materials under consideration. The maximum increment of 6% has been noted for insulating material while the minimum 1.2% is recorded for SiC.

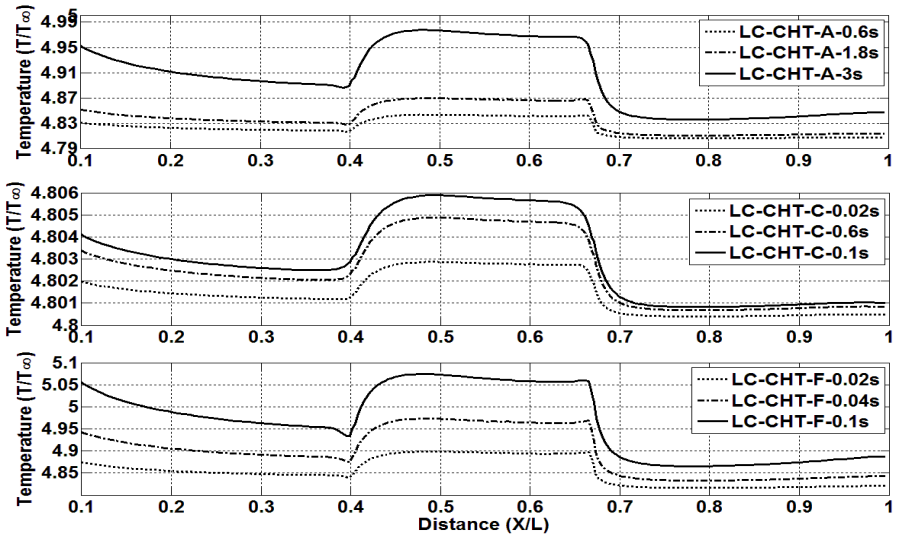

Fig. 8.7: Surface temperature distribution along the length for different wall materials.

The temperature traces for all the materials at 0.1s time are as shown in Fig. 8.8. The value at the leading edge is 300.25 K for SiC, 302.5 K for Macor and 313.12 K for insulating material in 0.1s. At the expected separation region, temperature values are 300.21 K, 301.25K and 303.75 K for SiC, Macor and Insulating materials are respectively. At the second wedge region, shock-boundary layer interaction takes places, in that region wall

heating rates drastically increased. The values of temperature for various walls materials (i.e, SiC, Macor and Thermal Insulating) are 303 K, 304.72 K and 318 K are respectively. Surface temperature along the length of the double wedge of adiabatic wall is shown in Fig. 8.9. Temperature rise is more compared to the CHT analysis; it is expected from this analysis, maximum temperature rise of 67.9 K, which is five times of CHT studies for insulting wall material.

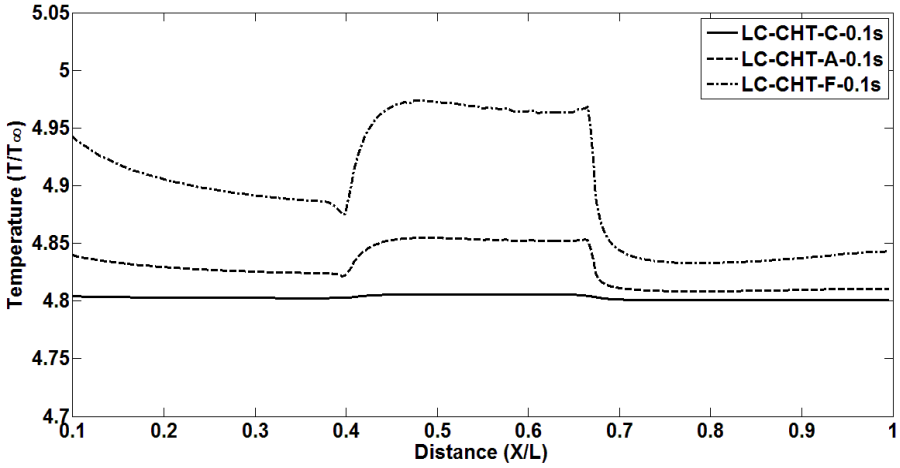

Fig. 8.8: Surface heat flux distribution along the length for different wall materials at 0.1s

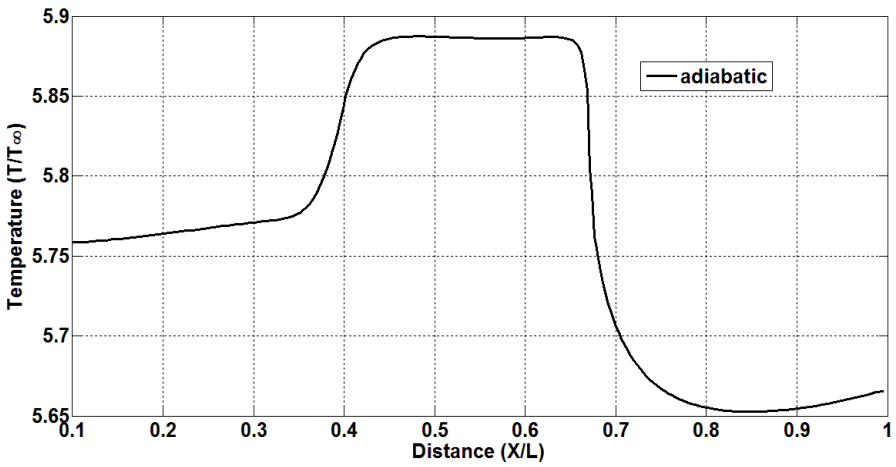

Fig. 8.9: Surface temperature distribution along the length used in adiabatic boundary case.

Trend of skin friction variation, for all wall boundary conditions and any time instance, is same as that of heat transfer rate. Such variation in skin friction coefficient along the length of the double wedge crosses the zero line close to the corner of the double wedge geometry. Hence the first crossover corresponds to separation of the flow while the second one corresponds to reattachment. This region of separation confirms the expectations about the same drawn from pressure trace (Fig. 8.3) and heat transfer profile (Figs.8.4 - 8.6).

Separation bubble length increases with wall temperature which can be observed from Figs. 8.10-8.11. In isothermal case, separation length is obtained as 3.77 mm at the wall temperature of 300 K. In CHT analysis, when silicon carbide (SiC) is considered as a wall, separation length is obtained as 3.77 mm at the wall temperature of 300.26 K near the separation region. The separation length in the above case is close to isothermal separation length. In case of Macor and Thermal insulator as wall materials, separation lengths obtained are 3.86 mm and 4.04 mm and corresponds temperatures in those regions are 305.76 K and 310.9 K respectively. In adiabatic case separation length is 4.69 mm at temperature of 360 K. From this figure it is clearly evident that the separation length increases with increase in wall temperature. Separation bubble length, traced for all the materials at 0.1s time is as shown in Fig. 8.12. It clearly shows that separation bubble length increases to a very low magnitude in SiC material, 3.79 mm for Macor and 3. 95 mm for the insulating material.

Heat diffusion in solid for all the materials at 0.1s is as shown in Fig. 8.13. It is observed that heat diffusion is more in high thermal conductivity material, for example 70% of heat diffused takes places in SiC, 10% and 7% diffusion take places in the Macor and thermal insulating material. From these studies, it is clear that heat diffusion is less in thermal insulating material compared to Macor and SiC materials, which are shown in Fig. 8.14. These figures clearly show that there are two regions of heat affected zones. First one is the leading wedge region and the other one is second wedge location. Near the first wedge heat transfer is more due to leading edge shock at this region and the surface temperature tremendously increases due to oblique shock at leading edge of the first wedge. Shock boundary layer interaction takes places in the second wedge location. The increase in surface temperature at the second wedge location is a direct result of this interaction. Therefore these two locations require more insulation.

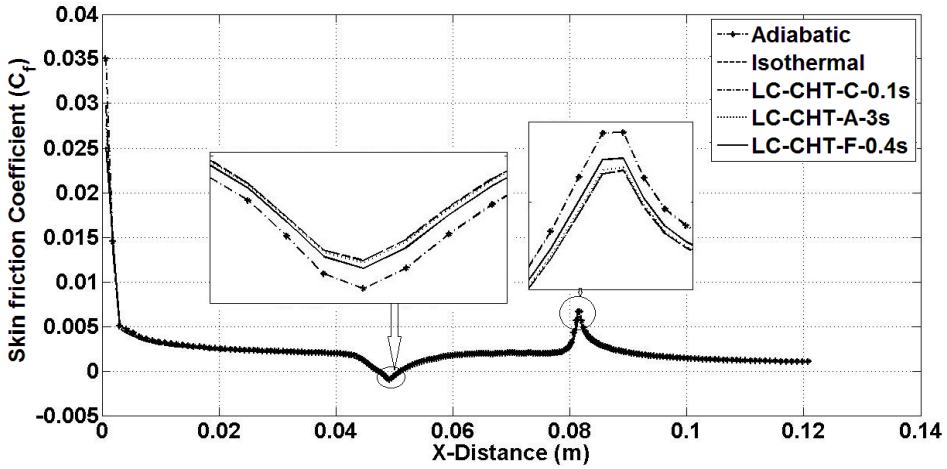

Fig. 8.10: Wall skin friction distribution along the length double wedge.

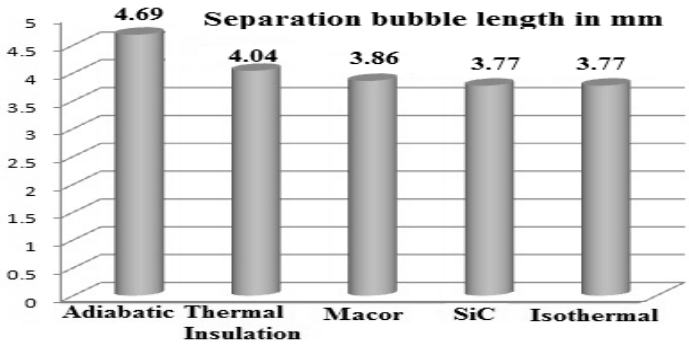

Fig. 8.11: Separation length in various wall materials used in CHT at the end of simulation time.

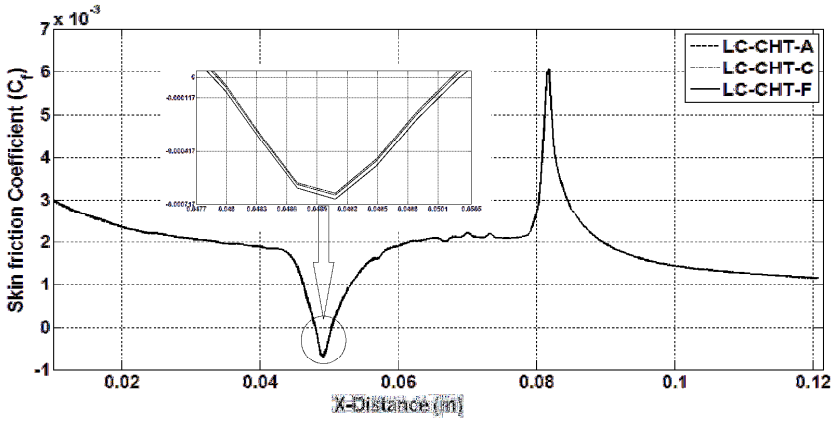

Fig. 8.12: Wall skin friction distribution along the length double wedge at time=0.1s

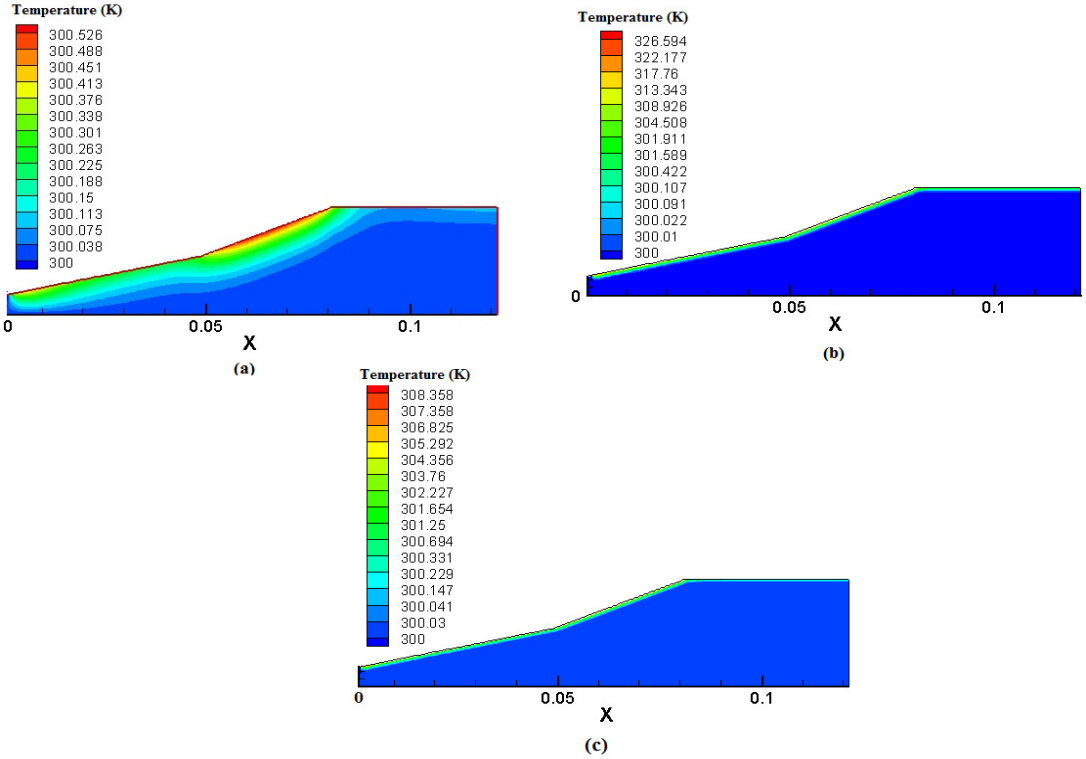

Fig. 8.13: Solid temperature contour at time 0.1 s; (a) SiC material (b) Thermal insulating; (c) Macor.

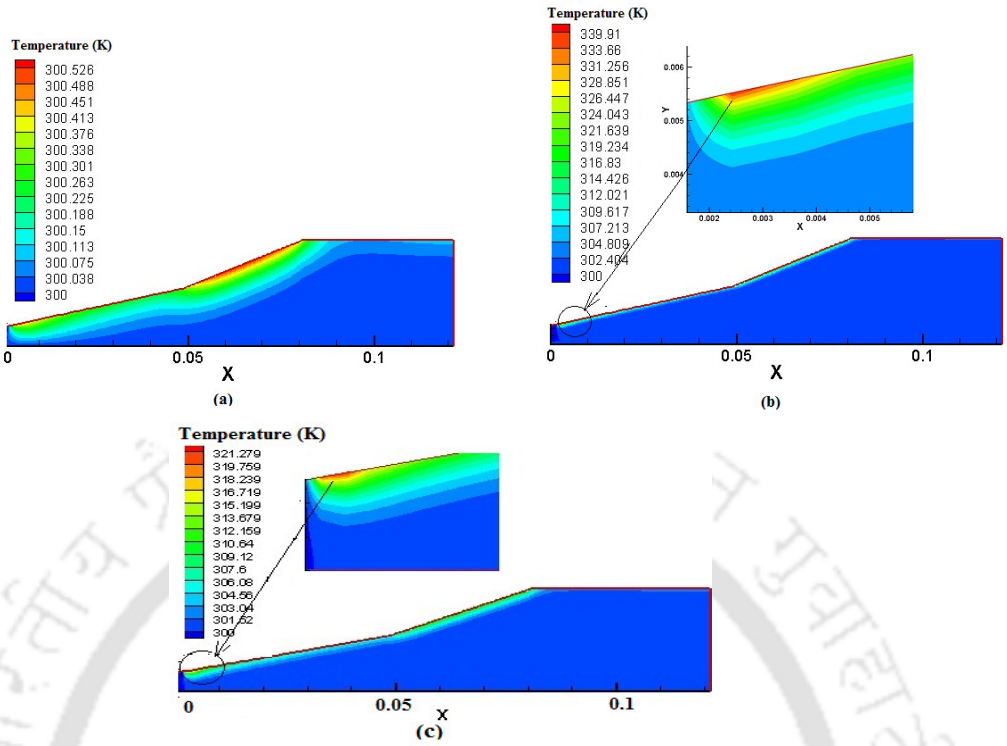

Fig. 8.14: Solid temperature contour; (a) SiC material at time=0.1s; (b) Thermal insulating at time=0.4s; (c) Macor at time= 3s.

8.4 Summary

The double wedge problem has been successfully investigated using the loosely coupled CHT solver for prediction of surface temperatures and heat flux, skin friction coefficient, pressure and separation bubble length respectively in different wall materials. This CHT technique is expected to bring out the exact prediction of separation bubble length heat flux, skin friction coefficient and pressure distributions in double wedge studies in hypersonic applications. In CHT studies, the wall materials used are thermal insulation, Macor and SiC, it clearly shows that while using Macor and thermal insulation wall material in CHT studies, interface temperature, skin friction coefficient, heat flux distribution along the length change significantly with increase in simulation time. In comparing the CHT results with fluid flow solver (N-S solver) isothermal and adiabatic boundary results, it clearly indicates that the fluid flow solver (N-S solver) results are either under predicting or over predicting the interface properties, but CHT studies gives an accurate prediction of separation length and interface properties. These studies are helpful for the efficient design of hypersonic vehicles.

CHAPTER 9

CONCLUSIONS AND FUTURE WORK

9.1 Conclusion

In this study, Conjugate Heat Transfer (CHT), solver is developed to understand the interface properties and flow properties due to change in wall heating rates. It is also useful to examine the heat penetration of solid in various wall materials with different time scales. This work mainly focuses on the accurate prediction of heat transfer, temperature at the interface and flow properties. This problem is critically important in efficient design of thermal protection system (TPS) for hypersonic vehicles. Such system, in-fact is traditionally designed with the help of one-dimensional heat transfer analysis. Since, uncertainties are more in these studies; CHT is used to overcome those uncertainties. From these studies, it is clear that thermal protection system can be optimally designed. The present investigations can be summarized in two main steps described as follows.

First stage involves, development of one-dimensional transient heat transfer analysis from known temperature history, using various analytical methods such as Laplace transform, Duhamel's integral, Schultz and Jones. Spline fitting (linear and cubic) and least square polynomial fitting techniques are used in temperature data for prediction of surface heat flux using above methods. In these studies, temperature signal obtained from numerical simulations, shock tunnel, and actual flight experiments has been used to recover the heat flux using above analytical methods. The conclusions drawn from one dimensional heat transfer studies are given below;

- Heat flux recovery from all the methods is well predicted with a reasonable accuracy of ±5%, for smooth temperature signal.
- In case of noisy temperature signal, polynomial based techniques were under predicting the heat flux. However, Spline based fitting techniques are found to be suitable for exact prediction of heat flux for all types of temperature signals.

In the second and foremost part of this work, the author has critically examined on conjugate heat transfer (CHT) techniques for various configurations, such as flow over a flat plate, cylinder, composite materials (flat plate and cylinder) and double wedge configurations.

Development of solvers for fluid flow and solid conduction

CHT solver development is grounded on the development of compressible fluid flow and conduction solver facilitated by the finite volume method. The AUSM-δ scheme is incorporated in the fluid flow solver for inviscid flux computations while the viscous fluxes are computed using discrete version of the Gauss theorem. Conduction solver is equipped with all required boundary conditions for transient heat conduction analysis.

- The developed solvers are validated for the standard test cases, hypersonic flow over isothermal plate for the fluid flow solver and transient heat conduction in a finite thickness flat plate.
- Encouraging agreement has been noticed for both the solvers with the respective analytical results.
- Possibility of simulation for composite domain conduction has also been successfully verified**.**

CHT Coupling Techniques and Decoupled CHT Studies

Coupling techniques are successfully implemented in the present solver. These techniques include strong and loose couplings between fluid flow and heat conduction solvers. The decoupled CHT technique is used in hypersonic flow over flat plate is considered for simulation with freestream Mach number 9.0. The conclusions drawn from flow over a flat plate are given below;

- The temperature contours of solid domain and the temperature traces at different locations clearly showed the necessity of multidimensional active coupling between fluid and solid domains for accurate prediction of surface properties.
- The decoupled CHT analysis with lesser computational cost is found to have limitation in the presence of non-uniform surface heating rates.
- This observation demands for the application of strong and loose coupling techniques for heat transfer analysis.

Flow over a flat plate

Hypersonic flow over a flat plate studies are carried out using conjugate heat transfer (CHT) techniques. These studies mainly focus on heat transfer measurements in shock tunnel and flight applications. It helps us to understand optimized design of experiments for small and large time scales, to find exact location of the thermal sensor so as to mount object in experiments and it is further used to reduce the experimental costs. Furthermore, the effect of wall heating rates on the fluid properties, thermal and velocity boundary layer thickness are studied.

- Coupled and decoupled CHT solvers are used for short and large duration transient temperatures and surface heat flux.
- Decoupled strategy is found equally effective as the strongly coupled technique to employ for simulating the heat transfer rate measurement for short test duration of 1 millisecond which relates with shock tunnel testing.
- From the fore mentioned studies, designing the experiment would be possible which in turn facilitates the selection of sensor and its mounting location.
- Extended study using loosely coupled CHT technique has showed significant effect of wall material on the fluid flow at moderately large time scales. This effect is noticed to be dependent on thermal diffusivity of the wall material.
- The material with higher thermal diffusivity is found to get disturbed more keeping the fluid domain relatively undisturbed. In line with this, the material with lower diffusivity is noticed to alter the boundary layer thickness and interface properties with lesser heat penetration in itself.
- Thermal boundary layer thickness increases around 29% from the leading edge location 0.01 m and 20% from the 0.09 m location at 0.1scc. Skin friction also increases with increase in simulation time and wall temperature.

Flow over a cylinder

This study deals with hypersonic flow over a cylinder using various CHT coupling techniques. The objective is to develop computationally time efficient CHT algorithms in

different time scales. In addition, the effect of simulation time on interface heat flux and fluid flow properties is analyzed.

- Various coupling techniques are successfully implemented and evaluated for their applicability in CHT analysis at various time scales.

- Loosely coupled CHT analysis is very much useful for large time scale applications (actual flight experiments). For simulation time of 1s, maximum discrimination at the stagnation point is seen for LC-CHT method where the heat flux is under-predicted by 65% as compared to DC-CHT technique. Moving along the surface of the cylinder from stagnation point to the flow deflection angle of 90º, the difference of surface heat flux reduces to 35%.

- At 1 s, stagnation point heat flux is decreased around 65% due to maximum rise in the wall temperature in that region around 842 K.

Flow over a composite material (flat plate and cylinder)

Exact prediction of heat transfer rates is essential for design of thermal protection systems for hypersonic vehicles and is possible using CHT techniques. Thermal protection system and aerodynamic surfaces are generally configured with multiple solids. Hence, composite CHT analysis is performed in the present study.

- A CHT solver for the composite solid domain analysis was successfully developed.
- It is observed that when insulating material is used in solid domain, the heat penetration and the magnitude of temperature rise was significantly less within the solid domain and is limited to the surface i.e. around 20%.

- The idea of using lower conductivity material at the leading edge and other such regions, where there was higher heat flux generation, will prominently help in thermal protection of vehicles.

- Thus, the developed solver is useful for design of thermal protection systems in hypersonic vehicles.

Flow over a double wedge

Shock wave boundary layer interaction phenomenon plays a critical role in the design of supersonic and hypersonic vehicles. These interactions induce extremely high heating and pressure loads on the surface of the vehicle. Loosely coupled CHT technique is used for the present analysis. This study mainly focuses on variation of separation bubble length, skin friction coefficient, and heat flux caused by change in wall heating rates with different wall materials and time scales.

- CHT technique establishes the exact prediction of heat flux, skin friction, pressure distributions, and separation bubble length in double wedge studies of hypersonic applications.
- The separation length in Isothermal case is same as in CHT analysis of SiC wall. Macor and Thermal insulator materials have 2.25% and 7.07% separation lengths increments at temperatures 321.76 K, 339.9 K respectively. In adiabatic case, separation length had 24% increment at temperature of 360 K. Hence, it is clearly evident that the separation length increases with increase in wall temperature.
- In CHT studies, the wall materials used are Thermal insulation, Macor and SiC. While using Macor and thermal insulation, it is evident that with increase in simulation time significant changes takes place in interface temperature, skin friction coefficient, heat flux distribution, and separation bubble length, along the surface.
- A similar study shows that as CHT simulation time increases, the wall temperature increases and more temperature rise is observed around 21 K in Macor wall material. Heat flux decreases by around 50% of initial value.
- While comparing the CHT results with fluid flow solver (N-S solver) isothermal and adiabatic boundary results, the Fluid flow solver (N-S solver) results are either under predicting or over predicting the interface properties. But CHT studies give an accurate prediction of interface properties.

9.2 Future Work

- In-house CHT solvers can be extended to composite solid domain axi-symmetric and 3D geometries.
- In-house CHT solvers can be extended to various typical hypersonic situations like shock-boundary layer interactions, shock-shock interactions, shock reflection etc. for axi-symmetric and 3D geometries.
- In-house fluid flow solver can be extended to non-equilibrium flows, real gas effect, and low density flows. Flow can be considered as turbulent to get more accurate and realistic results.
- In-house conduction solver can be extended to change in thermo-physical property considering temperature as function.
- Updated fluid flow and conduction solvers can be coupled in CHT techniques.

LIST OF PUBLICATIONS

Journal Papers

[1] Ravi K. Peetala, Niranjan Sahoo and Vinayak N. Kulkarni, "Prediction of short duration transient surface heat flux using various analytical techniques" *Journal of Asian Research: Heat Transfer,* (2013), **42**(6): 530-543.

[2] Ravi K. Peetala, Dipankar Das Vinayak N Kulkarni and Niranjan Sahoo"Conjugate heat transfer analysis for a finite thickness cylinder in a hypersonic flow" *International Journal of Heat Transfer Engineering*. (Under Review).

Conference Papers

[1] Ravi K. Peetala, Vinod Pandey, Vinayak N Kulkarni and Niranjan Sahoo "HMTC1300049: Conjugate heat transfer analysis for composite solids at hypersonic speeds" *Proceedings of the 22th National and 11th International ISHMT-ASME Heat and Mass Transfer Conference*, December 28-31, 2013, IIT Kharagpur, India.

[2] Ravi K. Peetala, Vinayak N Kulkarni and Niranjan Sahoo "ISSW-2757: Simple conjugate heat transfer analysis for hypersonic flows" *International Symposium on Shock Waves 28 (ISSW-28),* at University of Manchester UK, 17-28 July 2011.

Bio-data

Ravi Kumar Peetala received the B. Tech. degree in Mechanical Engineering from SRKR Engineering College, Bhimavaram, India in 2006. He obtained the M. Tech. from Indian Institute of Technology, Guwahati, India in 2009 in the area of Fluids and Thermal Sciences. Presently he is pursuing PhD in the Department of Mechanical Engineering, Indian Institute of Technology, Guwahati, India. His research interests are Heat Transfer Studies in Hypersonic Flow Applications and Computational Fluid Dynamics.

REFERENCES

Abderrahmane B, Najib L, Nacim A, and Zoubir Z, (2004), Fast transient conduction in infinite plate subject to violent thermal effect, Applied Thermal Engineering, **22**: 1–15.

Abram SD, (2010), Conjugate Problems in Convective Heat Transfer, CRC Press, Taylor & Francis Group, pp. 249-264.

Adam JC, Jack JM, (2010), Studies on fluid–thermal–structural coupling for aerothermoelasticity in hypersonic flow, AIAA Journal, 48 (8): 1721-1737

Alifanov AV, and Golub VM, (2003), Solution of the unsteady heat-conduction equation for a system of two bounded heterogeneous cylinders with the use of the integral transformations of Henkel and Laplace, Journal of Engineering Physics and Thermophysics, **76** (5): 1111-1118.

Al-Zaharnah IT, and yilbas BS, (2004), Thermal analysis in pipe flow: influence of variable viscosity on entropy generation, Journal of Entropy, **6**: 344-363.

Amin MR, and Greif D, (1999), Conjugate heat transfer during two-phase solidification process in a continuously moving metal using average heat capacity method, International Journal of Heat and Mass Transfer, **42**: 2883–2895

Anderson AM, (1994), Decoupling convective and conductive heat transfer using the adiabatic heat transfer coefficient, Journal of Electron Packaging, **116** (4): 310-317.

Anderson JD Jr., (2006), Hypersonic and High-Temperature Gas Dynamics, AIAA Education Series; Ed: J.A. Schetz, American Institute of Aeronautics and Astronautics, Virginia, Second Edition.

Arnal D, and Delery J, (2004) Laminar–turbulent transition and shock wave/boundary layer interaction. EN-AVT-116-04.

Beck JV, (1986), Green's functions and numbering system for transient heat conduction, AIAA Journal, **24**: 327-333.

Bertolazzi E, Battisti L, and Trivellato F, (2012), Numerical processing of thin-film thermometer data for determining transient heat fluxes, Applied Mathematical Modeling, **36**: 3645-3662.

Bibin J and Kulkarni V, (2014), Numerical assessment of correlations for shock wave boundary layer Interaction, Computers & Fluids, **90**: 42–50

Bibin J, Kulkarni V, and Natarajan G, (2014), Shock wave boundary layer interactions in hypersonic flows, International Journal of Heat and Mass Transfer, **70**: 81–90.

Blazek J, (2001), Computational Fluid Dynamics: Principles and Applications, Elsevier Publishing Company.

Blobner J, Hribersek M, and Kuhn G, (2000), Dual reciprocity BEM-BDIM technique for conjugate heat transfer computations, Comput. Mrthods Appl. Mech. Engrg, **190**: 1105-1116.

Boyce RR, and Hillier, R, (2000), Shock-induced three-dimensional separation of an axisymmetric hypersonic turbulent boundary layer, American Institute of Aeronautics & Astronautics, AIAA Paper 2000-2226.

Bulavin PE, and Kascheev VM, (1965), Solution of the non-homogeneous heat conduction equation for multilayered bodies, International Journal of Chemical Engineering, **1**: 112-115.

Carslaw HS, and Jaeger JC, (1959), Conduction of Heat in Solids, Oxford University Press, London, England, pp. 353-386.

Chandrashekhar V, Jayathi YM, and Sanjay M, (2010), A meshless finite difference method for conjugate heat conduction problems, Transactions of the ASME: Journal of Heat Transfer, **132** (8): 0813031-08130313.

Chantasiriwan S,(2002), Inverse determination of steady state heat transfer coefficient, Journal of International Communications in Heat and Mass Transfer, **27**: 1155-1164.

Chiu WKS, Richards CJ, and Jaluria Y, (2001), Experimental and numerical study of conjugate heat transfer in a horizontal channel heated from below, Transactions of the ASME: Journal of Heat Transfer, **123** (4): 688-697.

Clarissa RR, Renato MC, and Jian S, (2000), Improved lumped analysis of transient heat conduction in a nuclear fuel rod, International Journal of Heat and Mass Transfer, **27**: 357-366.

Cook WJ, and Felderman EJ, (1966), Reduction of data from thin-film heat-transfer gauges: concise numerical technique, AIAA Journal, **4**: 561-562.

Davis J, (1999), High enthalpy shock/boundary layer interaction on a double wedge, PhD thesis, California Institute of Technology, Pasadena, CA, USA.

Diego AM, (1987), Parameter selection by discrete mollification and the numerical solution of the inverse heat conduction problem, Journal of Computational and Applied Mathematics, **22**: 25-38.

Divo E, and Kassab AJ, (2006), Iterative domain decomposition meshless method modeling of incompressible viscous flows and conjugate heat transfer, Journal of Engineering Analysis with Boundary Elements, **30**: 465-478.

Divo E, Steinthorsson E, Kassab AJ, and Bialecki, (2002), An iterative BEM/FVM protocol for steady state multi-dimensional conjugate heat transfer in compressible flows, Journal of Engineering Analysis with Boundary elements, **22**: 447-454.

Dowell E, and Hall KC, (2001), Modeling of fluid structure interaction, Annual Review of Fluid Mechanics, **33**: 445-490.

Duchaine F, Corpron A, Pons L, Moureau V, Nicoud F, Poinsot T, (2009), Development and assessment of a coupled strategy for conjugate heat transfer with large eddy simulation. Application to a cooled turbine blade, International Journal of Heat and Fluid Flow, **30** (6): 1129-1141.

Ge SA, Zheng T, and Jian SB, (2009), Improved lumped models for transient heat conduction in a slab with temperature-dependent thermal conductivity, Applied Mathematical Modeling, **33** (1): 274–283.

Guosm, Lai CC, Jones TV, Oldfield MLG, Lock GD, Rawlinson AJ, (1998), The application of thin-film technology to measure turbine-vane heat transfer and effectiveness in a film

cooled engine simulated environment, International Journal of Heat and Fluid Flow, **19**: 594–600.

Haji SA, and Mashena M, (1987), Integral solution of diffusion equation-part I-general solution, Transactions of the ASME: Journal of Heat Transfer, **109**: 551-556.

Hashimoto T, (2003), Analytical and Experimental Study of Hypersonic Nozzle Flows in Free Piston Shock Tunnel, Ph. D. Thesis, Tohoku University, Japan.

Hassan B, Kuntz D, Potter DL, (1998), coupled fluid/thermal prediction of ablating hypersonic vehicle, *AIAA pape*r-168.

He M, Bishop P, Kassab AJ, Minardi A, (1995), A coupled FDM/BEM solution for the conjugate heat transfer problem, Numerical Heat Transfer. Part B Fundamentals, **28** (2): 139–154.

He M, Kassab AJ, Bishop PJ, and Minardi A, (1995), A coupled FDM/BEM iterative solution for the conjugate heat transfer problem in thick-walled channels: constant temperature imposed at the outer channel wall, Journal of Engineering Analysis, **15** (1): 43-50.

Heidmann J, Rigby D, and Ameri A, (2002), A three-dimensional coupled external/internal simulation of a film-cooled turbine vane, ASME Journal of Turbomachinery, **122**: 348-359.

Holman JP, (1989), Heat Transfer, McGraw-Hill, Inc 6th Editionm, pp.139.

Huang CH, and Tsai CC, (1998), An inverse heat conduction problem of estimating boundary fluxes in an Irregular domain with conjugate gradient method, International Journal of Heat and Mass Transfer, **34**: 47- 54.

Hui P, and Tan HS, (1994), A transmission-line theory for heat conduction in multilayer thin films, IEEE Transactions, Components, Packaging and Manufacturing Technology, Part B, Advanced Packaging, **17** (3): 426–434.

Hwang JJ, (1998), Conjugate heat transfer for developing flow over multiple discrete thermal sources flush-mounted on the wall, Transition of ASME; Journal Heat Transfer **120**: 510-521.

Incropera FP, and DeWitt DP, (2002), Fundamentals of Heat Transfer, John Wiley and Sons, Appendix A.

James MH, and Jeffrey ND, (1987), Heat conduction, Blackwell Scientific Publications, Oxford, USA, pp. 64-153.

James VB, (1970), Nonlinear estimation applied to the nonlinear inverse heat conduction problem, International Journal of Heat and Mass transfer, **13**: 703-716.

Jian S, (2001), Improved lumped models for asymmetric cooling of a long slab by heat convection, International Journal of Heat and Mass Transfer, **28**: 973-983.

Kai-Hsiung K, and Liou MS,(1997), Application of chimera/unstructured hybrid grids for conjugate heat transfer, AIAA Journal, **35** (9): 1472-1478.

Kaminski DA, and Prakash C,(1986), Conjugate natural convection in a square enclosure: effect of conduction in one of the vertical walls, International Journal of Heat and Mass Transfer, **29** (12): 1997-88.

Kanna PR, and Das MK, (2005) ,Conjugate forced convection heat transfer from a flat plate by laminar plane wall jet flow, International Journal of Heat and Mass Transfer, **48**: 2896–2910.

Kassab AJ, and Aliabadi MH, (eds.), (2001), Advances in boundary elements: Coupled field problems, WIT Press, Southampton and Boston.

Kim HK, and Oh SI, (2001), Evaluation of heat transfer coefficient during heat treatment by Inverse analysis, Journal of Material Processing Technology, **112**: 157-165.

Kim SK, Jung BS, and Lee W, (2007), An inverse estimation of surface temperature using the maximum entropy method, International Communications in Heat and Mass Transfer, **34**: 37–44.

Kolodziej P, (1997), Aerothermal performance constrains for hypervelocity small radius unswept leading edges and nose tips, NASA-TM-11204.

Kontinos DA, (1997), Coupled thermal analysis method with application to metallic thermal protection panels, Journal of Thermo Physics Heat Transfer, **11** (2): 173-81.

Kulkarni V and Reddy KPJ, (2008), Enhancement in counterflow drag reduction by supersonic jet in high enthalpy flows, Physics of Fluids, **20**: 16103.

Kulkarni V and Reddy KPJ, (2009), Effect of supersonic counter flow jet on blunt body heat transfer rates for oncoming high enthalpy flow, Journal of Engineering Physics and Thermophysics, **8**(1): 3-7.

Kulkarni V, Hegde GM, Jagadeesh G, Arunan E and Reddy KPJ, (2008), Aerodynamic drag reduction by heat addition into the shock layer for a large angle blunt cone in hypersonic flow, Journal of *Physics of Fluids,* **20** (8): 081703.

Kulkarni V, Viren M, and Reddy KPJ, (2010), Effectiveness of forward facing spike for drag reduction on a large angle blunt cone in hypersonic flow, Journal of Spacecraft and Rockets, **43** (3): 542-544.

Li H, and Kassab AJ, (1994), Numerical prediction of fluid flow and heat transfer in turbine blades with internal cooling, AIAA/ASME Paper 94-2933.

Liou MS, (1996), A Sequel to AUSM: AUSM+, Journal of Computational Physics, **129**: 364-382.

Lisa CM, John DW, and Gustave CF,(2001), Thin film sensors for surface measurements, 19th International Congress on Instrumentation in Aerospace Simulation Facilities (ICIASF 2001), NASA Glenn, and OAI, Cleveland, Ohio, August 27-30.

Liu FB, (2008), A modified genetic algorithm for solving the inverse heat transfer problem of estimating plan heat source, International Journal of Heat and Mass Transfer, **51**: 3745–3752.

Liu T, Cai Z, Lai J, Rubal J, and Sullivan JP, (2010), Analytical method for determining heat flux from temperature-sensitive-paint measurements in hypersonic tunnels, Journal of Thermophysics and Heat Transfer, **24**(1): 85-94.

Madhusudhan KN, Sivamurugan T, Kumar GVR, (2007), Conceptual thermal protection system design of a control surface of a wing body hypersonic vehicle, Symposium on Applied Aerodynamics and Design of Aerospace Vehicle (SAROD), November 22-23, 2007, Thiruvananthapuram, India.

Mahulikar SP, (2005), Theoretical aerothermal concepts for configuration design of hypersonic vehicles, Aerospace Science and Technology, **9** (8): 681-685.

Mallinson S, Gai S, and Mudford N, (1996), Upstream influence and peak heating in hyper velocity Shock wave / boundary-layer interaction," Journal of Propulsion and Power ,**12** (5): 984-990.

Mark EB, and Patankar SV, (1985), Analysis of laminar mixed convection in shrouded arrays of heated rectangular blocks, International Journal of Heat and Mass Transfer, **28** (9): 1699-1709.

Mehdi D, (2000), A finite difference method for a non-local boundary value problem for two-dimensional heat equation, Applied Mathematics and Computation, **112** (1): 133-142.

Mehta RC, Jayachandran T, Trivandrum and Sastri VMK, (1988), Finite element analysis of conductive and radiative heating of a thin skin calorimeter, Heat and Mass Transfer, **22**: 227-230.

Miller ST, and Hober RB, (2008), A space time discontinuous Galerkin method for hyperbolic heat conduction, Journal of Computer Methods in Applied Mechanics and Engineering, **198**: 194–209.

Ming-I C, Fu-Ping C, and Bo-Chen T, (2008), Inverse determination of thermal conductivity by differential quadrature method, Journal of International Communications in Heat and Mass Transfer, **35**: 113–119.

Mishra SC, and Roy HK, (2007), Solving transient conduction and radiation heat Transfer problems using the lattice Boltzmann method and the finite volume method, Journal of Computational Physics, **223**: 89–107.

Murthy MSRC, Manna, and Chakraborty D, (2013), Conjugate heat transfer analysis in high speed flows, Proc. IMechE Part G: Journal of Aerospace Engineering, **227** (10): 1672-1681.

Nakayama W, and Park SH, (1996), Conjugate Heat Transfer from a Single Surface-Mounted Block to Forced Convective Air Flow in a Channel, Transactions of the ASME: Journal of Heat Transfer, **118** (2): 301-309.

Narayanan VAB, and Zabaras N, (2004), Scholastic inverse heat conduction using a spectral approach, International Journal for Numerical Methods in Engineering, **60** (7): 1-24.

Nikas KSP, and Panagiotou AD, (2013), Numerical Investigation of conjugate heat transfer in a computer chassis, Journal of Advanced Mechanical Engineering, **1**: 40-57.

Olejniczak J, Candler GV and Wright MJ, (1999), Experimental and Computational Study of High Enthalpy Double-Wedge Flows, Journal of Thermophysics and Heat Transfer, **13** (4): 431–439.

Olejniczak J, Wright MJ, and Candler GV, (1997), Numerical Study of Inviscid Shock Interactions on Double-Wedge Geometries, AIAA Journal, **352**: 1-25.

Ostrogorsky AG, (2008), Transient heat conduction in spheres for Fo<0.3 and finite Bi, International Journal of Heat and Mass Transfer, **44**: 1557-1562.

Pagliarini G, (1991), Conjugate Heat Transfer for Simultaneously Developing Laminar Flow in a Circular Tube, Transactions of the ASME: Journal of Heat Transfer, **113** (3): 763-766.

Peyret R, and Taylor TD, (1983), Computational Methods for Fluid Flow, *Springer-Verlag* New York, pp: 230.

Pietro F, and Domenic D, (2008), A numerical method for conjugate heat transfer problems in hypersonic flows, 40th AIAA Thermophysics Conference, Seattle, Washington, 23-25 June, 2008, pp.4247.

Piotr D, Jan T, and Eberhard R, (2003), Inverse method for temperature and stress monitoring in complex-shaped bodies, Nuclear Engineering and Design, **227**: 331–347.

Qinghua W, and Yogesh J, (2004), Three-dimensional conjugate heat transfer in a horizontal channel with discrete heating, Transactions of the ASME: Journal of Heat Transfer, **126**: 642-647.

Radu V, Taylor N and Paffumi E, (2008) Development of new analytical solutions for elastic thermal stress components in a hollow cylinder under sinusoidal transient thermal loading, International Journal of Pressure Vessels and Piping, **85**: 885–893.

Rahim CP, Kassab AJ, and Cavalleri RA, (2000), Coupled dual reciprocity Boundary element/Finite volume method for transient conjugate heat transfer, Journal of Thermo Physics Heat Transfer, **14** (1): 27-38.

Rahim CP, Kassab AJ, Cavalleri R, (1997), Computational code for conjugate heat transfer problems: an experimental validation effort, AIAA paper 97-2487.

Ramesh S, Alfonso O, Choi CH, (1994), A numerical investigation of conjugate heat transfer from a flush heat source on a conductive board laminar channel flow, Thermal Phenomena in Electronic Systems, (I-THERM IV) Concurrent Engineering and Thermal Phenomena, Inter Society Conference, May 4-7, Washington, DC, USA, pp. 7803-1372.

Reza A, and Ahmad A, 2008, Applications of linear inverse finite element method in prediction of the optimum blank in sheet metal forming, Material & Design, **29** (10): 1965-1972.

Sadat H, (2006), A second order model for transient heat conduction in a slab with convective boundary conditions, Applied Thermal Engineering, **26**: 962–965.

Saha S, Rathod S, Murty MSRC, and Chakraborty, (2012), Numerical simulation of base flow of a long range flight vehicle, Acta Astronautica, **74**: 112-119.

Sahoo N, (2003), Simultaneous Measurement of Aerodynamic Forces and Convective Surface Heat Transfer Rates for Large Angle Blunt Cones in Hypersonic Shock Tunnel, PhD Thesis, Department of Aerospace Engineering, Indian Institute of Science, Bangalore, India.

Sahoo N, and Peetala RK, (2010), Transient temperature data analysis for a supersonic flight test, Transactions of the ASME: Journal of Heat Transfer, **132**: 084503-1-5.

Sahoo N, and Peetala RK, (2011), Transient surface heating rates from a nickel film sensor using inverse analysis, International Journal of Heat and Mass Transfer, **54** (5): 1297-1302.

Samuel SM, and John MF, (1995), An experimental and numerical study of hypersonic study of hypersonic flat plate flow, 12th Australasian Fluid Mechanics Conference, The University of Sydney, Australia, pp.803-806.

Saravanan S, Jagadeesh G, and Reddy KPJ, (2009), Convective heat-transfer rate distributions over a missile shaped body flying at hypersonic speeds, Experimental Thermal and Fluid Sciences, **33**: 782-790.

Schultz DL, and Jones TV, (1973), Heat transfer measurements in short-duration hypersonic facilities, AGARDograph-AG-165.

Shahani AR, and Nabavi SM, (2007), Analytical solution of the quasi-static thermoelasticity problem in a pressurized thick-walled cylinder subjected to transient thermal loading, Applied Mathematical Modeling, **31**: 1807–1818.

Sirilath JD, and Cho LC, (2008), Coupled boundary element method and finite difference method for the heat conduction in laser processing, Applied Mathematical Modeling, **32**: 2429–2458.

Sugavanam R, Ortega A, and Cho CY, (1995), A numerical investigation of conjugate heat transfer from a flush heat source on a conductive board in laminar channel flow, International Journal of Heat and Mass Transfer, **38** (16): 2969-2984.

Suresh BN, (2009), Road map of Indian space transportation, Acta Astronautica, **64**: 395-402.

Taler J, (1996[a]), Theory of transient experimental techniques for surface heat transfer, International Journal of Heat and Mass Transfer, **39** (17): 3733-3748.

Taler J, (1996[b]), A semi-numerical method for solving inverse heat conduction problem, International Journal of Heat and Mass Transfer, **31**: 105-111.

Taler J, Bohdan W, Wiestaw Z, Slawomir G and Marcin ZB, (1997), Monitoring of transient temperature and thermal stresses in pressure components of steam boilers, International Journal of Pressure Vessels and Piping, **72** (3): 231-241.

Tittle CW, (1965), Boundary value problems in composite media: quasi-orthogonal functions, Journal of Applied Physics, **36** (4): 1486-1488.

Veersteeg HK and Malalasekera W, (1995), An introduction to computational fluid dynamics (Finite volume method), *Longman Scientific and Technical*.

Walker DG, and Scott EP, (1998), Evaluation of estimation methods for high unsteady heat fluxes from surface measurements, Journal of Thermophysics and Heat Transfer, **12**: 543-551.

Walker DG, Scott EP, and Nowak RJ, (2000), Estimation methods for two-dimensional conduction effects of shock-shock heat fluxes, Journal of Thermophysics and Heat Transfer, **14**: 533-539.

Wang XYJ, (2000), Conjugate heat transfer analyses on the manifold for ramjet fuel injectors, NASA Report.

White F. M., "Viscous Fluid Flow", 2nd Edn, Mc Graw-Hill. New York, 1991.

Wieting AR, Dechaumphai P, Thornton EA, and Morgan K, (1991), Application of integrated fluid-thermal-structural analysis methods, Journal of Thin-Walled Structure, **11**: 1-23.

Wieting, AR, (1987), Experimental Study Shock Wave Interference Heating on a Cylindrical Leading Edge at Mach 6 and 8, AIAA 22nd Thermophysics Conference, June 8-10, Honolulu, Hawaii.

Wilson KSC, Cristy JR, and Yogesh J, (2001), Experimental and Numerical Study of Conjugate Heat Transfer in a Horizontal Channel Heated From Below, Transactions of the ASME: Journal of Heat Transfer, **123**: 688-697.

Woodbury KW, (1990), Effect of thermocouple sensor dynamics on surface heat flux predictions obtained via inverse heat transfer analysis, Journal of Heat and Mass Transfer, **33** (12): 2641-2649.

Xia JH, and Spel JMM, (1997), Structured surface definition and grid generation for complex aerospace configurations, 13th AIAA Computational Fluid Dynamic Conference- Open Forum, June 29-July 2.

Xiaoli Z, Zhenxu S, Longsheng T, and Gangtie Z, (2010), coupled flow-thermal-structural analysis of hypersonic aerodynamically heated cylindrical leading edge, Journal of Engineering Applications of Computational Fluid Mechanics, **5** (2): 170-179.

Yang L, Behtash HZ, Erdem E, and Kontis K, (2012), Application of AA-PSP to hypersonic flows: the double ramp model, Journal of Sensors and Actuators B: Chemical, **161**: 100-1007.

Yang L, Behtash HZ, Erdem E, and Kontis K, (2012), Investigation of the double ramp in hypersonic flow using luminescent measurement systems, Experimental Thermal and Fluid Science, **40**: 50-56.

Ye R, Kassab AJ, and Li HJ, (1998), FVM/BEM Approach for the Solution of Nonlinear Conjugate Heat Transfer Problems, Proceedings of the 20th International Conference on the Boundary Element Method, Orlando, Florida, August 19-21, pp. 679-689.

Yvonnet J, Umbrello D, Chinesta F, and Micari F, (2006), A simple inverse procedure to determine heat flux on the tool in orthogonal cutting, International Journal of Machine Tools and Manufacture, **46**: 820–827.

Zukhova VN, and Pimshtein PG, (1990), Thermally stressed state of a laminated cylinder exposed to internal pressure and steady-state external heating, Soviet Applied Mechanics, **25** (8): 808-813.